

<https://doi.org/10.15388/vu.thesis.392>

<https://orcid.org/0000-0003-0987-7119>

VILNIUS UNIVERSITY

STATE RESEARCH INSTITUTE CENTER FOR PHYSICAL SCIENCES AND
TECHNOLOGY

Eivydas Andriukonis

Yeast cell wall modification for improvements in biofuel cells

DOCTORAL DISSERTATION

Natural sciences,
Chemistry (N 003)

VILNIUS 2022

This dissertation was written between 2017 and 2021 at Vilnius University and State research institute Center for Physical Sciences and Technology. The research was supported the by Research Council of Lithuania.

Academic supervisor – Prof. Habil. Dr. Arūnas Ramanavičius (Vilnius University, Faculty of Chemistry and Geosciences, Natural sciences, Chemistry – N 003).

This doctoral dissertation will be defended in a public meeting of the Dissertation Defence Panel:

Chairman – Prof. Habil. Dr. Rimantas Ramanaukas (State research institute Center for Physical Sciences and Technology, Natural sciences, Chemistry – N 003).

Members:

Dr. Marius Dagys (Vilnius University, Natural sciences, Research field, N 004),

Doc. Dr. Tatjana Kochanė (Vilnius University, Natural sciences, Chemistry, N 003),

Dr. Vitali Syritski (Tallinn University of Technology, Natural sciences, Chemistry, N 003),

Prof. Dr. Vida Vičkačkaitė (Vilnius University, Faculty of Chemistry and Geosciences, Natural sciences, Chemistry, N 003).

The dissertation shall be defended at a public meeting of the Dissertation Defence Panel at 16:00 on 11th of November 2022 in lecture hall 141-NChA of the Faculty of Chemistry and Geosciences, Institute of Chemistry.

Address: Naugarduko st. 24, 141-NChA, Vilnius, Lithuania

Tel. +37061612338; eivydas.andriukonis@ftmc.lt

The text of this dissertation can be accessed at the library of Vilnius University, as well as on the website of Vilnius University:

www.vu.lt/lt/naujienos/ivykiu-kalendorius

<https://doi.org/10.15388/vu.thesis.392>

<https://orcid.org/0000-0003-0987-7119>

VILNIAUS UNIVERSITETAS
FIZINIŲ IR TECHNOLOGIJOS MOKSLŲ CENTRAS

Eivydas Andriukonis

Mielių sienelių modifikavimas siekiant pagerinti jų pritaikomumą biokuro elementuose

DAKTARO DISERTACIJA

Gamtos mokslai,
Chemija (N 003)

VILNIUS 2022

Disertacija rengta 2017– 2022 metais Vilniaus universitete Chemijos ir geomokslų fakultete ir Fizinių ir technologijos mokslų centre.
Mokslinius tyrimus rėmė Lietuvos mokslo taryba.

Mokslinis vadovas – prof. habil. dr. Arūnas Ramanavičius (Vilniaus Universitetas Chemijos ir geomokslų fakultetas, chemija – N 003).

Gynimo taryba:

Pirmininkas – prof. habil. dr. Rimantas Ramanauškas (Valstybinis mokslinių tyrimų institutas Fizinių ir technologijos mokslų centras, gamtos mokslai, chemija – N 003).

Nariai:

Dr. Marius Dagys (Vilniaus universitetas, gamtos mokslai, biochemija – N 004),

Doc. dr. Tatjana Kochanė (Vilniaus universitetas, gamtos mokslai, chemija – N 003),

Dr. Vitali Syritski (Talino technologijos universitetas, gamtos mokslai, chemija – N 003),

Prof. dr. Vida Vičkačkaitė (Vilniaus universitetas, gamtos mokslai, chemija – N 003).

Disertacija ginama viešame Gynimo tarybos posėdyje 2022 m. lapkričio mėn. 11 d. 16:00 val. Chemijos ir geomokslų fakulteto chemijos instituto 141-NChA auditorijoje. Adresas: Naugarduko g., 24, 141-NChA, Vilnius, Lietuva, tel. +37061612338 ; el. paštas eivydas.andriukonis@ftmc.lt

Disertaciją galima peržiūrėti Vilniaus universiteto bibliotekoje ir VU interneto svetainėje adresu:

<https://www.vu.lt/naujienos/ivykiu-kalendorius>

ABBREVIATIONS

AFM – Atomic force microscope
ATP – Adenosine triphosphate
ATRP – Atom transfer radical polymerization
AuNP – Gold nanoparticles
BC – Biofuel cell
CD – Carbon dots
CF – Carbon felt
CNT – Carbon nanotubes
DI – Deionized water
EA – Elemental analyzer
EBFC – Enzymatic biofuel cell
FIB SEM – Focused ion beam scanning electron microscope
FITC – Fluorescein isothiocyanate
FTIR – Fourier transform infrared spectroscopy
IRMS – Isotope ratio mass spectroscopy/spectrometer
MFC – Microbial fuel cell
MWCNT – Multi walled carbon nanotubes
PANI – Polyaniline
PBS - phosphate buffered saline
PDA – Polydopamine
Ppy – Polypyrrole
PU – Polyurethane
Py – Pyrrole
SDBS – Sodium dodecylbenzenesulfonate
SECM – Scanning electrochemical microscope

TABLE OF CONTENTS

INTRODUCTION.....	8
1. LITERATURE REVIEW	10
1.1. Enzymatic and Microbial biofuel cells	10
1.2. Microorganism adhesion on biofuel cell electrode	10
1.3. Common charge transfer materials	14
1.4. Cell modification for enhanced charge transfer	15
2. METHODOLOGY	21
2.1.1. Polypyrrole synthesis and kinetic studies	21
2.1.2. Synthesis and characterization of polydopamine.....	22
2.2.1. Cell preparation and modification with polypyrrole.....	22
2.2.2. Cell modification with polydopamine.....	23
2.2.3. Atomic force microscope imaging and force measurements	24
2.2.4. Isotope ratio mass spectrometry and isotope mixing model	26
2.2.5. Determination of polypyrrole localization in the cell wall	27
2.3.1. Chronoamperometric evaluation of modified yeast cells in a flow-through system.....	28
2.3.2. Evaluation of power generation by yeast cells modified with PDA and Ppy	28
3. RESULTS	30
3.1. Initial discovery. Principle of $[\text{Fe}(\text{CN})_6]^{4-}/[\text{Fe}(\text{CN})_6]^{3-}$ initiated formation of polypyrrole	30
3.2. Spectrophotometric evaluation of Ppy formation initiated by $[\text{Fe}(\text{CN})_6]^{3-}$ and formed particle characterization	32
3.2.1. Basis for an optical Ppy evaluation.....	32
3.2.2. Influence of oxygen and pH on polymerization kinetics	35
3.2.3. Polypyrrole doping in acidic medium and characterization of aggregates.....	37
3.2.4. Polydopamine synthesis optical assessment	39
3.3. Characterization of yeast and polymer composite	42

3.3.1. Atomic force microscope imaging and mechanical properties of modified yeast	42
3.3.2. Isotopic characterization of polypyrrole-yeast composite	46
3.3.3. Polypyrrole-yeast composite characterization using fluorescence staining	49
3.3.4. Enzymatic cell wall removal.....	49
3.3.5. Optical assessment of polydopamine uptake in yeast	52
3.4. Electrochemical behavior of yeast and polymer composites	54
3.4.1. Chronoamperometric evaluation of modified <i>S. cerevisiae</i> in the flow-through system.....	54
3.4.2. Performance of PDA and Ppy modified yeast cells in MFC.....	57
4. CONCLUSIONS	59
4.1. Polypyrrole and polydopamine synthesis.....	59
4.2. Yeast – polymer composite enhanced chemical and physical resistances	59
4.3. Altered electrical properties of yeast – polymer composite.....	60
4.4. Novelty and significance.....	60
LITERATURE	62
SANTRAUKA	74
PUBLICATION LIST AND OTHER PUBLICITY	83
PUBLICATION COPIES.....	86

INTRODUCTION

Biofuel cells are devices that produce electricity in the presence of a biological catalyst and medium with the appropriate substrate/substrates [1]. Over the past three decades, this research topic has attracted increasing attention as global energy consumption has been continuously increasing and 'green' technologies are gaining popularity. However, biofuel cells have become the gold standard for the remediation of wastewater in commercial [2] and probably domestic environments [3]. The fundamental principle of biofuel cells is that they can simultaneously perform wastewater treatment while producing electricity. Most common biofuel cells are equipped with either enzymes or living microorganisms. The basic difference is that one is using purified enzymes [4] and other living microorganisms [5], which can replenish the entire enzyme pool. Thus, microorganism-based fuel cells are the most promising as microorganisms are capable of reproducing themselves and there is no need for the purification of enzymes, which can often be expensive [6]. Microbial biofuel cells (MFCs) and enzymatic biofuel cells (EBFCs) operate at ambient temperatures, but MFCs are cheaper and simpler to make, as often bacteria samples are required, which are obtained from sludge, soil, and many other natural sources. However, the main delay for their wide application is a low charge transfer (CT) from the microorganism, or in other words, the electrical conductivity of the cell outer layers such as the cell wall and/or membrane is low. Typically, this problem is tackled by adding charge transfer improving materials into biofuel cell [6-14] or using 'specialized' microorganisms that can perform direct electron transfer [15-19]. Materials can range from redox-active organic or non-organic salts [20-24] to various types of conductive nanoparticles [10, 11], nanorods, or polymers [12-14]. These materials are targeted to enhance charge transfer at medium, fuel cell electrodes, or microorganism outer layers. In combination of the chosen materials and the charge transfer enhancement method, there have been a number of studies describing various combinations [7, 12, 25]. As an example, a typical system uses hydrophilic and lipophilic electron mediators to improve charge transfer through the microorganism membrane and water-based medium to the fuel cell electrode. On the other hand, one of the other common approaches is to modify a fuel cell electrode [26-28], which would promote all-together microorganism adhesion to the electrode and charge transfer. However, recently a new type of enhancement type emerged – in situ microorganism modification with conducting polymers [29-31]. Polymerization of monomers into polymers is promoted by microorganisms

or external factors, which further creates conductive polymer matrices or coatings around individual cells [32].

The modifications described here are performed explicitly on yeast *Saccharomyces cerevisiae*. The choice behind was influenced by many favorable traits of these cells. They are one of the most studied eukaryotic model microorganisms. Their genome [33] and metabolism [34] are well characterized and therefore are an invaluable resource in biotechnology and industrial applications [35]. This microorganism, that have been used longest by humanity [36], were also successfully applied in MFC designs [37, 38]. Yeasts are non-pathogenic, grow rapidly, have a wide substrate spectrum, high catabolic activity [34], ability to switch metabolism between aerobic and anaerobic (alcoholic fermentation)[39] thus these traits make their application in MFC promising.

This thesis covers studies that lay groundwork of yeast *Saccharomyces cerevisiae* modification with conductive polymers for application in biofuel cells. The majority of the thesis covers the principles of polymer formation around microorganisms, the physical and the chemical nature, and application in biofuel cells and other fields.

This work describes a discovery about localized polymer synthesis on the surface of yeast cells. The main objective of the thesis is to evaluate yeast cells *Saccharomyces cerevisiae* and conductive polymer composites and apply them in microbial fuel cells. In order to reach the set goal major tasks were designed:

- i) Evaluate polypyrrole synthesis using $K_3[Fe(CN)_6]$ under various conditions varying oxygen accessibility and buffer pH values. Characterize the synthesized polymer with optical methods;
- ii) Evaluate polydopamine synthesis at various buffer pH values. Characterize the synthesized polymer with optical methods;
- iii) Design yeast cell *Saccharomyces cerevisiae* modification methodologies with polypyrrole and polydopamine individually;
- iv) Characterize yeast-polypyrrole composite structure, composition, chemical and physical properties;
- v) Apply polymer-modified yeast cells in microbial biofuel cell design and evaluate some electrochemical properties.

1. LITERATURE REVIEW

The whole literature review is divided into several sections: principles of biofuel cells, CT systems, and conductive polymer application in cell coating methodologies. This segmentation ensures a better understanding behind the motivations and novelty of this theses.

1.1. Enzymatic and Microbial biofuel cells

Biofuel cells (BCs) are electrochemical devices that consist of at least two electrodes (anode, cathode), a biological catalyst, which is usually an enzyme or microorganism, and a medium with the substrate [1]. During the operation, the catalyst catalyzes a chemical reaction, which is a redox-type reaction, during which electrons are extracted from the substrate and then transferred to the electrode. There are two main types of biofuel cell: enzymatic biofuel cells (EBFC) [4] and microorganism-based biofuel cells (MFC) [5]. Each type has its *pro et contra*. In principle, both work similarly. In the simplest BC design, there are two compartments separated with a semi-permeable membrane, while enzymes/microorganisms are enclosed in an anode-containing compartment. The semipermeable membrane ensures and enables the migration of ions between compartments [1, 4, 5]. The main difference is that EBFC requires purified enzymes, whereas MBC does not. If the conditions are met, microorganisms can multiply, thus replenishing BC, thus MFC is much more cost-effective [6]. EBFCs are designed for specific substrates, whereas MFCs exhibit the ability to perform catalysis on a wider range of substrates. Lastly, EBFCs tend to perform better than MFCs [40]. However, the general principle is that both types of BC perform poorly on their own in terms of energy production [21]. Thus, various methodologies are applied to improve CT. The main physical barrier is the distance between the redox-active centers and the electrodes that must be ‘reduced’, ‘bridged’, or ‘wired’. Redox-active centers refer to enzyme-active centers or sometimes membrane cytochromes where subsequential transducers receive their electrons. Mainly, two techniques are applied: physical attachment of the catalyst to the electrode or introduction of soluble CT capable materials. Often a combination of both is applied.

1.2. Microorganism adhesion on biofuel cell electrode

The adhesion of microorganisms to the electrode surface plays one of the key roles in the CT process and the generated power density [41]. For physical

attachment, various materials, including polymers, are used to modify the electrode surfaces. These materials have to be biocompatible, have a high surface to the area ratio for the biocatalyst to adhere to, and in the case of MFC, be susceptible to the robust microbial attachment. At the same time, the materials used for it should promote or at least do not interfere with charge transfer.

The most utilized anode base material in MFCs is carbon-based materials. They are highly conductive, chemically stable in most cases, and relatively inexpensive. On the other hand, they exhibit hydrophobic properties that interfere with the attachment of enzymes or microorganisms. To resolve this, various chemical or physical modifications are applied in order to enhance properties of interest [42]. In most cases modifications boil down to balancing between features like: price, manufacturing, conductivity, biocompatibility, ability to adhere/attach enzymes/microorganisms and mechanical strength. Thus, the most popular electrode modification/ functionalization materials are carbon nano structures, metal oxides, semiconductor nanoparticles/nanocomposites, conducting polymers, and/or co-structures of all listed here.

Carbon is an electrode building material that can be shaped into many functional structures. One of the more popular structures used in MFCs is carbon felt (CF). It is commonly used as a low-cost anode material as it has a large surface area and high porosity. As a carbon-based structure, it has good electrical conductivity [43, 44]. However, the less hydrophobic nature of the polymers does not work well with water-based electrolyte solutions, thus charge transfer is limited. Because of the felt structure, it is somewhat favorable for biofilms, but its hydrophobic nature slows down the initial biofilm formation. To address this, materials such as polyethylenimine are used. The abundance of amine groups, which pose a positive charge, allows the compounds to interact with the carbon anode material [26, 27]. Other adhesion-promoting materials are polyurethane (PU), polyaniline (PANI) [45-47]. For example, PU is biocompatible [48] with living cells and has a porous structure; thus, it is reliable for biofilm formation. Few studies have shown that PU can also adsorb carbon nanotubes (CNT). PU with adsorbed CNTs and with bacterial/yeast biofilm can act as MFC for prolonged time [45, 49].

Techniques other than adsorption are also used for electrode modification. One example is layer-by-layer deposition. In one study, PANI/CNTs were deposited in multiple bilayers on an indium tin oxide electrode [46]. Performed MFC experiments with *Shewanella loihica* showed that modification improves the maximum power density in comparison to that with

the non-modified indium tin oxide electrode. PANI in this configuration not only improved CT, but also reduced CNT toxicity towards bacteria [46].

Redox-active polymers are also being applied for enhanced CT. Somewhat popular options are osmium polymers [50]. These polymers are used to bind cells to electrode. Binding is usually achieved via *in situ* polymerization with living cells, and thus cells are entrapped into the polymer matrix. Namely, flexible osmium polymers (poly(1-vinylimidazole)₁₂-[Os-(4,4'-dimethyl-2,2'-bi-pyridyl)₂Cl₂]^(+/2+) and poly(vinylpyridine)-[Os-(N,N'-methylated-2,2'-imidazole)₃]^(2+/3+) are used [51]. Cells closely surrounded by polymers can release and/or transfer electricity to the polymer more easily. This type of entrapment also appears to have some biological compatibility, as stability tests showed that cells after 6 h retain 73% of the initial response.

Simple techniques like entrapping cells in gel-like materials also were applied and reported. Carbon felt dipping into yeast cell alginate suspension was applied to coat the electrode with yeast cells by entrapping them into the alginate film. This ensures close cell proximity to the electrode, though it hinders cell mobility or exchangeability. As alginate is biological origin material, MFC had 44 days of stable performance [28].

Another somewhat popular approach is to modify carbon-based electrodes with nanostructures. For example, noble-metal and metal-based nanoparticles are often applied, as they tend to improve carbon-based anode conductivity electrocatalytic activity. In this way, the particles act as surface area enlargers and 'bridges' for electron transfer from enzymes or microorganisms. Unlike carbon materials, metal nanoparticles tend to suffer from corrosion or might be cytotoxic to cells [52, 53]. Though noble metal particles like gold (AuNPs) are considered biocompatible and suitable for electrochemical devices as they have high area/volume ratio and pose good electrical conductivity [54]. It was reported that the advanced biogenic gold nanoparticle composites 'decorated' by multiwall CNTs were used as an enhancer for MFC construction [55]. AuNPs were synthesized by *Shewanella oneidensis* bacteria, and thus AuNPs were fully biocompatible.

In case of advanced nanotechnologies, researchers reported application of flower-shaped AuNP's [56]. From a technological stand point carbon felt, which was functionalized with polyethyleneimine, was 'decorated' with gold nano flowers. These irregularly shaped structures were grown using surface-bound seeds. The shape proved to be beneficial for adhesion and inhabitation. Flower-type AuNPs were able to bridge the external cellular wall of yeast cells and the surface of carbon fibers, leading to direct electron transfer by 'local harvest' of electrons and accumulation of charge on the CF electrode [27].

Analogous systems were developed using manganese oxide-decorated iron oxide nanoflowers on the same carbon felt anode functionalized with polyethyleneimine. Metallic nanoflowers allowed the formation of yeast biofilms on carbon fibers, and an electrically efficient interface between the electrode and the biofilm was constructed. Enhanced adhesion of the biofilm was achieved using an anionic surfactant mediator, sodium dodecylbenzenesulfonate (SDBS). SDBS allowed nanostructures to stay firmly attached to the carbon felt. It was noted that external yeast cell polysaccharides reached around the individual FeMnNps on the electrode surface, creating strong electrochemical bridging effect [26].

A very different approach was applied in the work of Christwardana et al. [57]. Researchers used quorum-sensing molecules for the functionalization of MFC anode electrodes to improve biofilm adhesion/formation [58]. Quorum-sensing molecules are signaling molecules responsible for extracellular communication between the same/similar-type microorganisms. Biofilm formation on the electrode ensures biological fit, close proximity to the electrode, and short travel path for electrons. In addition, this functionalization has been shown to promote faster biofilm formation and extracellular polysaccharide in the biofilm to enhance electrode transfer and thus increase the power density of MFC.

Other microorganisms such as *Scedosporium dehoogii*, which are capable of forming biofilms and also metabolizing aromatic hydrocarbons, were used in the development of MFC. Toxic pharmaceutical compounds such as para-aminophenol belong to the aromatic hydrocarbons class of compounds, and it is essential to treat them from wastewater. Therefore, using *S. dehoogii*, the researchers were able to form biofilms on CF electrodes electrodeposited with poly-Ni (II) tetrasulfonated phthalocyanine [59, 60]. The MFC showed the ability to produce energy through cleaning water from toxic compounds, though since wastewater contained only small amounts of aromatic compounds, an additional cellulose based carbon source was used to maintain the viability of the fungi biofilms, thus attaining high power density for a long period of time (200 h).

As already mentioned, there have been numerous attempts to use carbon-based nanoscaled allotropies. Carbon nanotubes are often used to modify the surface of the anode which acts as a direct electron transfer promoter [6]. The yeasts are somewhat tolerant to MWCNTs in low dosages (2 µg/mL). These small concentrations are enough to greatly enhance the generated power. The same article describes that power generation was increased 69 times over the control sample.

These are just a few examples of compounds or materials that are being used to modify electrodes in MFCs to promote charge transfer from microorganisms to electrodes. Other techniques will be described in the next section.

1.3. Common charge transfer materials

Redox-active microorganisms used in MFCs are particularly exploited as versatile 'biocatalysts' suitable for the generation of bioelectricity [7, 61]. Many different organisms have been experimented with in the design of MFCs and depending on the need for the presence or absence of mediators to complete the redox reaction, two main types of MFCs have been reported: fuel cells based on mediated electron transfer and fuel cells with direct electron transfer [15]. *Shewanella putrefaciens* [16], *Geobacter sulfurreducens*, *Geobacter metallicreducens* [17], *Aeromonas hydrophila* [18], and *Rhodospirillum rubrum* [19], are the most common bacteria used in direct electron transfer-based MFCs. They either pose special protein based molecules or can excrete natural mediator molecules. Some microorganisms like yeast cells have a physical barrier like a cell wall, which hinders charge transfer from the inner part of cell, to electrode. Classical method to improve MFC's performance is to establish charge transfer *via* cell wall and/or membrane of microorganism. The preferred way is to apply redox compounds, which are capable of assisting charge transfer. These molecules are commonly known as redox mediators and have been well investigated in numerous studies [6-10]. Redox mediators can be assigned into few groups: (i) hydrophilic and (ii) lipophilic mediators, (iii) nanoparticles of various origin [10, 11], and (iv) conducting and/or redox polymer-based matrices [12-14]. Mediators usually are either non organic or organic compounds that have multiple oxidative stages and transition between them can be easily achieved. From electrochemical stand point, transition usually can be achieved with low electrical potentials (lower than 0.6 V). Common hydrophilic redox mediators are: methylene blue, riboflavin, thionine, and $K_3[Fe(CN)_6]/K_4[Fe(CN)_6]$ [20-24]. These hydrophilic mediators usually enhance MFC performance by interacting with cell transplasma membrane redox system and with MFC electrode [25]. The most common examples are various membrane-bound cytochromes [62]. Cytochromes generally possess a redox active center, a functional group, a coenzyme, or a whole cascade of them [63]. Usually, it is thought that hydrophilic mediators cannot pass through the membrane. Hence, here lipophilic mediators play their role in the charge transfer through the cell

membrane to directly interact with inner redox active metabolites like NAD or FAD. Most common organic mediators usually are benzoquinone or naphthoquinone derivatives. In more advanced applications specific hydrophilic and hydrophobic mediators are used in tandem to achieve better charge transfer [7, 12, 25], though the system becomes much more complex or is not cost effective for the application of biofuel cells.

1.4. Cell modification for enhanced charge transfer

Different microorganisms and living cells can be used in the development of BFCs, but electron transfer from microorganisms or cells to the electrode is very rarely observed; therefore, there is a challenge when these bioelectronic devices are designed [64-67]. The involvement of microorganism metabolic processes in the polymerization processes of conducting polymers is a very attractive strategy, which is useful during the modification of microorganisms [29, 68-70], because conducting polymers can improve electron transfer efficiency of microorganisms, which were modified in such way. It has been shown that stem cells [71, 72] and some microorganisms [12, 29] after the modification by CPs, retained viability, performed metabolic processes, and were applied for the generation of electrical current in biofuel cells. The formation of CPs within microorganisms is innovative and the application of such modified microorganisms in biofuel cells and biosensors is more progressive, because living cells remain biocatalytically active for a longer time [73] compared with the activity of polymer modified enzymes [9, 74]. For this reason, several types of mammalian cells [75], bacteria [76] fungi [69] and yeast [68] were engaged in the formation of various polymers, including conducting polymers.

However, various types, shapes, or origin nanomaterials are often applied in MFCs. Most often, carbon-based nanomaterials or metallic nanoparticles are applied [6, 77, 78]. Modification involves preparation of suspension [79] or attachment of nanoparticles to the cell surface, thus the electrical pathway from cells to electrodes is achieved. In this way, cells are conjugated with nanoparticles rather than anchored to electrodes [30]. This type of cell modification methodologies can be considered as 'traditional'. Recently, self-encapsulation of cells with polymers has emerged. In contrast to other methods, polymer matrices can be prepared in situ with cell culture or sometimes even produced by metabolic/chemical processes that are running inside of cells. Currently, the application of Ppy rises in the field [70]. The first study, which reports the bioassisted synthesis of Ppy, to our knowledge was published by our research group in 2016 [76]. It was reported that bacteria *Streptomyces spp.* were able to catalyze the formation of spherical Ppy

particles without any additional chemicals. Bacteria are able to secrete redox-enzymes (e.g., phenol-oxidase) to extracellular media. These enzymes were able to initiate polymerization of different phenol-based monomers such as pyrrole. Thus, it was demonstrated that phenol-oxidases could be exploited for the synthesis of polypyrrole. After 6 days of growth of *Streptomyces spp.*, bacteria were able to create favorable conditions for the formation of hollow Ppy microspheres. Hollow microspheres were of 10-20 μm in size. The researchers discussed that the shape was influenced by organic compounds present in the growth medium. Later, it was reported that it is possible to coat yeast *S. cerevisiae* cells with Ppy [29, 30], and the techniques are described in these theses. In this case, yeast cells were used 'to cycle' the redox mediator $[\text{Fe}(\text{CN})_6]^{3-}/[\text{Fe}(\text{CN})_6]^{4-}$ and therefore perform Ppy synthesis in situ, in a controlled manner (Fig. 1).

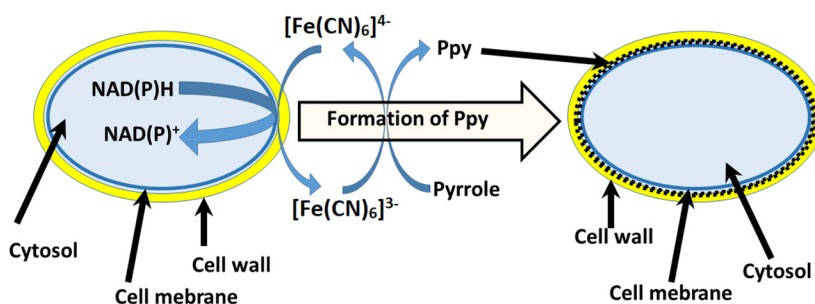


Fig. 1. Schematic representation of Ppy synthesis in cell wall of yeast [29]; Redox enzymes, located in plasma membrane, perform the oxidation of $[\text{Fe}(\text{CN})_6]^{4-}$ into $[\text{Fe}(\text{CN})_6]^{3-}$ that induces the polymerization reaction of pyrrole.

At a similar time, other researchers have shown that using iron nitride and iron (III) nitrate nonahydrate it was possible to form similar Ppy structures based on various bacteria: *Shewanella oneidensis* MR-1, *Escherichia coli*, *Ochrobacterium anthropic* or *Streptococcus thermophiles* [31]. During the preparation, bacterial cells were soaked with iron (III) nitrite nonahydrate, which was located in the outer layers and further initiated the polymerization of pyrrole. The bacterial cells remain viable and that the coating procedure did not affect proliferation. Taking into account the electrical properties, the modification with the conducting polymer-Ppy has improved the power density by 14.1 times compared to the unmodified *S. oneidensis* ($147.9 \mu\text{W}\cdot\text{cm}^{-2}$). A similar technique of self-encapsulation of microorganisms with Ppy also were performed and analyzed for MFC application using *Aspergillus niger* and *Rhizoctania sp.* [69, 70, 80]. For the evaluation of MFC, scanning electrochemical microscopy (SECM) was applied [12]. The study reported that during electrochemical probing on

immobilized modified cell culture the current output ($I_{\max} = 0.86$ nA) was three times higher compared to ($I_{\max} = 0.30$ nA) of the control group [12]. The results were determined by registering the surface approach curves. These experiments also showed how charge transfer efficiency, which is crucial for current generation in MFC, depends on several factors: (i) the distance between the SECM ultra-micro electrode and cells, and (ii) surface modification of the microorganism. The nominal current output when the ultra-micro electrode was 20 μm apart from the test sample was 0.47 nA, which was 1.5 times higher than that of the control sample.

White-rot fungal strains belonging to *Trametes spp.* were also modified with Ppy [70]. Researchers pointed out that Ppy formation in fungal hyphae was achieved using laccase enzyme, which is produced and secreted in growth medium by *Trametes spp.* fungi. The polymerization of pyrrole in crude enzyme extract and in cell culture growth medium was observed. Bioassisted polymer synthesis at that time was very innovative [81] and, to our knowledge, it was one of the first studies to facilitate the practical application of enzyme-assisted formation of conducting polymers [82-86], which later led to the formation of polymer-based coatings in cell culture [29, 68-70]. Therefore, it was shown that cells modified with conducting polymers have advanced electron transfer ability, which enables the use of these microorganisms in microbial biofuel cells (MFCs) [12] and biosensors [81, 86].

The most interesting application of living cell-induced Ppy formation was demonstrated by modification/coating of mammalian cells by Ppy [87]. Researchers have applied the synthesis method, which is described in this thesis [29] (Fig. 1), and were able to produce Ppy using suspension of the leukemia cell line, K562 cells. They determined that the previously suggested pyrrole polymerization mechanism could be driven by cell exudate molecules, not by plasma membrane oxidoreductase systems, different from the mechanism, which is presented in Fig. 1. During pyrrole polymerization, they observed cancer cell death, providing another application of this pyrrole polymerization mechanism as 'reverse pro drug' systems, meaning that cytotoxic pyrrole after cell death tends to polymerize, resulting in a biocompatible conducting polymer-polypyrrole [88] that is black and therefore can also be used as an optical indicator of dead cells. Subsequently, the implementation of the FeCl_3 compound with metal reduction-capable bacteria was reported: *Cupriavidus metallidurans*, *Escherichia coli* and *Clostridium sporogenes*, could initiate atom transfer radical polymerization (ATRP) of various monomers (poly (ethylene glycol methyl ether methacrylate); hydroxyethyl methacrylate; N-hydroxyethyl acrylamide; 2-acrylamido-2-methyl-1-propanesulfonic sodium; 2-(methacryloyloxy) ethyl dimethyl-(3- sulfopropyl) ammonium hydroxide [89]. The researchers suggested an interesting approach to designing cell-assisted polymerization.

The not-capable Fe (III) compound is reduced into Fe (II) in a controlled way, thus initiating the polymerization of monomers that are not toxic to cells, which are engaged in redox processes of Fe (II)/Fe (III). After ATRP polymerization, cells still maintain high viability.

In addition to Ppy, some other polymers are also used for cell modification to increase their performance in designed MFC. In a similar fashion, *S. xiamenensis* was coated with polydopamine (PDA) [90]. Selected bacteria can adhere to PDA during their formation *via* oxidative polymerization under aerobic, slightly alkali (pH 8) conditions. Researchers reported that PDA-modified bacteria *S. xiamenensis* cells were able to generate a power density, which was 6.1 times greater than that of electrodes based on nonmodified cells ($74.7 \text{ mW}\cdot\text{m}^{-2}$). The PDA additives were formed in 3 h, which is rather fast, and it also appears that bacteria modification just barely influences cell viability, which was reduced only reduced by 2–3%. Rather, popular bacteria for MFC design is *Shewanella oneidensis* MR-1, which was also coated with PDA. In the study [91], Yu *et al.* report that it is possible to use cell-assisted synthesis for the formation of conducting PDA or, using the same bacteria, to exploit biomineralization of FeS nanoparticles. The results show that different interfaces wire up cells at different levels, and thus their electrical/electrochemical properties are different. They also showed that by polysulfide reductase mineralized FeS nanoparticles interface the efficiency of MFC anodes increased to $3.2 \text{ W}\cdot\text{m}^{-2}$, which was 14.5 times higher than that of anodes modified by native *Shewanella oneidensis* cells ($0.2 \text{ W}\cdot\text{m}^{-2}$), while for PDA-coated anodes current density was of $\sim 0.6 \text{ W}\cdot\text{m}^{-2}$.

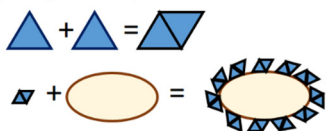
An alternative method was demonstrated in some other research [92, 93]. Researchers were able to feed or internalize pre-synthesized carbon dots (CD, carbon nanoparticles) into *Shewanella oneidensis* and *Shewanella xiamenensis*, accordingly [92, 93]. Both studies showed remarkable effects of carbon dots, because they are highly biocompatible. Furthermore, carbon dots can enhance metabolic activity, because levels of internal adenosine triphosphate (ATP) were significantly elevated. It was hypothesized that facilitated metabolism could also produce unwanted reactive oxygen species, but this was not the case. In addition, carbon dots form photoactive particles that promote the consumption of lactate together with current generation upon illumination. With *Shewanella oneidensis* MR-1 maximum current density achieved was $1.23 \text{ A}\cdot\text{m}^{-2}$ while the control was $0.19 \text{ A}\cdot\text{m}^{-2}$. Meanwhile, the maximum power density of the MFC with carbon dots was $0.491 \text{ W}\cdot\text{m}^{-2}$, which was by 6.46 times higher compared to that of the control based with the same not modified microorganisms ($0.076 \text{ W}\cdot\text{m}^{-2}$). *Shewanella xiamenensis* under illumination conditions and the sole lactate carbon source were able to reach a density of $329.4 \mu\text{A}\cdot\text{cm}^{-2}$, which was 4.8 times higher than that of the control electrode ($68.1 \mu\text{A}\cdot\text{cm}^{-2}$). Osmium redox polymers are also applied in

the development of MFC [51, 94-97]. In the study [94], cells were trapped and connected to the electrode surface *through* [Osmium (2,2 ' bipyridine) (polyvinylimidazole) 10Cl] Cl. The pre-synthesized polymer was used as a comediator and as a conductive binding matrix for bacterial cells of *Gluconobacter oxydans*. Electrodes were designed *via* drop-coating methodology onto a glassy carbon paste electrode. Researchers achieved a maximum charge density of 15.079 mA·cm⁻² and an open circuit potential value of 176 mV.

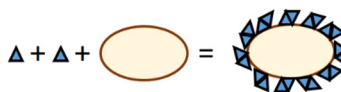
These are just a few examples of emerging technologies and methodologies to improve the performance of MFCs by introducing a modification agent into the cells themselves or by covering them. Summarizing these technologies, they can be classified as cell surface engineering, internalization, or artificial biofilm film formation (Fig. 2). The most promising cell modification technologies involve the formation of polymeric coatings and the internalization by living cells. Although there is clear evidence for this modification-based impact on charge transfer [12], there are still some drawbacks. As some modifications are quite complex, their application in 'real-life' MFCs could be troublesome. The main drawbacks revolve around the viability and proliferation, as newly formed cells in MFC should inherit or undergo the modification. Overall, modifications of the cell surface in conjunction with other methodologies listed in this thesis should yield synergetic effects on the output of electricity from MFCs.

a) Cell modification types based on formation:

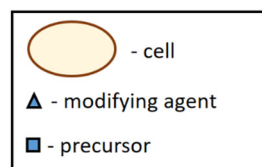
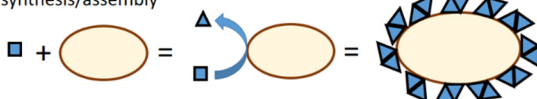
I) Pre synthesized/assembled modification agent



II) In situ synthesized/assembled modification agent



III) In situ microorganism assisted synthesis/assembly

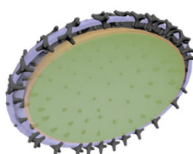


b) Cell modification depth/localization:

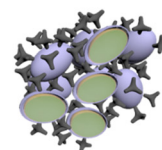
I) Surface interactions



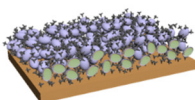
II) Surface bound/entrapped



III) Agglomerate formation/matrix bound



IV) Film formation



V) Internalization

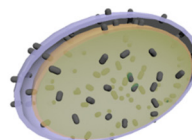


Fig. 2. Schematic representation of cell modification principles. Cells can be modified using pre-synthesized compounds (I), assembled/ synthesized in situ with living cells are present (II), and in situ when cell assists/catalyzes the assembly of modification agent; (B) Schematic representation of modifying agent localization in MFC applications: (I) surface interactions such as adsorption, electrostatic interactions etc.; (II) modifying agent is either covalently bonded or forms interlacing and inseparable structures with cell walls or other similar structures; (III) when modifying agent forms aggregates from its matrix and cells; (IV) higher agglomerate organization onto surfaces; (V) internalization of the modification agent [98].

2. METHODOLOGY

2.1.1. Polypyrrole synthesis and kinetic studies

The standard solutions used in this research consisted of 0.1 M phosphate buffered saline (PBS) of different pHs with 0.04 – 0.1 M $[\text{Fe}(\text{CN})_6]^{3-}$ and/or $[\text{Fe}(\text{CN})_6]^{4-}$. The visual test of Ppy formation was performed at 0.04 M concentration of $[\text{Fe}(\text{CN})_6]^{3-}$ or $[\text{Fe}(\text{CN})_6]^{4-}$ with 0.5 M Py. The exact compositions of the solutions and the visual evaluation of polymerization are indicated in Table 1. The same conditions were used to prepare Ppy for experiments with FTIR and focused ion beam scanning electron microscope (FIB SEM). The reaction was carried out for 24 h with the reaction mixture mixed by an orbital shaker at 200 revolutions per minute at 30°C. The synthesized polymer was centrifuged and the supernatant (reaction mixture) was decanted. The sediments were washed multiple times using 1 ml of distilled water. Subsequently, the polymer was dried by heating it to 90 °C under a gentle stream of nitrogen gas. The dried samples were then analyzed with an infrared spectrometer.

Table 1. Visual evaluation of Ppy formation (dark precipitant) in solutions with different compositions, performed at 0.04 M concentration of $[\text{Fe}(\text{CN})_6]^{3-}$ or $[\text{Fe}(\text{CN})_6]^{4-}$ with 0.5 M of pyrrole [30].

Sample Nr.	Composition of samples			Description of Result
	$[\text{Fe}(\text{CN})_6]^{3-}$	$[\text{Fe}(\text{CN})_6]^{4-}$	Pyrrole	
1	0.04 M	-	0.5 M	Ppy was formed instantly
2	-	0.04 M	0.5 M	Ppy distinctly appeared only after 1-2 days

The samples were prepared by mixing precalculated amounts of initial standard solutions directly prior to experiments. Reactions were performed in PBS solutions usually containing 0.5 mM $[\text{Fe}(\text{CN})_6]^{3-}$ or $[\text{Fe}(\text{CN})_6]^{4-}$ and a concentration of Py. Polymerization was studied at three different $[\text{Fe}(\text{CN})_6]^{4-}$ concentrations of 0.1, 0.5 and 1 mM and at two $[\text{Fe}(\text{CN})_6]^{3-}$ concentrations of 0.1 and 0.5 mM, at pH 3.0, 5.0, 7.0 and 9.0. The kinetics of the reactions were evaluated by measuring the absorption at wavelengths of 420 nm and 460 nm, which are related to optical absorption of $[\text{Fe}(\text{CN})_6]^{3-}$ [99] (Fig. 4a) and Ppy [85] (Fig. 4b). The optical extinction molar coefficient for $[\text{Fe}(\text{CN})_6]^{3-}$ is 1179 L/mol·cm, determined experimentally, while other authors describe a slightly lower value of 1040 L/mol·cm [100]. $[\text{Fe}(\text{CN})_6]^{4-}$ did not show any

significant absorption maximum in the visible light region (Fig. 4a). These measurements were performed under aerobic conditions with oxygen from the ambient atmosphere dissolved in the reaction mixture and under anaerobic conditions, when oxygen was removed by argon gas. For later experiments, oxygen was removed from the standard solutions by purging with argon gas for 20 min, after which the solutions were tightly sealed for later use. The cuvettes were also filled with argon and then sealed. To ensure oxygen-free reactions, cuvette filling was performed under a gentle argon gas stream and sealed with a cuvette cap. All measurements were made at least 3 times. The curves represented in the graphs are the average values of repeated measurements.

Samples for FIB SEM analysis after synthesis were collected by filtering through Milipore polycarbonate filters (pore size 0.22 μm) and lyophilized prior to analysis. For FIB SEM images, Ppy samples were suspended in methanol and suspension was transferred to microscopic glass. Samples were coated with a thin chrome layer prior to visualization.

2.1.2. Synthesis and characterization of polydopamine

The synthesis of an electrically conducting polymer, polydopamine (PDA), was conducted at varying buffer pH. Small PDA particles were synthesized by dissolving different concentrations of dopamine hydrochloride (13 mM and 26 mM) in a 50 mM TRIS buffer solution [101]. Buffer solutions with different pH ranged from 5.0 to 8.5, were used. Test tubes with 1.5 ml of reaction mixture were kept at 30 $^{\circ}\text{C}$ for 16 h. After this, the samples were centrifuged and only the supernatant was taken from each of the samples. The absorption of the supernatant was measured on a spectrophotometer at wavelengths ranging from 350 to 700 nm.

2.2.1. Cell preparation and modification with polypyrrole

The modification procedure has previously been described in detail [29]. In summary, yeast cells *Saccharomyces cerevisiae* (Y00000; *BY4741 Mata his3 Δ 1 leu2 Δ 0 met15 Δ 0 ura3 Δ 0*) (Euroscarf, Germany) were aerobically overnight (for 20-24 h, 30 $^{\circ}\text{C}$, YPD media: 1 % yeast extract, 2 % peptone and 2 % glucose), harvested then washed with neutral (pH 7.0) 0.1 M phosphate buffer saline (PBS). Cells were then incubated with shaking for 22 - 24 h in the same PBS buffer containing 0.2 M of glucose and different concentrations of $\text{K}_4[\text{Fe}(\text{CN})_6]$ (0.02 - 0.08 M) plus different concentrations of the pyrrole monomer (0.01 - 0.5 M). The harvested yeast cells and Ppy were washed from

the reaction mixture, and the resultant biocomposites were used in further experiments. Furthermore, in the isotope labeling mixtures both non-labeled pyrrole and pyrrole labeled with ^{15}N (400 - 4000 ‰) were used for polymerization. For the pyrrole adhesion experiment, cells were incubated as previously described, with the exception that the $\text{K}_4[\text{Fe}(\text{CN})_6]$ was not included. It is referred to as ‘not modified’, ‘intact’, or “control yeast cells” to indicate cells, which were incubated under the same conditions except that the pyrrole monomer was absent. For ease of navigation, abbreviations for cell modification will be used. A detailed description of the abbreviations is given in Table 2.

2.2.2. Cell modification with polydopamine

Three different 10 mL samples containing 100 mg of yeast cells were prepared in 0.05 M TRIS, pH 5.0 buffer. Subsequently, dopamine chloride salt was added to each sample to reach a final concentration of 0.013 M and 0.025 M. The samples were incubated for 1 h at 30 °C with a constant shaking at 250 rpm. Then 6.5 mL of 0.05 M TRIS, pH 8.5, buffer was added to change the pH of the sample to weak alkaline, pH 7.5, and incubated for another hour. Subsequently, the three samples were centrifuged and washed with 0.1 M PBS, pH 7.0 two times. All samples were suspended in 25 mL of 0.1 M PBS, pH 7.0, containing 0.005 M $\text{K}_4[\text{Fe}(\text{CN})_6]$.

Table 2. Yeast modification with polypyrrole abbreviations. Adapted from [102].

Abbreviation	Explanation
Y@Ppy-ctr	Yeast cell control sample. It was prepared by incubating 22-24 h in 0.1 M PBS, pH 7.0, containing 5 mM $K_4[Fe(CN)_6]$, and 0.2 M glucose.
Y@Ppy-X	Ppy modified yeast cells. Sample prepared by incubating 22-24 h in 0.1 M PBS, pH 7.0, containing 5 mM $K_4[Fe(CN)_6]$, 0.2 mM glucose and Py. Subsequently, cells were washed from reaction buffer. X stands for used pyrrole monomer concentration, typically 0.1, 0.3 or 0.5 M.
Y@ ¹⁵ N-Ppy-X	Ppy-modified yeast cell. Sample prepared by incubation 22-24 h in 0.1 M PBS, pH 7.0, containing 5 mM $K_4[Fe(CN)_6]$, 0.2 mM glucose and ¹⁵ N labeled Py. Subsequently, cells were washed from reaction buffer. X stands for used pyrrole monomer concentration, typically 0.1, 0.3 or 0.5 M.
Y@PDA-ctr	Yeast cell control sample. It was prepared by incubating 1 h in 0.05 M TRIS pH 5.0, containing 200 mM glucose and 13 mM, then the pH changed to pH 7.5 and incubated 1 h more. Subsequently, cells were washed from reaction buffer.
Y@PDA-X	PDA-modified yeast cells. The sample prepared by incubating them for 1 h in 0.05 M TRIS pH 5.0, containing 200 mM glucose and dopamine, then the pH changed to pH 7.5 and incubated for 1 h more. Subsequently, cells were washed from reaction buffer. X – stands for the concentration of the dopamine monomer used, typically 13 or 26 mM.

*Unless noted otherwise

2.2.3. Atomic force microscope imaging and force measurements

Custom-made silicon wafers of various size (4 – 12 μ m), etched with square pyramid-shaped holes, were used for the immobilization of yeast cells. Silicon wafers were manufactured using photoelectrochemical etching principles (Kaunas Technology University, Mechatronics Center, Panevezys, Lithuania). Before immobilization, silicon plates were sequentially cleaned by treating them with a ‘piranha’ solution ($H_2SO_4:H_2O_2$, ratio 3:1, for 15 min), then rinsed with deionized water (DI) and stored in 96 % ethanol. The plates were dried at room temperature and then covered with a layer of poly-l-lysine by spreading a solution of polylysine (0.01 % w/v) over them and leaving it to polymerize for 10 - 15 min. Excess unpolymerized poly-l-lysine was

removed with a copious amount of DI water. Before immobilization, washed cells were collected from the suspension of PBS and resuspended in DI water. A small volume of cell suspension was spread on silicon plates and allowed to dry for 15 min. The plates were then washed with DI water to remove excess cells. The atomic force microscope BioScope Catalyst II (Bruker, USA) was applied for the imaging and elasticity measurements of the yeast cell wall. In fluid, contact mode with a conventional silicon nitride tip (resonant frequency – 18 kHz, spring constant ~ 0.07 N/m, Bruker, Germany) was applied for surface visualization of Ppy-modified and unmodified yeast cells. The accurate spring constant of the cantilever was determined by the thermal fluctuation method, using the thermal tuning mode, which allowed analysis of thermal noise. Visualization and force curve measurements were performed in phosphate buffer, pH 7.0. Before and after the stiffness measurement, the topographical map of immobilized cells was produced in order to validate that cells were located in the silicon holes. Cell stiffness evaluation force (F) measurements were made using AFM. Four different types of Y@Ppy samples were analyzed: Y@Ppy-ctr, Y@Ppy-0.1, Y@Ppy-0.3, Y@Ppy-0.5. For each type of sample, between 8 and 10 cells were evaluated. Prior to cell analysis, normalization was achieved by measuring F by AFM on the solid surface of the same silica wafer but next to the immobilized yeast cell. During the analysis of a single yeast cell at least 5 indentation measurements were performed in the middle of the cell by the production of AFM based deflection-distance curves. Only cells inserted within holes of $6 \times 6 \mu\text{m}$ in size were evaluated. For data processing and calculation of Young's modulus, the Hertz-Sneddon model (Equation (1)) was applied [21]. Raw data were recalculated to force indentation curves and linearized by applying a root function, which allowed for the discrimination of small from deep indentation. Then it was fitted twice to the rooted Hertz-Sneddon stiffness modulus (Equation (2)). The fitting was performed on individual curves in two separate regions and Young's modulus (E) was calculated for small and deep indentations (δ). The Young modulus values were then used to describe different treatments.

$$F = \frac{2 \tan(\alpha) E}{\pi(1-\nu)} \cdot \delta^2 \quad (1)$$

Young's modulus E was evaluated after transformation of Eqs. (1) into (2):

$$\sqrt{F} = \sqrt{\frac{2 \tan(\alpha) E}{\pi(1-\nu)}} \cdot \delta \quad (2)$$

where Poisson ratio $\nu = 0.5$; α stands for the tip corner angle of the AFM probes, in our example $\alpha = 45^\circ$.

2.2.4. Isotope ratio mass spectrometry and isotope mixing model

Detailed methods of isotope ratio mass spectrometry have been previously described [103]. In summary, nitrogen isotope ratios in biocomposites were measured using a Flash EA1112 elemental analyzer (EA) coupled to an isotope ratio mass spectrometer (IRMS, Thermo delta plus advantage) *via* a ConFlo III interface (Thermo Electron GmbH, Germany). Yeast cells were freeze dried, before being weighed into tin-based capsules and combusted in the elemental analyzer in the presence of excess oxygen; Helium (grade 5.0) was used as the carrier gas. The gases, produced by combustion, passed sequentially through an oxidation column comprising CrO₃ granules at 1020°C, a copper wire reduction column at 650°C, then a magnesium perchlorate water trap. The resulting N₂ and CO₂ were separated by the chromatography column in the EA and transferred to the ConFlo III interface. This interface allowed the introduction of CO₂ and N₂ calibration gases from laboratory cylinders into the IRMS. The measured stable carbon and nitrogen isotope ratios are reported in the VPDB scale and in the air-N₂ scale, respectively. The reference material caffeine IAEA 600, $\delta^{13}\text{C} = -27.771\text{‰}_{\text{VPDB}}$, $\delta^{15}\text{N} = 1\text{‰}_{\text{air N}_2}$ [104] was used for the calibration of the laboratory N₂ and CO₂ cylinder.

If the isotope ratios of the starting substrates are known, isotope ratio mass spectrometry allows determination of the amount of ‘substrate’ material in the reaction product [105]. In order to determine the amounts of polymer mass and biomass, an isotope mixing model was applied. When the isotopic composition of the initial substrates polypyrrole and yeast cells (respectively: δ_{PPy} and the δ_{Y}) and isotopic composition of the composite material (δ_{SAMPLE}) are known, it can be expressed as follows:

$$\delta_{\text{SAMPLE}} = (\delta_{\text{PPy}}) * f_1 + (\delta_{\text{Y}}) * f_2 \quad (3)$$

Also,

$$f_1 + f_2 = 1 \quad (4)$$

where f_1 and f_2 are the fractions of polypyrrole and yeast cells in the sample, respectively. Combining Equations 3 and 4 gives:

$$f_1 = (\delta_{\text{SAMPLE}} - \delta_{\text{Y}}) / (\delta_{\text{PPy}} - \delta_{\text{Y}}) \quad (5)$$

$$f_2 = 1 - f_1 \quad (6)$$

The δ notation is used in isotope ratio mass spectrometry to describe the sample isotope ratio compared to an internationally accepted isotope standard and is expressed in parts per million. In the case of nitrogen isotopes, it would be:

$$\delta^{15}N = \left(\frac{R_{sample}}{R_{standard}} - 1 \right) * 1000 \quad (7)$$

where R_{sample} is the isotope ratio in the sample and $R_{standard}$ is the isotope ratio according to the international standard (defined by the IEAE).

2.2.5. Determination of polypyrrole localization in the cell wall

To determine the location of the Ppy location in yeast cells, two approaches were used, followed by bright-field and fluorescence light microscopy. First, Ppy-modified and unmodified cells were stained with fluorescently labeled concanavalin A, a cell wall-specific protein. To stain cells with fluorescent label, yeast, after the modification procedure described above, were washed twice with TRIS buffer (0.05 M TRIS; 0.15 M NaCl; 0.004 M CaCl₂; pH 7.2) and collected by centrifugation. Staining was performed using the simplified methodology described in the *Saccharomyces cerevisiae* Morphological Database (<http://scmd.gi.k.u-tokyo.ac.jp>). Labeled concanavalin A was diluted with TRIS buffer prior to use to a final concentration of 100 mg/ml. Approximately 10⁶ yeast cells were then incubated in 1 ml of diluted stain for 15 min at room temperature. The stained cells were washed with the same buffer three times and collected by centrifugation. Cells were then fixed to microscope slides by drying and inspected with a fluorescence microscope. Digestion experiments were performed with the lyticase enzyme using isotopically labeled pyrrole. Samples Y@¹⁵Ppy-ctr and Y@¹⁵Ppy-0.5 were prepared. After modification, cells were pelleted, twice washed, and suspended in lyticase-specific buffer. The lyticase buffer contained 1.2 M sorbitol, 0.5 mM MgCl₂ and 35 mM K₂HPO₄, adjusted to pH 6.0 [106]. The suspension volume was adjusted according to the initial cell optical density, set to approximately 1.5 arbitrary units. A further, 25 μ g /ml of lyticase was added to each cell sample, which was then incubated at 30 °C for 2 hours. To prove that the lyticase enzyme was active, the optical density of the control sample suspension was also measured. The optical density was measured at 600 nm before and after the incubation cycle. After digestion, the samples were inspected with a bright-field optical microscope and analyzed by IRMS. Before IRMS measurement, Ppy-modified cells were centrifuged to separate cells from digested cell wall debris, which could contain isotopically labeled

Ppy*. Centrifugation was initially performed using a small relative centrifugal force (RCF), and then after a pellet from the supernatant was separated, the supernatant was centrifuged at a higher RCF. Thus, performing short centrifugations (2 min) at 400, 800, 2000, 6000 and 12000 RCF allowed to separate fractions of cells, which were relatively large and sedimented faster than smaller debris particles. The cell and debris particle fractions were analyzed by IRMS.

2.3.1. Chronoamperometric evaluation of modified yeast cells in a flow-through system

After modification, Y@PDA or Y@Ppy were subjected to a flow-through system. Each sample was passed through an electrochemical cell where a 0.4 V potential was applied for the working electrode and the correspondingly generated electric current was measured with a sampling rate of 300 ms. To register the current value at steady state, first, the current was recorded for 5 min without solution flow to reach steady state of background current. Then the solution flow was turned on at a flow rate of 35 mL/min. After 5 min glucose solution was added to the samples to achieve a final concentration of 200 mM (in 0.1 M PBS, pH 7.0, supplemented with 5 mM $K_4[Fe(CN)_6]$) and measurements were continued for another 10 min. The samples were subjected to a three-electrode cell: platinum wire was used as the working electrode, stainless steel tube was used as the auxiliary electrode, and Ag/AgCl reference electrode filled with 3 M KCl was used as the reference electrode.

2.3.2. Evaluation of power generation by yeast cells modified with PDA and Ppy

A two-electrode-based electrochemical cell with two separate containers and a bridge was used to evaluate Y@PDA and Y@Ppy performance. A graphite electrode was used as a working electrode and was immersed in a container with 25 mL of Y@PDA or Y@Ppy samples that were constantly stirred (at 100 rpm) to prevent cell sedimentation. A copper electrode was used as an auxiliary electrode and it was immersed in a 1 M $CuSO_4$ solution. The two reservoirs were connected with a salt bridge filled with a 1 M KCl solution and covered by semipermeable membranes (200 μ L 40 % acrylamide, 2 μ L ammonia persulfate, 0.5 μ L, and TEMED). During potential measurements, external resistors (of 10 Ω , 100 Ω , 220 Ω , 330 Ω , 1 k Ω , 2 k Ω , 5.1 k Ω , 10 k Ω ,

100 k Ω , 1 M Ω) were connected in parallel to the electrical circuit to mimic the load and to assess the power density of the Y@PDA and Y@Ppy samples.

The electric power formula was obtained from Ohm's law (8). Where P is power in watts (W), V is voltage in volts (V), and R is the resistance in ohms (Ω). The power density was calculated by dividing electric power per exposed working electrode surface, measured in square meters (m^2).

$$P = \frac{E^2}{R} \quad (8)$$

3. RESULTS

3.1. Initial discovery. Principle of $[\text{Fe}(\text{CN})_6]^{4-}/[\text{Fe}(\text{CN})_6]^{3-}$ initiated formation of polypyrrole

Upon witnessing the polymerization of the pyrrole phenomenon in the presence of a yeast cell in an electrochemical cell that had $[\text{Fe}(\text{CN})_6]^{4-}/[\text{Fe}(\text{CN})_6]^{3-}$ mediator system, investigation began to rout out its cause. In the first part of this investigation, the formation of Ppy was evaluated under different combinations of initial compounds (Table 3)(Fig. 3).

Table 3. Evaluation of Ppy formation in solutions of different compositions. Each added substance is indicated in grey, while absent substances are indicated by dashes (-) in white cells. The concentrations of added substances are listed in the table [29].

Nr.	Composition of samples					Indication of Ppy formation
	$[\text{Fe}(\text{CN})_6]^{3-}$	$[\text{Fe}(\text{CN})_6]^{4-}$	Pyrrole	Yeast cells	Glucose	
1	0.04 M	-	0.5 M	-	-	+ (Instant)
2	-	0.04 M	0.5 M	-	-	- (very slow)
3	-	-	0.5 M	+	-	- (after 24 h)
4	-	-	0.5 M	-	0.04 M	- (after 24 h)
5	-	-	0.5 M	+	0.04 M	- (after 24 h)
6	0.04 M	-	0.5 M	+	0.04 M	+ (Instant, Fig. 3d)
7	-	0.04 M	0.5 M	+	0.04 M	+ (Fig. 3e)
8	0.04 M	-	0.5 M	+	-	+ (Instant)
9	-	0.04 M	0.5 M	+	-	- (very slow)

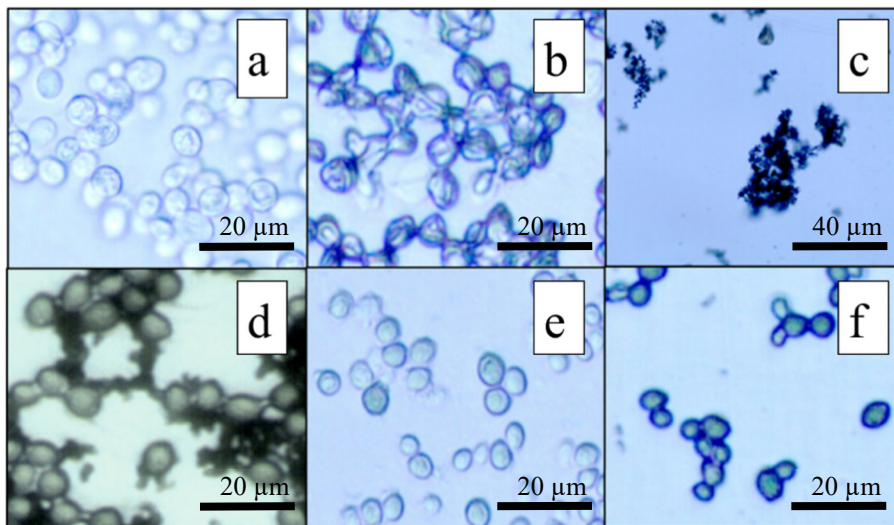


Fig. 3. Evaluation based on optical microscopy of Ppy formation. (a) Control sample based on yeast cells, which was incubated in PBS buffer with 0.2 M glucose but without $[\text{Fe}(\text{CN})_6]^{3-}$ or $[\text{Fe}(\text{CN})_6]^{4-}$ and Py. (b) not modified yeast cells, which were consequently immobilized, incubated in PBS, and dried. (c) Ppy particle agglomerates, which were formed from 0.5 M Py and 0.04 M of $[\text{Fe}(\text{CN})_6]^{3-}$ in the absence of yeast cells; (d) Immobilized yeast cells, which were incubated in cell growth media with 0.5 M of Py, 0.2 M glucose and 0.04 M of $[\text{Fe}(\text{CN})_6]^{3-}$; (e) immobilized yeast cells, which were incubated in the cell growth media with 0.5 M of Py, 0.2 M of glucose and 0.04 M of $[\text{Fe}(\text{CN})_6]^{4-}$; (f) immobilized yeast cells, which were incubated in the cell growth media with 0.5 M of Py, 0.2 M of glucose and 0.04 M of $[\text{Fe}(\text{CN})_6]^{4-}$ and then dried [29].

In several reaction mixtures, various results were inspected. In images (Fig. 3a–c) represent control/reference samples: native yeast cells (Fig. 3a); the same cells immobilized using poly-L-lysine and glutaraldehyde on glass microscope slides, then dried (Fig. 3b). As is seen from Fig. 2b, after drying, the cells became wrinkled as they lose water. In Fig. 3c and polypyrrole particle agglomerates are shown. They were synthesized from 0.5 M Py and 0.04 M $[\text{Fe}(\text{CN})_6]^{3-}$ (Fig. 3c). From Fig. 3d it can be observed that the yeast cells, which were incubated in the reaction mixture containing $[\text{Fe}(\text{CN})_6]^{3-}$, glucose, and Py, were surrounded by dark Ppy particles, which are distributed mainly in the space between the cells. The Ppy-based structures had the same pattern as that observed in the control measurement, which is represented in Fig. 3c. These structures were formed because $[\text{Fe}(\text{CN})_6]^{3-}$ acted as an oxidator and induced fast Py polymerization, which was followed by the formation of Ppy-based particles of different sizes and shapes and thus entrapping/incorporating cells during polymerization. In contrast, if yeast cells were incubated in the solution containing $[\text{Fe}(\text{CN})_6]^{4-}$, Py and glucose,

then a dark ‘envelope’ is formed from Ppy within the cell wall or periplasm (Fig. 3e and f). But in this case no other Ppy structures were formed, neither within nor outside the cells, and no separated particles or structures were observed within the yeast cell wall (Figs. 3e and f). In other words, the sample took dark Ppy color, though no visible Ppy micro particles are present only darkened cell wall. In such a case, the Ppy-based ‘envelope’ became even more distinctly visible when yeast cells were immobilized on substrates and dried (Fig. 3f). During the drying process, the cells with the Ppy ‘envelope’ did not shrink or wrinkle like the control sample (Fig. 3b). This leads to an early belief that Ppy reinforces the cell wall, as cells can retain shape after drying. For this reason, it was assumed that Ppy synthesis of Ppy was the most intensive within the periplasm and/or the cell wall. Early experiments also raised the hypothesis that in the reaction mixture there are two oxygen users: yeast and $[\text{Fe}(\text{CN})_6]^{4-}$ and that yeast are the dominant one. Thus, this leads to the second hypothesis that $[\text{Fe}(\text{CN})_6]^{4-}$ oxidation occurs in close proximity to yeast cells.

Further, experimental data is presented. Data are divided into a few main sections describing “evolution of scientific thought” on the yeast-polymer compound based on experiments performed. These major sections can be divided into: Ppy and PDA particle formation and its particle characterization; yeast-Ppy composite characterization; yeast composite application.

3.2. Spectrophotometric evaluation of Ppy formation initiated by $[\text{Fe}(\text{CN})_6]^{3-}$ and formed particle characterization

3.2.1. Basis for an optical Ppy evaluation

The formation of Ppy initiated by $[\text{Fe}(\text{CN})_6]^{3-}$ was evaluated by UV-Vis spectrophotometry. Polymerization experiments were started by adding Py to a reaction buffer containing $[\text{Fe}(\text{CN})_6]^{3-}$ or $[\text{Fe}(\text{CN})_6]^{4-}$. Measurements were made at wavelength ranges where selected compounds showed almost independent optical absorption. The spectra of $[\text{Fe}(\text{CN})_6]^{3-}$, $[\text{Fe}(\text{CN})_6]^{4-}$, and Ppy, which was formed using $[\text{Fe}(\text{CN})_6]^{3-}$, were measured in the range between 300 and 900 nm (Fig. 4). $[\text{Fe}(\text{CN})_6]^{3-}$ has an absorption maximum at 420 nm (Fig. 4a). $[\text{Fe}(\text{CN})_6]^{4-}$ does not show any distinct absorption maximum in the visible light region (Fig. 4a). A poorly expressed optical absorption maximum of Ppy was recorded at 460 nm (Fig. 4b), which is consistent with data reported in other investigations [85, 107]. As described in the literature this is a typical double bond absorption, which is measurable when delocalized electrons are transferred from bonding orbitals to non-bonding orbitals (π - π^*),

though this type of absorption is only characteristic of relatively short chains or small particles of Ppy [107]. Ppy spectra were recorded in different samples with varying concentrations of initial materials to evaluate whether the absorption maximum of Ppy remained at a constant wavelength. The results show that the absorption maximum is constant and does not shift sideways. In all of these reactions, no additional chemicals were used, which can affect the size of Ppy particles.

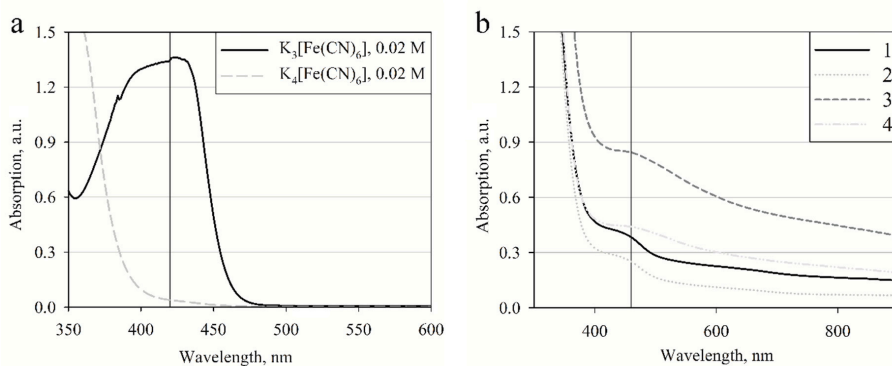


Fig. 4. (a) Optical absorbance spectra of 0.02 M of $[\text{Fe}(\text{CN})_6]^{3-}$ and 0.02 M of $[\text{Fe}(\text{CN})_6]^{4-}$. The vertical line indicates the absorption maximum at 420 nm; (b) Optical absorbance spectra of Ppy synthesized under different conditions: (1) polymerization solution containing 0.5 M of Py and 0.04 M of $[\text{Fe}(\text{CN})_6]^{3-}$, spectrum was registered after 24 h from the initialization of the polymerization reaction, (2) supernatant collected after 24 h of polymerization followed by centrifugation at 12,000 g for 10 min, (3) 0.375 M of Py and 0.1 M of the $[\text{Fe}(\text{CN})_6]^{3-}$ spectrum registered after 24 h of polymerization, (4) 1.5 M of Py and 0.25 M of the $[\text{Fe}(\text{CN})_6]^{3-}$ spectrum registered after 24 h of polymerization. All spectra were recorded in a 0.1 M PBS, pH 7.0. The vertical line indicates a poorly expressed absorption maximum at 460 nm [30].

Further changes of spectra during the course of polymerization initiated by $[\text{Fe}(\text{CN})_6]^{3-}$ were inspected. Polymerization was carried out in 0.1 M PBS, pH 7.0, with 0.5 mM $[\text{Fe}(\text{CN})_6]^{3-}$ and 0.5 M Py. Absorption spectra were registered at chosen time intervals (Fig. 5a). In this experiment, the optical absorption at $\lambda = 420$ nm has decreased, indicating that $[\text{Fe}(\text{CN})_6]^{3-}$ is involved in the reaction with Py monomers and is reduced by Py. The origin of optical absorbance increases in the range from 450 to 700 nm, which is probably related to the interconnection of shorter Ppy polymer chains. Such prolongation of conjugated double-bond systems induces a bathochromic absorption shift. In this particular experiment, the polymerization reaction initiated with 0.5 mM $[\text{Fe}(\text{CN})_6]^{3-}$ was relatively slow. In Fig. 5a an isosbestic point was observed at $\lambda = 450$ nm. This indicates that during a time frame that

lasts up to 2 h from the initialization of the polymerization reaction, the spectra of $[\text{Fe}(\text{CN})_6]^{3-}$ and Ppy are still not overlaying each other. This allows for spectrophotometric measurement of both $[\text{Fe}(\text{CN})_6]^{3-}$ and Ppy independently.

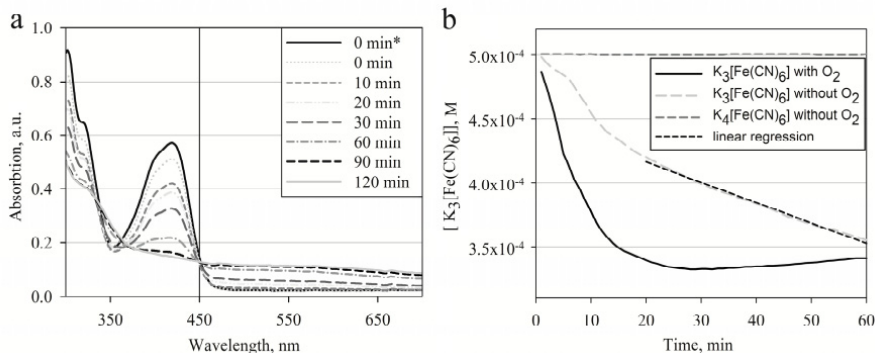


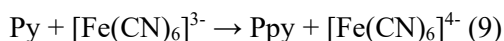
Fig. 5. (a) Change in the absorption spectra of a sample containing 0.5 mM $[\text{Fe}(\text{CN})_6]^{3-}$ and 0.5 M Py at different incubation periods; (b) evolution of absorption at 420 nm versus incubation time in a solution consisting of 0.5 M of Py with 0.5 mM of $[\text{Fe}(\text{CN})_6]^{3-}$ or 0.5 mM of $[\text{Fe}(\text{CN})_6]^{4-}$ at pH 7.0, under aerobic and anaerobic conditions. Linear regression from $t = 20$ min was observed with $R^2 = 0.9933$; 0 min*, spectra registered before the addition of Py to the reaction mixture [30].

Similar experiments were performed measuring optical absorption at $\lambda = 420$ nm while the reaction was performed under aerobic and anaerobic conditions. In these experiments, the reduction of $[\text{Fe}(\text{CN})_6]^{3-}$ by Py to $[\text{Fe}(\text{CN})_6]^{4-}$ was observed. In Fig. 5b, curves indicate $[\text{Fe}(\text{CN})_6]^{3-}$ concentration changing over time under aerobic and anaerobic conditions are presented. In a reaction mixture that contained 0.5 M of Py and 0.5 mM of $[\text{Fe}(\text{CN})_6]^{3-}$ under aerobic conditions the process reaches equilibrium during the 35th minute after the initialization of the polymerization reaction. The formed $[\text{Fe}(\text{CN})_6]^{4-}$ is reoxidized back into $[\text{Fe}(\text{CN})_6]^{3-}$ by oxygen dissolved in the solution, and the concentration of $[\text{Fe}(\text{CN})_6]^{3-}$ remains constant after this point. The concentration of dissolved oxygen in a reaction mixture of 0.1 M PBS, pH 7.0, at 25 °C is ~ 250 μM [108, 109]. Alternatively, under anaerobic conditions $[\text{Fe}(\text{CN})_6]^{3-}$ reacts slowly with Py and the concentration of $[\text{Fe}(\text{CN})_6]^{3-}$ steadily decreases. The decrease in $[\text{Fe}(\text{CN})_6]^{3-}$ concentration from the 20th minute after the initialization of the polymerization reaction can be approximated using a linear function with a regression coefficient $R^2 > 0.99$. This suggests that during polymerization, the formed $[\text{Fe}(\text{CN})_6]^{4-}$ is not oxidized back into $[\text{Fe}(\text{CN})_6]^{3-}$. From this graph it is possible to determine that under anaerobic conditions with an excess of Py, the polymerization reaction ends when all $[\text{Fe}(\text{CN})_6]^{3-}$ is consumed or has reached its lowest thermodynamically favorable concentration. Under aerobic conditions, the

cycling of oxidation and reduction reactions takes place, which only stops when all Py is polymerized into polypyrrole. In both reactions, Ppy formation was observed; however, this is not represented in figures. Under anaerobic conditions, the reaction between $[\text{Fe}(\text{CN})_6]^{4-}$ and Py was also inspected and no transition or oxidation was observed from $[\text{Fe}(\text{CN})_6]^{4-}$ to $[\text{Fe}(\text{CN})_6]^{3-}$ or the formation of Ppy was observed (Fig. 5b). Constant oxidation of $[\text{Fe}(\text{CN})_6]^{4-}$ to $[\text{Fe}(\text{CN})_6]^{3-}$ under aerobic conditions without Py, was observed, although the data are not presented. The experiment described here proves that the reoxidation step of $[\text{Fe}(\text{CN})_6]^{4-}$ is essential in order to produce Ppy efficiently at relatively low initial concentrations of $[\text{Fe}(\text{CN})_6]^{3-}$. This shows that $[\text{Fe}(\text{CN})_6]^{3-}/[\text{Fe}(\text{CN})_6]^{4-}$ is reusable in the initiation of Ppy polymerization reactions. Few studies have shown that iron compounds such as FeCl_3 and Fe_2O_3 can be regenerated and reused in the synthesis of Ppy and polyaniline when they are coupled with an oxidation cycle by oxygen [110, 111].

3.2.2. Influence of oxygen and pH on polymerization kinetics

As shown above, the reoxidation of $[\text{Fe}(\text{CN})_6]^{4-}$ into $[\text{Fe}(\text{CN})_6]^{3-}$ has been carried out by oxygen dissolved in PBS under standard conditions. In order to control this process, it is important to find conditions where the influence of dissolved oxygen on the reaction is the lowest or has no impact at all. In Fig. 6 graphs represent both the variation rate of $[\text{Fe}(\text{CN})_6]^{3-}$ concentration and the rate of Ppy formation at different pH values measured at 420 and 460 nm. Measurements were performed in a 0.1 M PBS at different pHs. 0.5 M Py was present in all these reaction mixtures and 0.5 mM $[\text{Fe}(\text{CN})_6]^{3-}$ or 0.5 mM of $[\text{Fe}(\text{CN})_6]^{4-}$ were added to the polymerization solution. At different pH values, polymerization of Ppy using $[\text{Fe}(\text{CN})_6]^{3-}$ according to reaction Equation (9).



In this polymerization reaction (Equation (9)), the rate of $[\text{Fe}(\text{CN})_6]^{3-}$ concentration change over time was evaluated and is represented in Fig. 6a. The Ppy formation rate was evaluated and is represented in Fig. 6c. The other two graphs represent the kinetic parameters of the subsequent cascade of reactions (Equation (10)):

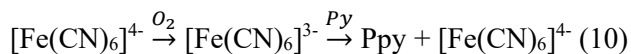


Fig. 6b represents the rate of change in the concentration of $[\text{Fe}(\text{CN})_6]^{3-}$ concentration and Fig. 6d addresses the formation rate of Ppy. In Fig. 6b the

represented rates correspond to changes of the overall concentration of $[\text{Fe}(\text{CN})_6]^{3-}$. During the experiment, a constant increase in $[\text{Fe}(\text{CN})_6]^{3-}$ concentration was observed, illustrating that the oxidation of $[\text{Fe}(\text{CN})_6]^{4-}$ to $[\text{Fe}(\text{CN})_6]^{3-}$ is faster than the reduction of $[\text{Fe}(\text{CN})_6]^{3-}$ by Ppy. In Fig. 6a, the concentration decrease rates of $[\text{Fe}(\text{CN})_6]^{3-}$ concentration decrease ($v = 1.75 \times 10^{-7} \text{ mol}\cdot\text{s}^{-1}$ and $v = 4.74 \times 10^{-7} \text{ mol}\cdot\text{s}^{-1}$) indicate that the reaction is faster under neutral pH (pH 7.0) and under basic conditions (pH 9.0). In Fig. 6b the formation of $[\text{Fe}(\text{CN})_6]^{3-}$ from $[\text{Fe}(\text{CN})_6]^{4-}$ due to oxidation by dissolved ambient oxygen is represented. The slowest oxidation of $[\text{Fe}(\text{CN})_6]^{4-}$ into $[\text{Fe}(\text{CN})_6]^{3-}$ occurs at pH 7.0 with a reaction rate of $v = 3.10 \times 10^{-9} \text{ mol}\cdot\text{s}^{-1}$. This process is approximately two orders of magnitude slower than that described above. Figures 6c and 6d represent the Ppy formation rates in the presence of $[\text{Fe}(\text{CN})_6]^{3-}$ and $[\text{Fe}(\text{CN})_6]^{4-}$ respectively. In both cases, the polypyrrole particles form the slowest at pH 7.0. In the presence of 0.5 mM $[\text{Fe}(\text{CN})_6]^{3-}$ the reaction rate was $v = 2.24 \times 10^{-6} \text{ DA}\cdot\text{s}^{-1}$, and in the presence of 0.5 mM $[\text{Fe}(\text{CN})_6]^{4-}$ it was equal to $v = 9.35 \times 10^{-7} \text{ DA}\cdot\text{s}^{-1}$. From these results it can be estimated that if $[\text{Fe}(\text{CN})_6]^{4-}$ is in the same reaction mixture with Py under aerobic conditions and at pH 7.0 then the oxidation process (Equation (10)) is the rate-determining step for the entire polymerization process. Consequently, the variation of pH can be exploited to control the reaction kinetics.

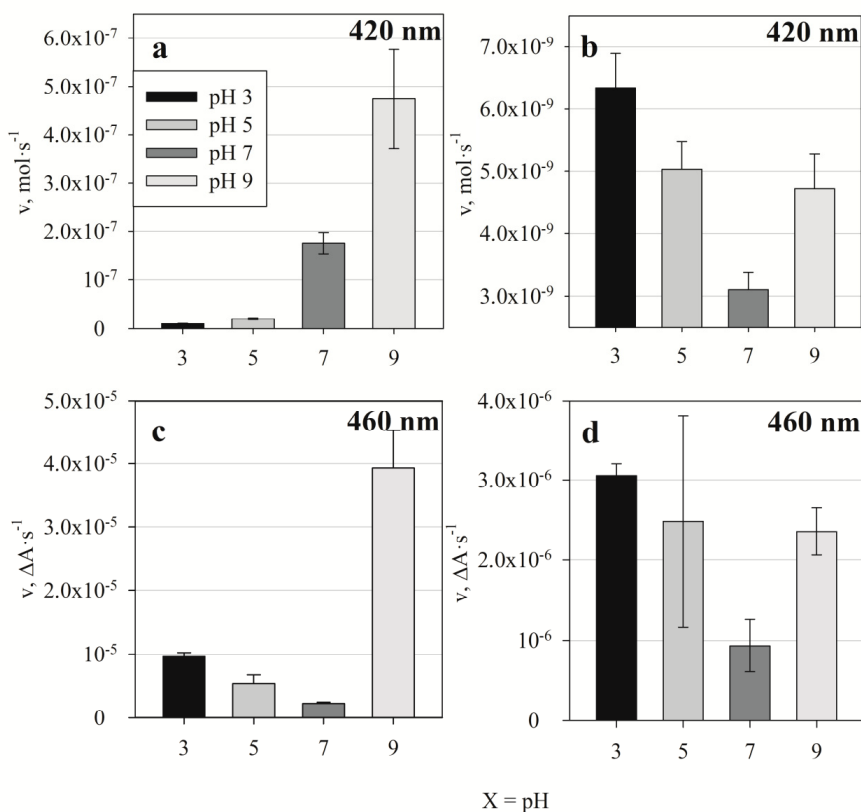


Fig. 6. Reaction rates at different pH values: (a) the $[\text{Fe}(\text{CN})_6]^{3-}$ concentration decrease rate was measured at 420 nm in the presence of $[\text{Fe}(\text{CN})_6]^{3-}$ and Py due to the formation of Ppy; (b) the $[\text{Fe}(\text{CN})_6]^{3-}$ concentration increase rate due to the re-oxidation of $[\text{Fe}(\text{CN})_6]^{4-}$ by dissolved oxygen was measured at $\lambda = 420$ nm; (c) Ppy polymerization rate in the presence of $[\text{Fe}(\text{CN})_6]^{3-}$ measured at $\lambda = 460$ nm; (d) Ppy polymerization rate in the presence of $[\text{Fe}(\text{CN})_6]^{4-}$ at 460 nm. In all samples 0.5 M Py and 0.5 mM of $[\text{Fe}(\text{CN})_6]^{3-}$ or 0.5 mM $[\text{Fe}(\text{CN})_6]^{4-}$ were used. All reactions were performed under aerobic conditions. Error bars indicate standard deviation of the calculated reaction rate [30].

3.2.3. Polypyrrole doping in acidic medium and characterization of aggregates

Polypyrrole powders prepared at different pH values were analyzed by FTIR. All Ppy samples were synthesized using $\text{K}_3[\text{Fe}(\text{CN})_6]$ in PBS at pH values of 3.0, 5.0, 7.0 and 9.0. FTIR spectra (Fig. 7) showed main characteristics peaks at 774, 1039, 1183, 1563, and 1690 cm^{-1} and a broad band at $\sim 3100\text{--}3500$ cm^{-1} . These peaks were observed in all samples. A variable peak at 2071 cm^{-1} was observed in Ppy, which was formed in an

acidic polymerization solution. The main FTIR characteristic peaks agree well with those presented by other researchers [112]. The bands at 774 cm^{-1} and 1684 cm^{-1} , which are ascribed to the C-N bond, and 1563 cm^{-1} correspond to fundamental vibrations of the polypyrrole ring. The band at 1039 cm^{-1} is based on the =C-H in-plane vibrations, and the band at 1196 cm^{-1} corresponds to the C-N stretching vibrations. The peak at $\sim 3100\text{--}3500\text{ cm}^{-1}$ corresponds to the N-H bond. The band at 2071 cm^{-1} corresponds to the C-N stretching of $\text{K}_x[\text{Fe}(\text{CN})_6]$. The absorption band for $[\text{Fe}(\text{CN})_6]^{x-}$ varies between 2040 and 2120 cm^{-1} [113]. This band is most likely to represent $[\text{Fe}(\text{CN})_6]^{4-}$ [114]. These FTIR spectra suggest that $[\text{Fe}(\text{CN})_6]^{4-}$ remains in the Ppy layer as a dopant if Ppy is synthesized in an acidic medium. This is a common feature for Ppy doping in an acidic medium because Ppy becomes positively charged and can incorporate negative ions into its structure [113]. Consequently, the efficiency of Ppy doping by $[\text{Fe}(\text{CN})_6]^{4-}$ can be controlled by varying the pH of the polymerization solution.

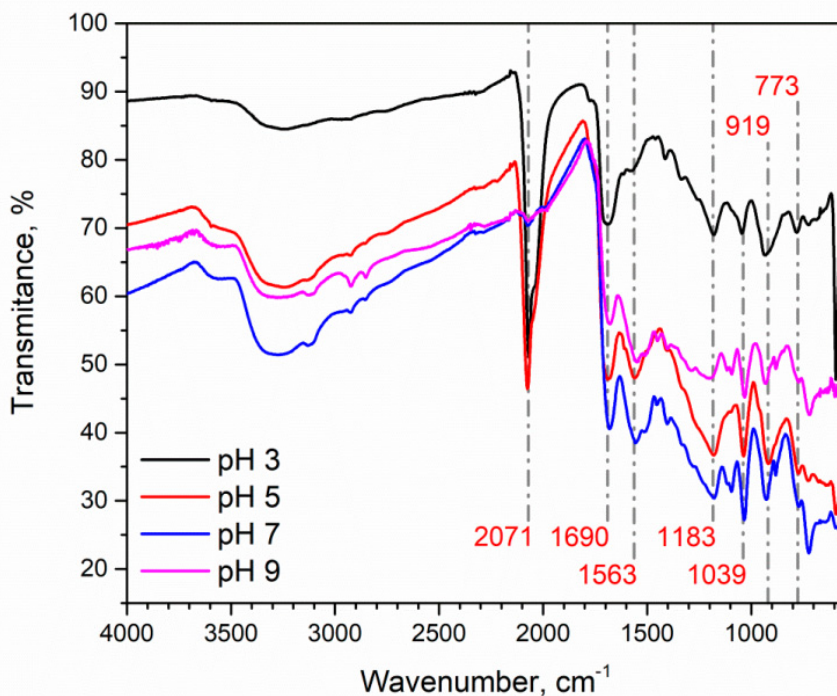


Fig. 7. FTIR spectra of Ppy synthesized at different pH values. 0.5 M Py and 0.04 M $\text{K}_3[\text{Fe}(\text{CN})_6]$ were used for the synthesis of Ppy in 0.1 M PBS buffers of four different pH levels: 3.0 , 5.0 , 7.0 and 9.0 [30].

Analysis of FTIR spectra reveals that it is possible to achieve doping with $[\text{Fe}(\text{CN})_6]^{4-}$ directly without using an additional oxidizer or an external electric stimulus, and to produce the $\text{Ppy}/[\text{Fe}(\text{CN})_6]^{4-}$ composite in one step, which corresponds to the results published in [115] additional oxidizer was used. This finding corresponds to that presented in other research, reporting that in acidic mediums anions tend to remain within the Ppy matrix [116].

FIB SEM images revealed that commonly reported Ppy aggregates consisted of smaller spherical shaped units shaped units (Fig. 8). On further inspection, variations among spherical unit size were observed, which were altered by pH value. Ppy prepared at different pHs (3.0, 5.0, 7.0 and 9.0) were formed respectively of 152 ± 12 nm, 76 ± 26 nm, 52 ± 15 nm and 54 ± 14 nm size base units. Thus, Ppy synthesized under more acidic conditions tended to form larger Ppy units. However, the Ppy unit size was lower under neutral and basic conditions. The FIB SEM study, in agreement with the FTIR data, suggests that the incorporation of $[\text{Fe}(\text{CN})_6]^{4-}$ into the Ppy structure increases its porosity. This is possible because the $\text{Ppy}(\text{H}^+)/[\text{Fe}(\text{CN})_6]^{4-}$ ion pairs formed in acidic medium, according to the FTIR results, could be hydrated and produce larger constituent units of Ppy.

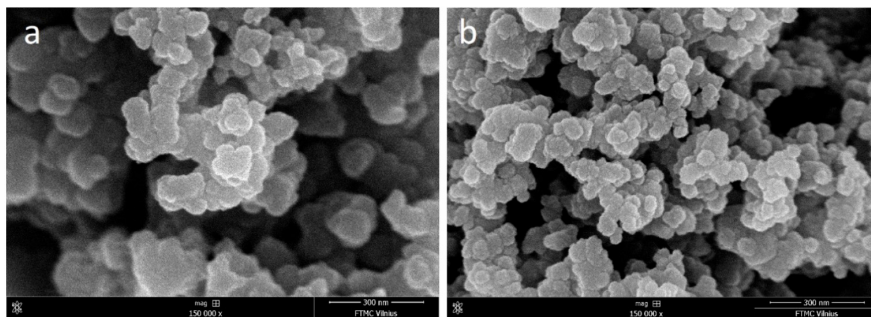


Fig. 8. FIB SEM images of Ppy aggregates synthesized using 0.5 M Py and 0.04 M $\text{K}_3[\text{Fe}(\text{CN})_6]$. (a) Synthesis was performed in 0.1 M PBS, pH 3.0; (b) Synthesis was performed in 0.1 M PBS, pH 9.0. Both images were obtained using a 150k magnification [30].

3.2.4. Polydopamine synthesis optical assessment

Polydopamine synthesis was investigated by applying buffers with various pH values to test the semi-auto polymerization of PDA. Reaction mixtures and products were inspected with a spectrophotometer and an FTIR spectrophotometer. From spectrophotometric data, it was concluded that PDA is rarely synthesized in acidic or neutral mediums. In basic medium, dopamine undergoes autopolymerization (Fig. 9). This agrees with the literature reported

[117]. These findings prove only that PDA synthesis can be controlled by changing the acidity and alkalinity of the reaction mixture.

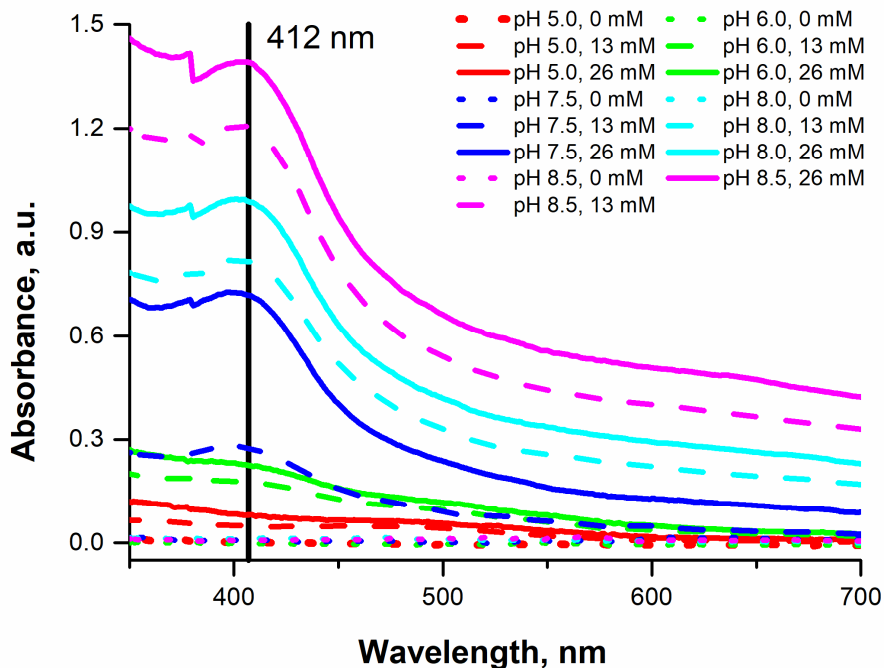


Fig. 9. Optical absorbance spectra of PDA particles at 350 - 700 nm wavelengths. The legend shows the pH of the buffer used in each sample and the concentration of dopamine used [102].

Synthesized polymer particles were also inspected with FTIR. FTIR was used to verify that the newly synthesized particles/agglomerates consisted of PDA. The remaining precipitates, after the supernatant was removed in the UV-VIS spectroscopy experiment, were washed with water and ethanol and then dried. The dried particles were collected and the absorbance was measured using an FTIR spectrometer. The results of this experiment are shown in Fig. 10. The FTIR spectra have some similarities to those of the previous studies [118, 119]. Peaks at 1650 (O-H), 1505 (C=O or N-H), and 1340 cm^{-1} (CNC) were detected in all samples, and they were at wavenumber matching those reported in previous studies.

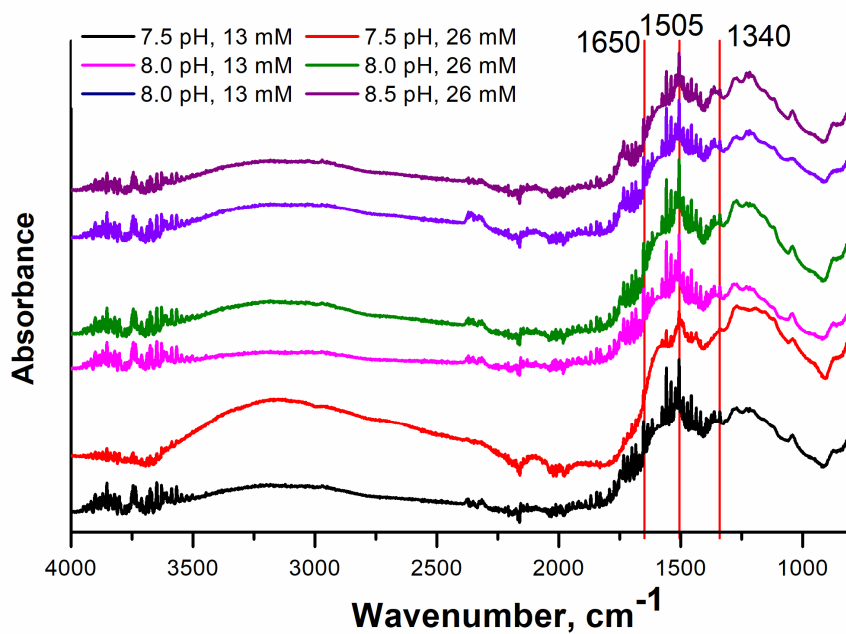


Fig. 10. FTIR spectrogram of PDA particles, at dopamine concentrations used in PDA synthesis of 13 mM at pH of 7.5, 8.0, 8.5, and 26 mM dispersed in 0.1 M PBS at pH of 7.5, 8.0, 8.5 [102].

3.3. Characterization of yeast and polymer composite

3.3.1. Atomic force microscope imaging and mechanical properties of modified yeast

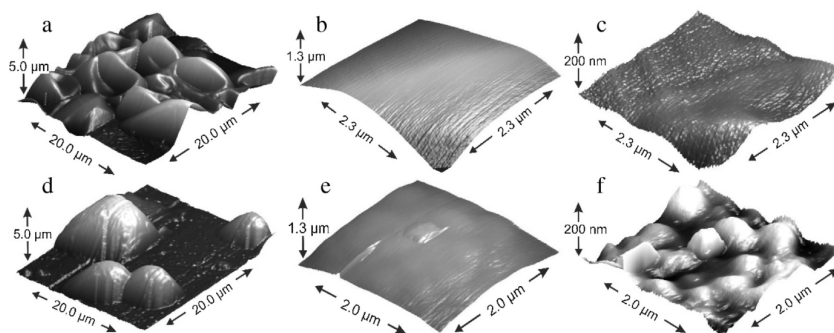


Fig. 11. AFM images obtained in contact mode: a–c— Y@Ppy-ctr; d–f— Y@Ppy-0.5. Images a and d represent AFM contact mode investigations of whole cells, which were dried on the Si surface, scan area is $20 \times 20 \mu\text{m}^2$; Images b and e represent the apex of unmodified and modified cells, image size is $2 \times 2 \mu\text{m}^2$; a second-order ‘surface flattening’ procedure was applied for the formation of c and f images from images b and e, respectively [29].

Atomic force microscopy was used to compare Y@Ppy-ctr with Y@Ppy. The surface morphology and elasticity of the cells were evaluated. For these experiments, yeast cells were grown and modified with pyrrole as described in Section 2.3.1.1, and then the modified cells were (i) dried on a conventional silica-based substrate, which is polished to a high degree of flatness, therefore, it was suitable for AFM based imaging, or (ii) immobilized in custom made silicon wafers with inclined square holes for AFM-based stiffness measurement. The results obtained from the AFM images are presented in Fig. 11. After 12 h of drying, it was observed that Y@Ppy-ctr have lost its initial round shape and became wrinkled, as can be seen in both the AFM (Fig. 11a) and optical (Fig. 11b) images. On the contrary, the Y@Ppy-0.5 have retained their spherical shape (Fig. 11d). Shape retention by Y@Ppy can be explained by two hypotheses. First, Ppy possesses highly hydrophilic properties that are caused by a large concentration of positively charged nitrogen atoms, which are present in the polymeric backbone of polypyrrole. The overall positive charge of nitrogen must be compensated with negatively charged ions and/or hydroxyl ions, which form hydrogen bonds with water molecules. Second, additionally formed polymeric structures increase the thickness of the cell wall, and as a result a thicker cell wall significantly slows down some of the cell drying related processes or reinforces the cell wall and

helps to retain the initial spherical form even if some water evaporates from the cell. For a detailed surface examination, high-resolution images of the cell's surface were taken (Fig. 11b,e). The surfaces of yeast cells Y@Ppy0.5 were observed to have some round-shaped features, while the surfaces of Y@Ppy-ctr were almost smooth. Figs. 11c,f were derived from scans, which are represented in Fig. 11b,e, by a second-order 'surface flattening' algorithm. These computed images showed that the modification of yeast cells with Ppy also increases the roughness of the cell surface. The spherical features observed in the AFM images suggested that polypyrrole is synthesized in small spherical structures, which most likely were located close to the redox enzymes of the PMOR system or the Ppy nucleation sites.

The stiffness profiles of individual cells were evaluated using the AFM-based force measurement technique [120-123], allowing the impact of the polymer layer on stiffness to be investigated. The data obtained were normalized to the solid surface stiffness model and reproduced as rooted force/indentation graphs (Fig. 12). From these results, Young's modulus for individual cells was calculated using modifications described in the Hertz-Sneddon model (Table 4). The model with the highest overall R^2 value was chosen for a further evaluation of the results in the following discussion. The stiffness profiles for all types of samples were dispersed, but clear tendencies for the different samples could be distinguished (Fig. 12, color clouds). Treatment with Py tended to form a relatively uniform cell population in a reaction solution. However, further analysis and modelling of the stiffness indicated that the cell wall could be treated as a system of two components. One component is more associated with smaller indentations and a second component is more associated with larger indentations. Therefore, two independent fittings were performed on the individual stiffness profile (Table 4). At small indentations the cell wall was soft, whereas at large indentations the stiffness was increased 350 times (0.0033 and 1.1939 MPa respectively, Table 4). The calculated Young's modulus showed that the stiffness of the outer layer of the cell wall, measured at small indentations and that of the inner layer measured at larger indentations, both decreased after incubation in 0.5 M of Py without polymerization inducing redox species (Table 4). However, a different influence on the cell wall was observed after Ppy treatment. The formation of Ppy within the outer layer of the cell wall slightly increased its stiffness (from 0.0033 MPa to 0.0046 MPa) in the presence of 0.1 M Py; the stiffness increased further as the concentration of Py increased. On the contrary, the inner layers of the modified cell became almost 3.5 times softer (from 1.1939 to 0.3385 MPa) in the presence of 0.1 M Py. This suggests that the formation of Ppy polymers crosslinks the outer layer of the cell wall structures, and thus increases the rigidity. However, the formation of Ppy in the inner cell wall layer acts differently and initiates

disruption of the natural cell wall structure. However, if the concentration of Py used for the polymerization was higher, then the stiffness of both inner- and outer-layers of the cell wall increased.

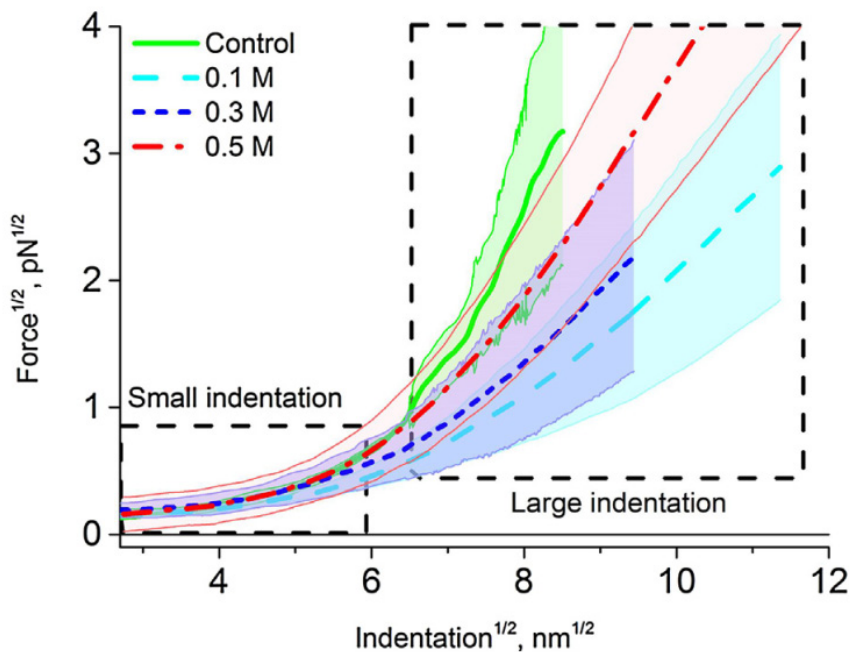


Fig. 12. Force indentation curves, linearized according to the Hertz-Sneddon elasticity model. Average lines were generated from different treatments; Clouds (shaded areas) represent the standard deviation ($n < 10$) in a particular indentation; Square zones represent fitting ranges for small or large indentations [68].

A pilot AFM-based force measurement study has revealed that Ppy incorporation within the cell wall changed the mechanical properties of Y@Ppy [29]. Currently, force/indentation measurements were used to determine Young's modulus of individual Ppy-modified and unmodified cells. Young's modulus is considered the most representative parameter for the evaluation of mechanical properties of encapsulated cells [124-127]. To evaluate mechanical properties of yeast cells using AFM, several cell immobilization techniques are available [103, 121, 122, 128]. Immobilization of yeast cells within pores of polycarbonate membranes is often reported to be unreliable [129, 130]. Therefore, yeast cells were immobilized within specially prepared holed silica wafers, which contained pyramid-shaped holes of similar dimensions to those of yeast cells. Despite this using current method of immobilization, Young's modulus of Y@Ppy-ctr were almost identical and comparable (Table 4) to those reported by the other authors [127]. Our current

AFM-based research additionally showed that incorporation of formed Ppy increases the rigidity of outer cell wall layer (Table 4, 1st fitting range) but has differing effects on the inner layers of the cell wall, depend and on the concentration of Py used (Table 4, 2nd fitting range). Y@Ppy-0.1 cells (Table 4, No. 1, second fitting range) had softer cell walls compared to Y@Ppy-ctr (Table 4, No. 2, second fitting range). Although Y@Ppy-0.1 (Table 4, No. 2, second fitting range) compared to those that were only incubated with high Py concentrations (0.5 M, without polymerization initiator; Table 4, No. 5, second fitting range), their inner layer of the cell wall lost its stiffness by the same amount, and Young's modulus decreases from ~ 1.19 down to ~ 0.34 MPa. This suggests that adsorption of Py and Ppy with β -glucan disturbs or destabilizes the structure of the natural cell wall. Yeast cells incubated in reaction solutions containing higher Py concentrations showed increased stiffness of cell walls. This suggests that larger Ppy particles or matrices are formed that, instead of further distorting the natural cell wall, start to act as a binding agent through the formation of more complex polymeric structures. The gradually increasing value of Young's modulus also illustrates possible cross-linking between Ppy clusters randomly distributed within the cell wall or within other structural units. This prediction agrees with the results showing that the lowest CV% value was observed after incubation of yeast cells in solutions containing the highest evaluated Py concentrations (Table 4, CV values). These results suggest that the Ppy might undergo different degrees of cross-linking as the stiffness of Ppy-modified cells gradually increases, with increasing Py concentration in the reaction media, ultimately forming a more uniform structure. Previous studies on the mechanical properties of chitosan/Ppy composites stated that increasing the pore size of this composite significantly softens the material [131]. This fact might help to understand the loss of stiffness, observed currently; Ppy formed within yeast cell wall structures could act similarly to increase pores in chitosan/Ppy composites. The same study showed that the incorporation of Ppy within chitosan makes this composite material more flexible and softer. These findings also suggest that similarly acting composites were formed within yeast cell walls. In summary: Ppy acts on the outer layers of the cell wall as a hardening agent, which crosslinks β -glucan. In addition, Ppy acts as a plasticizer, softening the cell wall by disrupting, weakening, and redistributing essential bonds, such as hydrogen bonds between different molecules and/or layers of chitin- or chitosan-type polycarbohydrates. Different accessibility of Ppy-modified and unmodified cell wall by lyticase and the mechanically different effects on the yeast cell wall prove that the

yeast cell wall probably acts as a double layered system [120]. This unexpected tendency can only be explained by the destabilization of the cell wall when low concentrations of pyrrole are used for polymerization, while at higher concentrations a more advanced Ppy polymer matrix is formed. Therefore, incubation of yeast cells at a higher pyrrole concentration containing the polymerization initiation solution increased the toughness of the inner layer of the yeast cell.

Table 4. Young's modulus of Ppy modified yeast cells and respective coefficient of variance (CV), $n \geq 10$ [68].

Type of sample	Young's modulus, MPa, 1st fitting range	CV, %	Young's modulus, MPa, 2nd fitting range	CV, %
1. Y@Ppy-ctr	0.0033 ± 0.0017	52	1.1939 ± 0.6825	57
2. Y@Ppy-0.1	0.0046 ± 0.0024	52	0.3385 ± 0.13	38
3. Y@Ppy-0.3	0.0064 ± 0.0017	27	0.4169 ± 0.3188	76
4. Y@Ppy-0.5	0.0425 ± 0.0183	43	0.7758 ± 0.1225	16
5. *Y@Ppy-0.5 without K ₄ [Fe(CN) ₆]	0.0019 ± 0.0011	58	0.3562 ± 0.268	75

*without K₄[Fe(CN)₆] the polymerization reaction was not initiated.

3.3.2. Isotopic characterization of polypyrrole-yeast composite

Isotope ratio mass spectroscopy was used to determine the location of Ppy in the cells and to evaluate monomer adsorption on the cell structures. Various mixtures of not labeled and isotopically labeled pyrrole at varied ¹⁵N enrichments were used (Py*, M_r=68 g/mol). Most of the experiments were carried out using lightly enriched pyrrole ($\delta^{15}\text{N}(\text{Py}^*) = 400 \text{ ‰}$), but in some experiments pyrrole with higher enrichment ($\delta^{15}\text{N}(\text{Py}^*) \sim 4000 \text{ ‰}$) was used. Initial experiments were carried out to check the tendency of pyrrole to adhere to or dissolve within cell structures; for these, K₄[Fe(CN)₆] was not added into the Py* containing samples. The mass of pyrrole in the biocomposite, using an initial concentration of 0.5 M of pyrrole, reached ~ 1.9 % after 22 h (Table 5a). Yeast cells from the same batch incubated under the same

conditions, though without pyrrole, were used as a control. The data indicate that the amount of Py* dissolved within cells increased in time from 2 to 22 h.

Altering the concentration of Py* in incubation (Table 5b) suggests that the amount of Ppy and Ppy*, trapped within cell structures, increases concomitantly with the concentration of Py* monomer used. Similarly, from the measured Ppy* concentrations a gradual increase in produced polymer was observed with an increasing concentration of added K₄[Fe(CN)₆] (Table 5c). Further experiments where Py* was applied at a higher ¹⁵N enrichment (~4000 ‰) were performed in order to compare yeast samples with Ppy formed in/on the cell and pyrrole adsorbed on/in the cell structure with better resolution and higher precision. This allowed investigation of yeast cells incubated with lower concentrations of Py*.

Using solutions, containing 0.5 M of Py* and 0.04 M of K₄[Fe(CN)₆], for the modification of yeast cells, higher concentrations of Ppy* were formed, compared to solutions without K₄[Fe(CN)₆] (Fig. 13). However, for both treatments, an increased concentration of pyrrole resulted in higher total Ppy production (Fig. 13). At low Py* concentration (up to 0.1 M), no significant differences between polymerized Ppy* formed and intercalated/adsorbed Py* were observed. The differences only became apparent when yeast cells were incubated in solutions containing more than 0.1 M Py*. In cells incubated in solution with 0.5 M pyrrole, the amount of Ppy* (squares) was approximately three times the amount of adsorbed Py* monomers (triangles).

Table 5. The concentrations of Py* and formed Ppy*, adsorbed on/within the yeast cells, were quantified by IRMS. Numerical data provided with SD, n ≥ 3 [68].

Section 'a'; quantification of adsorbed Py*	
¹⁵ N enrichment	~ 400 ‰
[Py*] = const.	0.50 M
Time	Adsorbed Py* amount in comparison to total mass, %
2 h	0.77 ± 0.05
22 h	1.85 ± 0.07
Section 'b', quantification of Ppy* formed on/within cell	
¹⁵ N enrichment	~ 400 ‰
Time = const.	22 h
[Py*], M	The amount of formed Ppy* in comparison to total mass, %
0.10	0.06 ± 0.06

0.30	0.34 ± 0.03
0.50	2.30 ± 0.09

Section 'c', quantification of Ppy* formed on/within the cell at different initial $K_4[Fe(CN)_6]$ concentrations

^{15}N enrichment	$\sim 400 \text{ ‰}$
Time = const.	22 h
$[Py^*] = \text{const.}$	0.50 M
$[K_4[Fe(CN)_6]]$, M	Adsorbed Ppy* amount in comparison to total mass, %
0.02	$4.34 \pm 0.02\%$
0.04	$5.76 \pm 0.51\%$
0.08	$6.61 \pm 0.54\%$

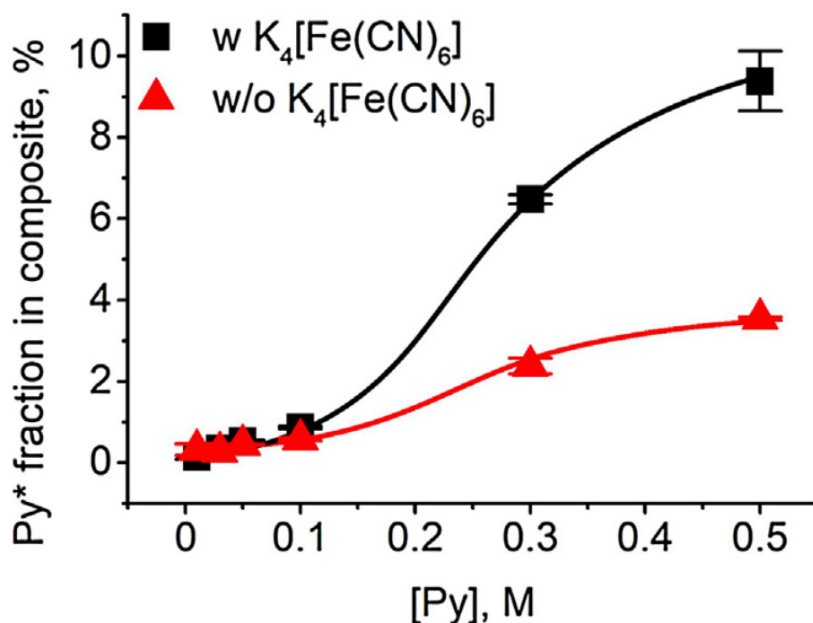


Fig. 13. Formed Ppy (squares) and adsorbed Py (triangles), in a biocomposites from total mass, using different initial monomer concentrations. Squares indicate Ppy formed using Py^* and $K_4[Fe(CN)_6]$; triangles – Py^* that only adsorbed to cells. Fractions were determined with IRMS from freeze-dried samples. The experiment was carried out using a mixture of isotopically labeled monomers (Py^*) and unlabeled monomers (Py) with isotopic enrichment $\sim 4000 \text{ ‰}$. 0.04 M of $K_4[Fe(CN)_6]$ were used for Py^* synthesis. Error bars indicate the variation between samples ($n \geq 3$) [68].

3.3.3. Polypyrrole-yeast composite characterization using fluorescence staining

The yeast cell wall is partially composed of polysaccharides, which interact with some specific proteins such as concanavalin A. Ppy-modified and unmodified yeast cells were stained with FITC-labeled concanavalin A (Fig. 14). After staining, a similar FITC fluorescence intensity was observed for the unmodified and Ppy-modified cells. Therefore, the binding of concanavalin A to cells is independent of the initial concentration of pyrrole, suggesting that, as Ppy forms, the cell wall polysaccharides remain available to bind with the labeled concanavalin A. In turn, this suggests that Ppy, when formed, is most probably embedded inside the cell wall.

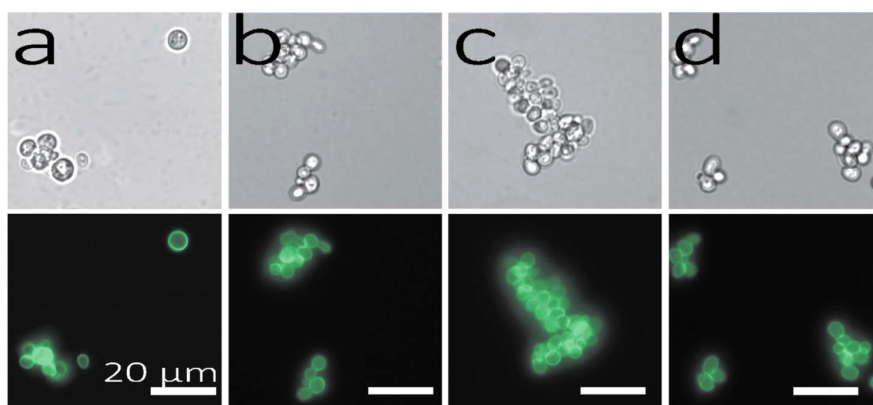


Fig. 14. Yeast cells stained with FITC-labeled concanavalin A; bright field versus fluorescence light microscopy; a – unmodified cells; b–d Ppy-modified cells using 0.1; 0.3 and 0.5 M Py [68].

3.3.4. Enzymatic cell wall removal

Yeast spheroplasts were produced [106], and subjected to IRMS investigation. Yeast cells were modified with Ppy* using isotopically labeled Py* and after which their wall was removed/digested with the enzyme – lyticase, which acts simultaneously as an endoglucanase and a protease [132]. Different fractions of digested samples were collected from the reaction mixture by centrifugation; spheroplasts were separated from the other debris from the digested yeast cells. The $\delta^{15}\text{N}$ values of both spheroplasts and the other debris of digested yeast cells were determined. The samples were also taken before enzymatic digestion, and their $\delta^{15}\text{N}$ values were treated as control reference points. It was determined that the $\delta^{15}\text{N}$ of unmodified cells

(untreated with Ppy*) was 2.3 ‰ while the $\delta^{15}\text{N}$ value of Ppy* was 101.7 ‰ (Table 6).

Comparison of the $\delta^{15}\text{N}$ values of unmodified cells before 2.3 ‰ and after 2.6 ‰ digestion illustrated that the effect of lyticase digestion was not significant. However, in samples prepared from Ppy*-modified cells, the shift in $\delta^{15}\text{N}$ was more pronounced, decreasing from 101.7 down to 91.4 ‰ (Table 6). The decrease in $\delta^{15}\text{N}$ indicates that during lyticase cell digestion, part of the formed Ppy* became free and did not precipitate with other larger cell debris.

Table 6. Comparison of $\delta^{15}\text{N}$ (‰) measured from unmodified yeast cells and Ppy* modified. Whole cells and cell debris obtained by centrifugation using different RCFs were analysed. The analytical precision for $\delta^{15}\text{N}$ was better than 0.20 ‰ [68].

Sample	Fractions collected at RCF	$\delta^{15}\text{N}$, ‰
1. Y@Ppy-ctr before digestion of the cell wall with lyticase	12000	2.3
2. Y@ ¹⁵ Ppy-0.5 before digestion of the cell wall with lyticase	12000	101.7
3. Y@Ppy-ctr after cell wall digestion with lyticase	12000	2.6
4. Y@ ¹⁵ Ppy-0.5 after the digestion with lyticase	12000	91.4
5. Precipitate fraction of Y@ ¹⁵ Ppy-0.5 after digestion with lyticase collected at different RCF:	200	75.9
	400	92.0
	800	92.5
	1200	84.1
	2000	90.6
	6000	97.2

The collection of samples at various RCF allowed the separation of cell wall debris by size. The results showed, little or no relationship between particle (debris) size and $\delta^{15}\text{N}$ values, suggesting that the incorporated Ppy* is randomly distributed between debris. The pure spheroplast fraction (as well as containing the largest cell wall debris), collected at 200 RCF, had the lowest $\delta^{15}\text{N}$ value, confirming that the majority of Ppy* was located within the cell wall. Furthermore, it indicates that enzymatic wall digestion was incomplete and that some parts of the cell wall and Ppy* remained together.

Ppy-modified and unmodified Ppy cells were evaluated with an optical microscope to determine their size before and after enzymatic cell wall digestion.

The removal of the cell wall with lyticase led to the successful formation of Y@Ppy-ctr spheroplasts, causing these cells to swell/expand and almost double in size (Table 7). However, the complete formation of the Y@Ppy spheroplast was not very obvious and the increase in cell size was less significant (Table 7). In spheroplasts obtained from Y@Ppy-ctr, all inner yeast cell structures were visible, however, Y@Ppy were opaque (Fig. 15). These observations led to the conclusion that Ppy may interfere with the ability of lyticase to fully digest the cell wall.

Table 7. Average size of yeast cells before and after enzymatic removal of their wall. Size represented with SD; $n \geq 20$ per treatment [68].

Sample	Y@Ppy-ctr, in μm	Y@Ppy-0.5, in μm
Before digestion of the cell wall with lyticase	9.57 ± 3.03	9.89 ± 0.89
After digestion of the cell wall with lyticase	15.95 ± 1.36	11.43 ± 1.63

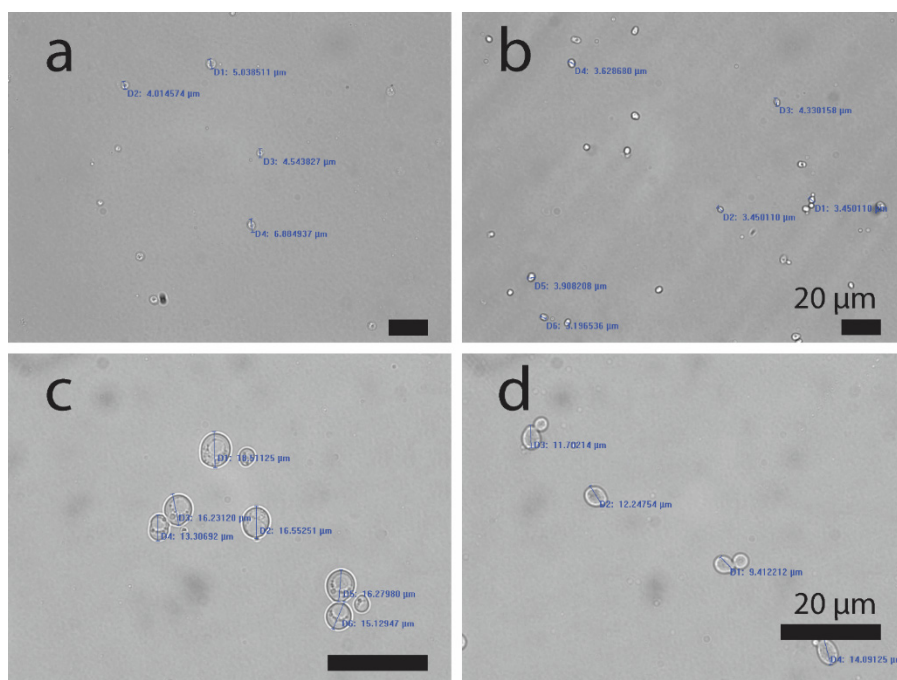


Fig. 15. Yeast before (a, b) and after (c, d) enzymatic wall digestion with lyticase. b, d – Polypyrrole entangled yeast cells; a, c – intact cells. 200 times magnified – a, c and 400 times – c, d [68].

3.3.5. Optical assessment of polydopamine uptake in yeast

On the verification of successful chemical PDA synthesis, polymerization was applied for yeast cell modification. To assess the formation of a Y@PDA composite in the reaction mixture, samples were prepared by centrifuging modification mixtures. The supernatants were collected and optically evaluated. Small molecular weight PDA leftovers in the supernatant generated a peak of absorbance at 412 nm. In Table 8 ‘supernatant’ section, PDA absorbance values are represented. The control samples and the samples that contained dopamine differ in magnitude, which shows a successful formation of PDA. Samples modified in the absence of glucose (Y@PDA-26 w/o glu) had higher absorbance (0.879 a.u.) than those modified with 200 mM glucose (Y@PDA-26, 0.644 a.u.). Cells with/and PDA particles were washed out of the reaction mixture with PBS buffer to remove any PDA leftovers and resuspended in PBS before measuring at 600 nm wavelength. Measurements at 600 nm wavelength are common when assessing cell count in samples (Table 8, cell suspension). The results show that the modified samples without glucose also had lower absorbance (Y@PDA26 w/o glu, 0.722 a.u.) than those of Y@PDA-26 (0.806 a.u.). The results show that during PDA modification, if 200 mM glucose was used, more PDA was bound to the cells and less free floating PDA was present in the supernatants. This leads to the belief that glucose might promote dopamine adsorption/uptake to cells. Although it was unclear why the control samples (Y@PDA-ctr w/o glu, Y@PDA-ctr) had higher absorbance values than those of modified cells (Y@PDA-26 w/o glu, Y@PDA-26). A possible explanation might be that dopamine slows down yeast cell budding.

Table 8. *Optical assessment of yeast modification with PDA reaction mixture. N=3 [102].*

Supernatant	Average absorbance at 412 nm, a.u.
Y@PDA-ctr w/o glu	0.040
Y@PDA-26 w/o glu	0.879
Y@PDA-ctr	0.022
Y@PDA-26	0.644
Cell suspension	Average absorbance at 600 nm, a.u.
Y@PDA-ctr w/o glu	0.818

Y@PDA-26 w/o glu	0.722
Y@PDA-ctr	0.848
Y@PDA-26	0.806

3.4. Electrochemical behavior of yeast and polymer composites

3.4.1. Chronoamperometric evaluation of modified *S. cerevisiae* in the flow-through system

A controlled flow-through system with free-flowing yeast cells was created to imitate a part of a simplified commercial microbial fuel cell system. In this system, yeast cells were subjected to an electrochemical cell, where a 0.4 V potential was applied and the resulting current was recorded. First, the effect of dopamine saturation time effect on yeast cell electrical properties was evaluated. The chronoamperogram showed that 60 min saturation at pH 5, had a minor improvement over 30 min, while 90 min long saturation resulted in reduced current generation (Fig. 16a). Then the dopamine polymerization time was evaluated by letting the yeast incubate in a weak alkaline environment (pH 7.5). Yeast cells treated by 1 h lasting dopamine polymerization showed a pronounced current generation compared to yeast cells treated by 3 h and 6 h lasting polymerization (Fig. 16b). Finally, 1 h lasting dopamine saturation at pH 5.0 followed by 1 h polymerization at pH 7.5 was chosen for all subsequent dopamine modifications of yeast cells.

Different dopamine concentrations were tested to modify yeast cells. Y@PDA-13 and Y@PDA-26 produced very similar electrical response in the flow-through system (Fig. 16c). Compared to the control sample, the currents produced were approximately 20 % higher. However, upon addition of glucose, the signals have slightly dropped. These current decreases were probably induced by changes in the fluid concentrations or density. However, the addition of glucose allowed to separate the generated signals to be separated, which showed that Y@PDA-13 performed slightly better than Y@PDA-26. As constant flux is present in the flow-through system, our results suggest that an additional amount of PDA polymers may reduce glucose uptake to cells. Thus, Y@PDA-26 generated slightly smaller current. The addition of polymers to the natural cell interface has produced mechanically more rigid biocomposites [37], which also change the rate of the glucose uptake.

Yeast cell modification utilizing Ppy was designed in previous experiments. However, the 24 h long modification resulted in reduced cell viability and changed physical properties [30, 68]. Since Ppy is known to possess good electrical conductivity [133], it was necessary to test if a shorter modification time could improve cell viability while maintaining sufficient electrical properties. Our initial data using a 24 h and shorter 8 h modification

in the flow-through system have produced weak electrical signal (Fig. 16e). When short (2 h lasting) modification to long (24 h and even 8 h lasting) modification were compared, a rough three time decrease in electrochemical signal was observed. Furthermore, it was decided to reduce the yeast modification period down to 2 h, because after this modification, yeast cells produced the highest electrical current. Furthermore, based on our previous work with pyrrole monomer labeled with ^{15}N , it was determined that during 2 h of modification yeast cells were capable of absorbing and subsequently polymerizing around $0.77 \pm 0.05\%$ of the pyrrole monomer [68].

Y@Ppy samples were subjected to a flow-through system, where a 0.4 V potential was applied to the working electrode and the resulting electrical current was measured. The results showed that Y@Ppy alters electrical properties but inconsistently, as depicted in the chronoamperogram (Fig. 16d). In a flow-through system, Y@Ppy-ctr were able to generate around $85 \mu\text{A}$ in the presence of the $\text{K}_4[\text{Fe}(\text{CN})_6]$ mediator, while Y@Ppy-100 were able to generate a current as high as $140 \mu\text{A}$ current in a flow-through system. The Y@Ppy-300 modification had a significantly increased current generation compared to the other samples. During the evaluation of both Y@Ppy-100 and Y@Ppy-500, it was detected that the increase in the generated current was small and was similar to that detected in the control sample (Y@Ppy-ctr). This effect could be due to insufficient Ppy bridging or due to the poisoning of yeast cells by the high pyrrole/Ppy-concentrations applied, which indicated that after 24 h of lasting modification the viability of yeast cells has decreased significantly in the case of Y@Ppy-500 sample Y @ Ppy-500 [68]. Thus, results indicate that Y@Ppy-300 in 2 h lasting modifications were sufficient at bridging, as charge transfer was increased, while no poisoning effect was observed.

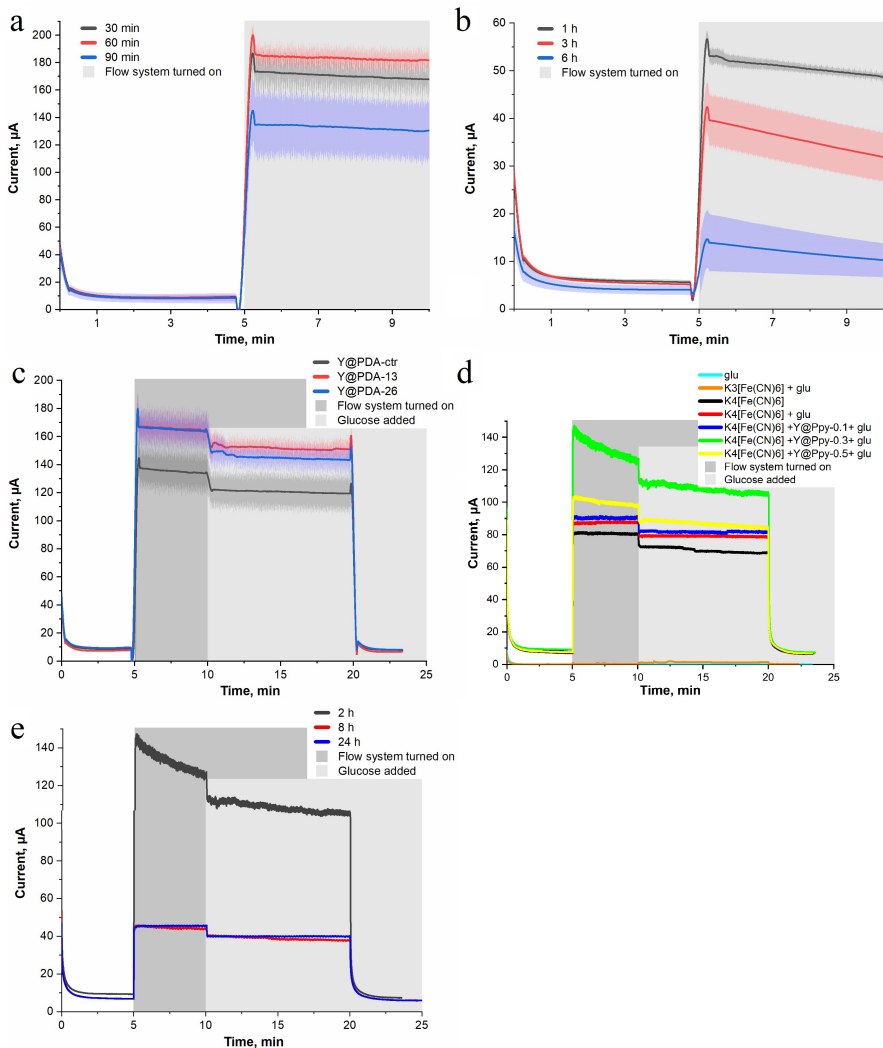


Fig. 16. The chronoamperogram of modified yeast cells subjected to a flow-through system containing 0.1 M PBS solution, pH 7.0, where 0.5 mM $K_4[Fe(CN)_6]$ was used as redox mediator. The system flow rate was set to 35 mL/min and turned on at 5 min mark. Where noted, glucose was added at the 10 min mark with a final concentration of 200 mM. (A) Current registered using Y@PDA-26 at different incubation durations (30, 60, and 90 min) at pH 5.0, with the following 1 h polymerization at pH 7.5. (B) Current registered using Y@PDA-26 firstly incubated 1h at pH 5.0 then polymerized at pH 7.5 with different incubation durations (1, 3, and 6 h). (C) Current registered using Y@PDA-13 and Y@PDA-26 and their response to the addition of glucose. (D) Current registered using Y@Ppy-100, Y@Ppy-300, and Y@Ppy-500 and their response to addition of glucose, additional control samples are presented. (E) Comparison of time of 2, 8, and 24 h using Y@Ppy-300. Data depicted in A, B, and C as the average signal value \pm SD [102].

3.4.2. Performance of PDA and Ppy modified yeast cells in MFC

To assess the electrochemical properties of the modified yeast, the open circuit potential and loaded circuit potential were measured, and the generated power density was subsequently calculated in the classical two-compartment MFC system. To evaluate the influence of polymer modification on charge transfer only, during the measurements, the modified yeast cells were not fed glucose. Measurements began by evaluating open circuit potential in MFC, and afterward various resistances were connected into the circuit to create circuit load, and the changes of the potential were registered. The potential was considered to reach steady state when the potential value has not changed for 10 consecutive seconds.

Two variants of Y@PDA were explored: one batch of the yeast cells were not fed with glucose during modification (Fig. 17a) and the other batch fed with 200 mM glucose during modification (Fig. 17b). In both cases, the majority of MFCs with Y@PDA samples the usual maximal calculated power density has been reached when 5.1 k Ω external resistance was applied (Fig. 17a and b). The only exception was the control system without glucose (Fig. 17a, Y@PDA-ctr w/o glu), which achieved a maximum value of power density when 10 k Ω external resistance was applied to the system. In the sample Y@PDA-13 without glucose, the maximum value of 113 $\mu\text{W}/\text{m}^2$ power density was reached at 21 mV compared to the control sample value 36 $\mu\text{W}/\text{m}^2$ at 17 mV (Fig. 17a, Y@PDA-ctr w/o glu). When yeast cells were modified in the presence of 200 mM glucose, reproducible measurements were achieved. In the electrochemical system based on Y@PDA-26 a maximum current value of 113 $\mu\text{W}/\text{m}^2$ was observed at 21 mV compared to the electrochemical system based on Y@PDA-ctr that had maximum values of 50 $\mu\text{W}/\text{m}^2$ at 14 mV (Fig. 17b). Meanwhile, the majority of control samples gave a value of 23 $\mu\text{W}/\text{m}^2$ at 9 mV. These results suggest that, when yeast cells were modified with PDA and fed glucose during modification, their possible vital functions were retained because less variance between identical biofuel systems was observed (Fig. 17b).

In comparison, Y@Ppy (Fig. 17c), which were fed with glucose during modification and during measurements, showed lower reproducibility. The maximum calculated power density was reached using 5.1 k Ω external circuit load for most of the samples modified with pyrrole. Only except for the Y@Ppy-500 sample, which reached the peak value at 10 k Ω . In the Y@Ppy-100 sample, the maximum power density of 115 $\mu\text{W}/\text{m}^2$ was reached at 21 mV, which was just slightly higher than that of the Y@Ppy-ctr sample

($84 \mu\text{W}/\text{m}^2$ at 18 mV) (Fig. 17c). Overall, the influence of Ppy modification on charge transfer in our MFC setup is deemed poor because the control sample often outperformed the modified ones.

Evaluation of Y@PDA by potentiometry reveals that polydopamine is a good agent to improve charge transfer from yeast cells. It was observed that on average the power density generated by Y@PDA-26 increased up to 5-6 times e.g. at $5.1 \text{ k}\Omega$ circuit load compared to Y@PDA-ctr MFC (Fig. 17b). These findings are similar to those previously reported in the other systems, likewise bacteria *S. xiamenensis* was also modified with PDA [91]. Evaluation of experimental results reveals that Y@PDA are well suited for biofuel cells and biosensing cell activity, while Y@Ppy, with poor MFC performance, are more suitable for biosensing cell metabolic activity in a three-electrode based amperometric setup.

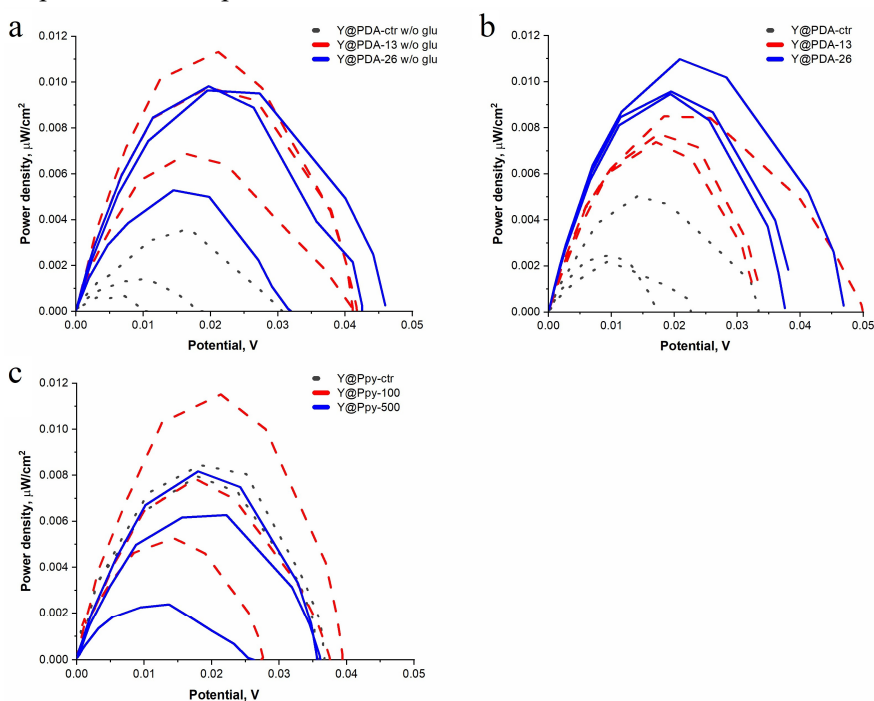


Fig. 17. Dependence of the calculated power density on the generated potential in a two compartment MFC, which consisted of (a) Y@PDA in PBS with 5 mM of $\text{K}_4[\text{Fe}(\text{CN})_6]$, (b) yeast modified with dopamine in PBS with 5 mM of $\text{K}_4[\text{Fe}(\text{CN})_6]$, and 200 mM glucose, and (c) yeast modified with Ppy in PBS with 5 mM of $\text{K}_4[\text{Fe}(\text{CN})_6]$ and 200 mM glucose. All measurements were performed in a two-electrode based electrochemical cell [102].

4. CONCLUSIONS

4.1. Polypyrrole and polydopamine synthesis

Herein the evaluation of the polymerization of pyrrole initiated by $[\text{Fe}(\text{CN})_6]^{3-}$ and controlled PDA synthesis is reported and here are main findings:

- If $[\text{Fe}(\text{CN})_6]^{4-}$ is initially added to a bulk polymerization solution must be oxidized into $[\text{Fe}(\text{CN})_6]^{3-}$ by dissolved oxygen. The formed $[\text{Fe}(\text{CN})_6]^{3-}$ then acts as the initiator of the pyrrole polymerization reaction.
- Using $[\text{Fe}(\text{CN})_6]^{3-}$ the polymerization rate of pyrrole can be controlled by varying the pH value of the polymerization bulk solution. The slowest polypyrrole formation rate was observed when the reaction was carried out at neutral pH (pH 7.0).
- There is some evidence that polypyrrole-based particle size increases by doping with $[\text{Fe}(\text{CN})_6]^{4-}$ and such doping is more efficient in an acidic medium.
- It was shown that polydopamine can be synthesized in a controlled manner by manipulating reaction solutions pH from 5.0 to 7.5.

4.2. Yeast – polymer composite enhanced chemical and physical resistances

The current results broaden our understanding of Ppy synthesis based on the redox cycling of $[\text{Fe}(\text{CN})_6]^{3-/4-}$ by yeast cells. Various indirect techniques were applied for the evaluation of Ppy-modified yeast cell biocomposite. The main findings of this research section are as follows:

- From AFM, concavalin A labeling, and lyticase digestion experiments, it was determined that polypyrrole forms small structural units within the yeast cell wall.
- AFM force indentation experiments revealed that polypyrrole changes yeast wall mechanical properties by disrupting normal wall structure in the inner layers while strengthening outer layers.
- Yeast cells modified at higher concentrations of pyrrole form a more uniform Ppy-modified cell wall matrix.
- From isotopical labeling experiments it was determined that the localization of formed Ppy is predetermined by the initial adsorption of the pyrrole monomer within the components of the cell wall, which ensures close proximity, and thus polypyrrole effectively forms only in cell wall structures.

- Ppy enhances the chemical resilience of yeast cell walls; therefore, polypyrrole can provide advanced protection of Ppy-modified yeast cells from some environmental factors.

4.3. Altered electrical properties of yeast – polymer composite

Electrochemical investigations revealed these main findings:

- Chronoamperometric experiments in the flow-through system concurred with the hypothesis that a short (2 h lasting) modification time of yeast cells with both polymers is more beneficial in terms of electrical current generation.
- Potentiometry experiments using different external resistances revealed that yeast cells modified with conducting polymers improved charge transfer in microbial fuel cells. The microbial fuel cell based on polydopamine modification generated a maximum power density of $113 \mu\text{W}/\text{m}^2$ at 21 mV compared to the untreated samples that had a maximum value of $50 \mu\text{W}/\text{m}^2$ at 14 mV. Microbial fuel cell based on polypyrrole modification generated a maximum power density of $115 \mu\text{W}/\text{m}^2$ at 21 mV compared to the untreated samples, which had a maximum value of $84 \mu\text{W}/\text{m}^2$ at 18 mV.

4.4. Novelty and significance

To the best of our knowledge, we showed for the first time the influence of oxygen on the redox-cycled synthesis of Ppy. Kinetic reaction control in this case is crucial, because only through limitation of reaction speed in free medium desired polymer localization is achieved in yeast external cell wall layers.

Some of the experiments described here are unique. Uniqueness originates from the complexity of the research object, the yeast polymer biocomposite. Due to the ‘strange’ features of the biocomposite, many conventional techniques were not suitable fit for its evaluation, therefore new methodologies had to be designed or invented. It leads to indirect approaches to characterize biocomposites. Atomic force microscopy force indentation experiments are one of them. Initially, it was believed that uniform coatings and overall stiffness were increased of the yeast cell wall, which was proven to be wrong. While isotope labeling worked well to evaluate the composition, it proved to be a good tool for polymer tracking after enzymatic digestion.

Prior to these studies, polymeric coatings were mostly associated with cell encapsulation for drug delivery or immunization. These studies were among

the first to point out the coating of yeast cells with conducting polymer polypyrrole. Subsequently, other research groups and thus emerged, studies based on the original work described in this thesis.

LITERATURE

1. Santoro, C., C. Arbizzani, B. Erable, and I. Ieropoulos, *Microbial fuel cells: From fundamentals to applications. A review*. Journal of Power Sources, 2017. **356**: p. 225-244.
2. Tsekouras, G.J., P.M. Deligianni, F.D. Kanellos, V.T. Kontargyri, P.A. Kontaxis, N.M. Manousakis, and C.N. Elias, *Microbial Fuel Cell for Wastewater Treatment as Power Plant in Smart Grids: Utopia or Reality?* Frontiers in Energy Research, 2022. **10**.
3. Puig, S., M. Serra, M. Coma, M.D. Balaguer, and J. Colprim, *Simultaneous domestic wastewater treatment and renewable energy production using microbial fuel cells (MFCs)*. Water Science and Technology, 2011. **64**(4): p. 904-909.
4. Haque, S.u., N. Duteanu, S. Ciocan, A. Nasar, and Inamuddin, *A review: Evolution of enzymatic biofuel cells*. Journal of Environmental Management, 2021. **298**: p. 113483.
5. Logan, B.E., R. Rossi, A.a. Ragab, and P.E. Saikaly, *Electroactive microorganisms in bioelectrochemical systems*. Nature Reviews Microbiology, 2019. **17**(5): p. 307-319.
6. Bruzaite, I., J. Rozene, I. Morkvenaite-Vilkonciene, and A. Ramanavicius, *Towards Microorganism-Based Biofuel Cells: The Viability of Saccharomyces cerevisiae Modified by Multiwalled Carbon Nanotubes*. Nanomaterials, 2020. **10**(5): p. 954.
7. Rozene, J., I. Morkvenaite-Vilkonciene, I. Bruzaite, A. Dzedzickis, and A. Ramanavicius, *Yeast-based microbial biofuel cell mediated by 9,10-phenanthrenequinone*. Electrochimica Acta, 2021. **373**: p. 137918.
8. Rozene, J., I. Morkvenaite-Vilkonciene, I. Bruzaite, A. Zinovicius, and A. Ramanavicius, *Baker's Yeast-Based Microbial Fuel Cell Mediated by 2-Methyl-1,4-Naphthoquinone*. Membranes, 2021. **11**(3): p. 182.
9. Van der Zee, F.P. and F.J. Cervantes, *Impact and application of electron shuttles on the redox (bio)transformation of contaminants: A review*. Biotechnology Advances, 2009. **27**(3): p. 256-277.
10. Zhou, M., J. Yang, H. Wang, T. Jin, D.J. Hassett, and T. Gu, *Chapter 9 Bioelectrochemistry of Microbial Fuel Cells and their Potential Applications in Bioenergy*, in *Bioenergy Research: Advances and Applications*. 2014. p. 131-152.
11. Ramanaviciene, A., G. Nastajute, V. Snitka, A. Kausaite, N. German, D. Barauskas-Memenas, and A. Ramanavicius, *Spectrophotometric evaluation of gold nanoparticles as red-ox mediator for glucose oxidase*. Sensors and Actuators B: Chemical, 2009. **137**(2): p. 483-489.
12. Kisieliute, A., A. Popov, R.-M. Apetrei, G. Cârâc, I. Morkvenaite-Vilkonciene, A. Ramanaviciene, and A. Ramanavicius, *Towards*

- microbial biofuel cells: Improvement of charge transfer by self-modification of microorganisms with conducting polymer – Polypyrrole*. Chemical Engineering Journal, 2019. **356**: p. 1014-1021.
13. Rudra, R., D. Pattanayak, and P. Kundu, *Conducting Polymer-Based Microbial Fuel Cells*. 2019. p. 173-187.
 14. Oztekin, Y., A. Ramanaviciene, Z. Yazicigil, A.O. Solak, and A. Ramanavicius, *Direct electron transfer from glucose oxidase immobilized on polyphenanthroline-modified glassy carbon electrode*. Biosensors and Bioelectronics, 2011. **26**(5): p. 2541-2546.
 15. Aiyer, K.S., *How does electron transfer occur in microbial fuel cells?* World Journal of Microbiology and Biotechnology, 2020. **36**(2): p. 19.
 16. Gorby, Y.A., S. Yanina, J.S. McLean, K.M. Rosso, D. Moyles, A. Dohnalkova, T.J. Beveridge, I.S. Chang, B.H. Kim, K.S. Kim, D.E. Culley, S.B. Reed, M.F. Romine, D.A. Saffarini, E.A. Hill, L. Shi, D.A. Elias, D.W. Kennedy, G. Pinchuk, K. Watanabe, S.i. Ishii, B. Logan, K.H. Nealson, and J.K. Fredrickson, *Electrically conductive bacterial nanowires produced by Shewanella oneidensis strain MR-1 and other microorganisms*. Proceedings of the National Academy of Sciences, 2006. **103**(30): p. 11358-11363.
 17. Bond, D.R. and D.R. Lovley, *Electricity Production by Geobacter sulfurreducens Attached to Electrodes*. Applied and Environmental Microbiology, 2003. **69**(3): p. 1548-1555.
 18. Pham, C.A., S.J. Jung, N.T. Phung, J. Lee, I.S. Chang, B.H. Kim, H. Yi, and J. Chun, *A novel electrochemically active and Fe(III)-reducing bacterium phylogenetically related to Aeromonas hydrophila, isolated from a microbial fuel cell*. FEMS Microbiology Letters, 2003. **223**(1): p. 129-134.
 19. Chaudhuri, S.K. and D.R. Lovley, *Electricity generation by direct oxidation of glucose in mediatorless microbial fuel cells*. Nature Biotechnology, 2003. **21**(10): p. 1229-1232.
 20. Gunawardena, A., S.D. Fernando, and F. To, *Performance of a Yeast-mediated Biological Fuel Cell*. International Journal of Molecular Sciences, 2008. **9**: p. 1893 - 1907.
 21. Ganguli, R. and B.S. Dunn, *Kinetics of Anode Reactions for a Yeast-Catalysed Microbial Fuel Cell*. Fuel Cells, 2009. **9**(1): p. 44-52.
 22. Babanova, S., Y. Hubenova, and M. Mitov, *Influence of artificial mediators on yeast-based fuel cell performance*. Journal of Bioscience and Bioengineering, 2011. **112**(4): p. 379-387.
 23. Bennetto, H.P., J.L. Stirling, K. Tanaka, and C.A. Vega, *Anodic reactions in microbial fuel cells*. Biotechnology and Bioengineering, 1983. **25**(2): p. 559-568.
 24. Wilkinson, S., J. Klar, and S. Applegarth, *Optimizing Biofuel Cell Performance Using a Targeted Mixed Mediator Combination*. Electroanalysis, 2006. **18**(19-20): p. 2001-2007.

25. Rawson, F.J., A.J. Downard, and K.H. Baronian, *Electrochemical detection of intracellular and cell membrane redox systems in Saccharomyces cerevisiae*. Scientific Reports, 2014. **4**: p. 9.
26. Duarte, K.D.Z. and Y. Kwon, *Enhanced extracellular electron transfer of yeast-based microbial fuel cells via one pot substrate-bound growth iron-manganese oxide nanoflowers*. Journal of Power Sources, 2020. **474**: p. 228496.
27. Duarte, K.D.Z., D. Frattini, and Y. Kwon, *High performance yeast-based microbial fuel cells by surfactant-mediated gold nanoparticles grown atop a carbon felt anode*. Applied Energy, 2019. **256**: p. 113912.
28. Mardiana, U., C. Innocent, M. Cretin, Buchari, H. Setiyanto, R. Nurpalah, and M. Kusmiati, *Applicability of Alginate Film Entrapped Yeast for Microbial Fuel Cell*. Russian Journal of Electrochemistry, 2019. **55**(2): p. 78-87.
29. Ramanavicius, A., E. Andriukonis, A. Stirke, L. Mikoliunaite, Z. Balevicius, and A. Ramanaviciene, *Synthesis of polypyrrole within the cell wall of yeast by redox-cycling of $[Fe(CN)_6]^{3-}/[Fe(CN)_6]^{4-}$* . Enzyme and Microbial Technology, 2016. **83**: p. 40-47.
30. Andriukonis, E., A. Ramanaviciene, and A. Ramanavicius, *Synthesis of Polypyrrole Induced by $[Fe(CN)_6]^{3-}$ and Redox Cycling of $[Fe(CN)_6]^{4-}/[Fe(CN)_6]^{3-}$* . Polymers, 2018. **10**(7): p. 12.
31. Song, R.-B., Y. Wu, Z.-Q. Lin, J. Xie, C.H. Tan, J.S.C. Loo, B. Cao, J.-R. Zhang, J.-J. Zhu, and Q. Zhang, *Living and Conducting: Coating Individual Bacterial Cells with In Situ Formed Polypyrrole*. Angewandte Chemie International Edition, 2017. **56**(35): p. 10516-10520.
32. Yang, S.H., S.M. Kang, K.-B. Lee, T.D. Chung, H. Lee, and I.S. Choi, *Mussel-inspired encapsulation and functionalization of individual yeast cells*. Journal of the American Chemical Society, 2011. **133**(9): p. 2795-2797.
33. Peter, J., M. De Chiara, A. Friedrich, J.-X. Yue, D. Pflieger, A. Bergström, A. Sigwalt, B. Barre, K. Freil, A. Llored, C. Cruaud, K. Labadie, J.-M. Aury, B. Istace, K. Lebrigand, P. Barbry, S. Engelen, A. Lemainque, P. Wincker, G. Liti, and J. Schacherer, *Genome evolution across 1,011 Saccharomyces cerevisiae isolates*. Nature, 2018. **556**(7701): p. 339-344.
34. Lian, J., S. Mishra, and H. Zhao, *Recent advances in metabolic engineering of Saccharomyces cerevisiae: New tools and their applications*. Metabolic Engineering, 2018. **50**: p. 85-108.
35. Parapouli, M., A. Vasileiadis, A.-S. Afendra, and E. Hatziloukas, *Saccharomyces cerevisiae and its industrial applications*. AIMS Microbiology, 2020. **6**(1): p. 1-31.
36. Aouizerat, T., I. Gutman, Y. Paz, M. Maeir Aren, Y. Gadot, D. Gelman, A. Szitenberg, E. Drori, A. Pinkus, M. Schoemann, R.

- Kaplan, T. Ben-Gedalya, S. Copenhagen-Glazer, E. Reich, A. Saragovi, O. Lipschits, M. Klutstein, and R. Hazan, *Isolation and Characterization of Live Yeast Cells from Ancient Vessels as a Tool in Bio-Archaeology*. *mBio*, 2019. **10**(2): p. e00388-19.
37. Raghavulu, S.V., R.K. Goud, P.N. Sarma, and S.V. Mohan, *Saccharomyces cerevisiae as anodic biocatalyst for power generation in biofuel cell: Influence of redox condition and substrate load*. *Bioresource Technology*, 2011. **102**(3): p. 2751-2757.
38. Sayed, E.T., N.A.M. Barakat, M.A. Abdelkareem, H. Fouad, and N. Nakagawa, *Yeast Extract as an Effective and Safe Mediator for the Baker's-Yeast-Based Microbial Fuel Cell*. *Industrial & Engineering Chemistry Research*, 2015. **54**(12): p. 3116-3122.
39. Otterstedt, K., C. Larsson, R.M. Bill, A. Ståhlberg, E. Boles, S. Hohmann, and L. Gustafsson, *Switching the mode of metabolism in the yeast Saccharomyces cerevisiae*. *EMBO reports*, 2004. **5**(5): p. 532-537.
40. Lapinsonnière, L., M. Picot, and F. Barrière, *Enzymatic versus Microbial Bio-Catalyzed Electrodes in Bio-Electrochemical Systems*. *ChemSusChem*, 2012. **5**(6): p. 995-1005.
41. Yang, Y., M. Xu, J. Guo, and G. Sun, *Bacterial extracellular electron transfer in bioelectrochemical systems*. *Process Biochemistry*, 2012. **47**(12): p. 1707-1714.
42. Hindatu, Y., M.S.M. Annuar, and A.M. Gumel, *Mini-review: Anode modification for improved performance of microbial fuel cell*. *Renewable and Sustainable Energy Reviews*, 2017. **73**: p. 236-248.
43. Huong Le, T.X., M. Bechelany, and M. Cretin, *Carbon felt based-electrodes for energy and environmental applications: A review*. *Carbon*, 2017. **122**: p. 564-591.
44. Mouhib, M., A. Antonucci, M. Reggente, A. Amirjani, A.J. Gillen, and A.A. Boghossian, *Enhancing bioelectricity generation in microbial fuel cells and biophotovoltaics using nanomaterials*. *Nano Research*, 2019. **12**(9): p. 2184-2199.
45. Uscátegui, Y.L., L.E. Díaz, and M.F. Valero, *In vitro and in vivo biocompatibility of polyurethanes synthesized with castor oil polyols for biomedical devices*. *Journal of Materials Research*, 2019. **34**(4): p. 519-531.
46. Wu, W., H. Niu, D. Yang, S. Wang, N. Jiang, J. Wang, J. Lin, and C. Hu, *Polyaniline/Carbon Nanotubes Composite Modified Anode via Graft Polymerization and Self-Assembling for Microbial Fuel Cells*. *Polymers*, 2018. **10**(7): p. 759.
47. Humpolicek, P., V. Kasparkova, P. Saha, and J. Stejskal, *Biocompatibility of polyaniline*. *Synthetic Metals*, 2012. **162**(7): p. 722-727.

48. Nguyen, H.H., S.H. Lee, U.J. Lee, C.D. Fermin, and M. Kim, *Immobilized Enzymes in Biosensor Applications*. Materials, 2019. **12**(1): p. 121.
49. de Oliveira, A.H.P., J.J. Alcaraz-Espinoza, M.M. da Costa, M.L.F. Nascimento, T.M. Swager, and H.P. de Oliveira, *Improvement of Baker's yeast-based fuel cell power output by electrodes and proton exchange membrane modification*. Materials Science and Engineering: C, 2019. **105**: p. 110082.
50. Habermüller, K., A. Ramanavicius, V. Laurinavicius, and W. Schuhmann, *An Oxygen-Insensitive Reagentless Glucose Biosensor Based on Osmium-Complex Modified Polypyrrole*. Electroanalysis, 2000. **12**(17): p. 1383-1389.
51. Coman, V., T. Gustavsson, A. Finkelsteinas, C. von Wachenfeldt, C. Hägerhäll, and L. Gorton, *Electrical Wiring of Live, Metabolically Enhanced Bacillus subtilis Cells with Flexible Osmium-Redox Polymers*. Journal of the American Chemical Society, 2009. **131**(44): p. 16171-16176.
52. Liu, Y., X. Zhang, Q. Zhang, and C. Li, *Microbial Fuel Cells: Nanomaterials Based on Anode and Their Application*. Energy Technology, 2020. **8**(9): p. 2000206.
53. Bahadar, H., F. Maqbool, K. Niaz, and M. Abdollahi, *Toxicity of Nanoparticles and an Overview of Current Experimental Models*. Iranian Biomedical Journal, 2016. **20**: p. 1 - 11.
54. Guo, S. and E. Wang, *Synthesis and electrochemical applications of gold nanoparticles*. Analytica Chimica Acta, 2007. **598**(2): p. 181-192.
55. Wu, X., X. Xiong, G. Owens, G. Brunetti, J. Zhou, X. Yong, X. Xie, L. Zhang, P. Wei, and H. Jia, *Anode modification by biogenic gold nanoparticles for the improved performance of microbial fuel cells and microbial community shift*. Bioresource technology, 2018. **270**: p. 11-19.
56. Al-Akraa, I.M., A.M. Mohammad, M.S. El-Deab, and B.E. El-Anadouli, *Flower-shaped gold nanoparticles: Preparation, characterization, and electrocatalytic application*. Arabian Journal of Chemistry, 2017. **10**(6): p. 877-884.
57. Christwardana, M., D. Frattini, K.D.Z. Duarte, G. Accardo, and Y. Kwon, *Carbon felt molecular modification and biofilm augmentation via quorum sensing approach in yeast-based microbial fuel cells*. Applied Energy, 2019. **238**: p. 239-248.
58. Albuquerque, P. and A. Casadevall, *Quorum sensing in fungi – a review*. Medical Mycology, 2012. **50**(4): p. 337-345.
59. Mbokou, S.F., I.K. Tonle, and M. Pontié, *Development of a novel hybrid biofuel cell type APAP/O₂ based on a fungal bioanode with a Scedosporium dehoogii biofilm*. Journal of Applied Electrochemistry, 2017. **47**(2): p. 273-280.

60. Pontié, M., E. Jaspard, C. Friant, J. Kilani, A. Fix-Tailler, C. Innocent, D. Chery, S.F. Mbokou, A. Somrani, B. Cagnon, and P.Y. Pontalier, *A sustainable fungal microbial fuel cell (FMFC) for the bioremediation of acetaminophen (APAP) and its main by-product (PAP) and energy production from biomass*. Biocatalysis and Agricultural Biotechnology, 2019. **22**: p. 101376.
61. Ramanavicius, S. and A. Ramanavicius, *Charge Transfer and Biocompatibility Aspects in Conducting Polymer-Based Enzymatic Biosensors and Biofuel Cells*. Nanomaterials, 2021. **11**(2): p. 371.
62. Holmes, D.E., T. Ueki, H.-Y. Tang, J. Zhou, J.A. Smith, G. Chaput, and D.R. Lovley, *A Membrane-Bound Cytochrome Enables &Methanosarcina acetivorans To Conserve Energy from Extracellular Electron Transfer*. mBio, 2019. **10**(4): p. e00789-19.
63. Okamoto, A., S. Kalathil, X. Deng, K. Hashimoto, R. Nakamura, and K.H. Nealon, *Cell-secreted Flavins Bound to Membrane Cytochromes Dictate Electron Transfer Reactions to Surfaces with Diverse Charge and pH*. Scientific Reports, 2014. **4**(1): p. 5628.
64. Pankratova, G., L. Hederstedt, and L. Gorton, *Extracellular electron transfer features of Gram-positive bacteria*. Analytica Chimica Acta, 2019. **1076**: p. 32-47.
65. Pankratova, G., D. Pankratov, R.D. Milton, S.D. Minter, and L. Gorton, *Extracellular Electron Transfer: Following Nature: Bioinspired Mediation Strategy for Gram-Positive Bacterial Cells*. Advanced Energy Materials, 2019. **9**(16): p. 1970055.
66. Güven, G., P. Lozano-Sanchez, and A. Güven, *Power Generation from Human Leukocytes/Lymphocytes in Mammalian Biofuel Cell*. International Journal of Electrochemistry, 2013. **2013**: p. 706792.
67. Ayato, Y., K. Sakurai, S. Fukunaga, T. Suganuma, K. Yamagiwa, H. Shiroishi, and J. Kuwano, *A simple biofuel cell cathode with human red blood cells as electrocatalysts for oxygen reduction reaction*. Biosensors and Bioelectronics, 2014. **55**: p. 14-18.
68. Andriukonis, E., A. Stirke, A. Garbaras, L. Mikoliunaite, A. Ramanaviciene, V. Remeikis, B. Thornton, and A. Ramanavicius, *Yeast-assisted synthesis of polypyrrole: Quantification and influence on the mechanical properties of the cell wall*. Colloids and Surfaces B: Biointerfaces, 2018. **164**: p. 224-231.
69. Apetrei, R.-M., G. Carac, G. Bahrim, A. Ramanaviciene, and A. Ramanavicius, *Modification of Aspergillus niger by conducting polymer, Polypyrrole, and the evaluation of electrochemical properties of modified cells*. Bioelectrochemistry, 2018. **121**: p. 46-55.
70. Apetrei, R.-M., G. Carac, A. Ramanaviciene, G. Bahrim, C. Tanase, and A. Ramanavicius, *Cell-assisted synthesis of conducting polymer – polypyrrole – for the improvement of electric charge transfer*

- through fungal cell wall*. Colloids and Surfaces B: Biointerfaces, 2019. **175**: p. 671-679.
71. Vaitkuviene, A., V. Kaseta, J. Voronovic, G. Ramanauskaite, G. Biziuleviciene, A. Ramanaviciene, and A. Ramanavicius, *Evaluation of cytotoxicity of polypyrrole nanoparticles synthesized by oxidative polymerization*. Journal of Hazardous Materials, 2013. **250-251**: p. 167-174.
 72. Vaitkuviene, A., V. Ratautaite, L. Mikoliunaite, V. Kaseta, G. Ramanauskaite, G. Biziuleviciene, A. Ramanaviciene, and A. Ramanavicius, *Some biocompatibility aspects of conducting polymer polypyrrole evaluated with bone marrow-derived stem cells*. Colloids and Surfaces A: Physicochemical and Engineering Aspects, 2014. **442**: p. 152-156.
 73. Magennis, E.P., F. Fernandez-Trillo, C. Sui, S.G. Spain, D.J. Bradshaw, D. Churchley, G. Mantovani, K. Winzer, and C. Alexander, *Bacteria-instructed synthesis of polymers for self-selective microbial binding and labelling*. Nat Mater, 2014. **13**(7): p. 748-755.
 74. German, N., A. Ramanaviciene, and A. Ramanavicius, *Formation and Electrochemical Evaluation of Polyaniline and Polypyrrole Nanocomposites Based on Glucose Oxidase and Gold Nanostructures*. Polymers, 2020. **12**(12): p. 3026.
 75. Niu, J., D.J. Lunn, A. Pusuluri, J.I. Yoo, M.A. O'Malley, S. Mitragotri, H.T. Soh, and C.J. Hawker, *Engineering live cell surfaces with functional polymers via cytocompatible controlled radical polymerization*. Nature Chemistry, 2017. **9**(6): p. 537-545.
 76. Stirke, A., R.-M. Apetrei, M. Kirsnyte, L. Dedelaite, V. Bondarenka, V. Jasulaitiene, M. Pucetaite, A. Selskis, G. Carac, G. Bahrim, and A. Ramanavicius, *Synthesis of polypyrrole microspheres by Streptomyces spp*. Polymer, 2016. **84**: p. 99-106.
 77. Sharma, T., A.L. Mohana Reddy, T.S. Chandra, and S. Ramaprabhu, *Development of carbon nanotubes and nanofluids based microbial fuel cell*. International Journal of Hydrogen Energy, 2008. **33**(22): p. 6749-6754.
 78. Zhao, C.-e., J. Chen, Y. Ding, V.B. Wang, B. Bao, S. Kjelleberg, B. Cao, S.C.J. Loo, L. Wang, W. Huang, and Q. Zhang, *Chemically Functionalized Conjugated Oligoelectrolyte Nanoparticles for Enhancement of Current Generation in Microbial Fuel Cells*. ACS Applied Materials & Interfaces, 2015. **7**(26): p. 14501-14505.
 79. Cui, Q., X. Wang, Y. Yang, S. Li, L. Li, and S. Wang, *Binding-Directed Energy Transfer of Conjugated Polymer Materials for Dual-Color Imaging of Cell Membrane*. Chemistry of Materials, 2016. **28**(13): p. 4661-4669.
 80. Apetrei, R.-M., G. Cârâc, G. Bahrim, and P. Camurlu, *Sensitivity enhancement for microbial biosensors through cell Self-Coating with*

- polypyrrole*. International Journal of Polymeric Materials and Polymeric Biomaterials, 2019. **68**(17): p. 1058-1067.
81. Ramanavicius, A., A. Kausaite, and A. Ramanaviciene, *Polypyrrole-coated glucose oxidase nanoparticles for biosensor design*. Sensors and Actuators B-Chemical, 2005. **111**: p. 532-539.
 82. Ramanavicius, A., A. Kausaite, and A. Ramanaviciene, *Self-encapsulation of oxidases as a basic approach to tune the upper detection limit of amperometric biosensors*. Analyst, 2008. **133**(8): p. 1083-1089.
 83. Olea, D., O. Viratelle, and C. Faure, *Polypyrrole-glucose oxidase biosensor: Effect of enzyme encapsulation in multilamellar vesicles on analytical properties*. Biosensors and Bioelectronics, 2008. **23**(6): p. 788-794.
 84. Mazur, M., A. Krywko-Cendrowska, P. Krysiński, and J. Rogalski, *Encapsulation of laccase in a conducting polymer matrix: A simple route towards polypyrrole microcontainers*. Synthetic Metals, 2009. **159**(17): p. 1731-1738.
 85. Ramanavicius, A., A. Kausaite, A. Ramanaviciene, J. Acaite, and A. Malinauskas, *Redox enzyme – glucose oxidase – initiated synthesis of polypyrrole*. Synthetic Metals, 2006. **156**(5): p. 409-413.
 86. Apetrei, R.-M., G. Cârâc, G. Bahrim, and P. Camurlu, *Utilization of enzyme extract self-encapsulated within polypyrrole in sensitive detection of catechol*. Enzyme and Microbial Technology, 2019. **128**: p. 34-39.
 87. Sherman, H.G., J.M. Hicks, A. Jain, J.J. Titman, C. Alexander, S. Stolnik, and F.J. Rawson, *Mammalian-Cell-Driven Polymerisation of Pyrrole*. ChemBioChem, 2019. **20**(8): p. 1008-1013.
 88. Ramanaviciene, A., A. Kausaite, S. Tautkus, and A. Ramanavicius, *Biocompatibility of polypyrrole particles: an in-vivo study in mice*. Journal of Pharmacy and Pharmacology, 2007. **59**(2): p. 311-315.
 89. Bennett, M.R., P. Gurnani, P.J. Hill, C. Alexander, and F.J. Rawson, *Iron-Catalysed Radical Polymerisation by Living Bacteria*. Angewandte Chemie International Edition, 2020. **59**(12): p. 4750-4755.
 90. Liu, S.-R., L.-F. Cai, L.-Y. Wang, X.-F. Yi, Y.-J. Peng, N. He, X. Wu, and Y.-P. Wang, *Polydopamine coating on individual cells for enhanced extracellular electron transfer*. Chemical Communications, 2019. **55**(71): p. 10535-10538.
 91. Yu, Y.-Y., Y.-Z. Wang, Z. Fang, Y.-T. Shi, Q.-W. Cheng, Y.-X. Chen, W. Shi, and Y.-C. Yong, *Single cell electron collectors for highly efficient wiring-up electronic abiotic/biotic interfaces*. Nature Communications, 2020. **11**(1): p. 4087.
 92. Yang, C., H. Aslan, P. Zhang, S. Zhu, Y. Xiao, L. Chen, N. Khan, T. Boesen, Y. Wang, Y. Liu, L. Wang, Y. Sun, Y. Feng, F. Besenbacher, F. Zhao, and M. Yu, *Carbon dots-fed Shewanella oneidensis MR-1*

- for bioelectricity enhancement*. Nature Communications, 2020. **11**(1): p. 1379.
93. Liu, S., X. Yi, X. Wu, Q. Li, and Y. Wang, *Internalized Carbon Dots for Enhanced Extracellular Electron Transfer in the Dark and Light*. Small, 2020. **16**(44): p. 2004194.
94. Aslan, S., P.Ó. Conghaile, D. Leech, L. Gorton, S. Timur, and U. Anik, *Development of an Osmium Redox Polymer Mediated Bioanode and Examination of its Performance in Gluconobacter oxydans Based Microbial Fuel Cell*. Electroanalysis, 2017. **29**(6): p. 1651-1657.
95. Yuan, Y., H. Shin, C. Kang, and S. Kim, *Wiring microbial biofilms to the electrode by osmium redox polymer for the performance enhancement of microbial fuel cells*. Bioelectrochemistry, 2016. **108**: p. 8-12.
96. Timur, S., B. Haghghi, J. Tkac, N. Pazarlıoğlu, A. Telefoncu, and L. Gorton, *Electrical wiring of Pseudomonas putida and Pseudomonas fluorescens with osmium redox polymers*. Bioelectrochemistry, 2007. **71**(1): p. 38-45.
97. Hasan, K., E. Çevik, E. Sperling, M.A. Packer, D. Leech, and L. Gorton, *Photoelectrochemical Wiring of Paulschulzia pseudovolvox (Algae) to Osmium Polymer Modified Electrodes for Harnessing Solar Energy*. Advanced Energy Materials, 2015. **5**(22): p. 1501100.
98. Andriukonis, E., R. Celiesiute-Germaniene, S. Ramanavicius, R. Viter, and A. Ramanavicius, *From Microorganism-Based Amperometric Biosensors towards Microbial Fuel Cells*. Sensors, 2021. **21**(7): p. 2442.
99. Chakrabarti, M.H. and E.P.L. Roberts, *Analysis of Mixtures of Ferrocyanide and Ferricyanide using UV-Visible Spectroscopy for Characterisation of a Novel Redox Flow Battery*. Journal of the Chemical Society of Pakistan, 2008. **30**(6): p. 817-823.
100. Appleby, C.A. and R.K. Morton, *Lactic dehydrogenase and cytochrome b(2) of baker's yeast. Purification and crystallization*. Biochemical Journal, 1959. **71**(3): p. 492-499.
101. Ball, V., D.D. Frari, V. Toniazzo, and D. Ruch, *Kinetics of polydopamine film deposition as a function of pH and dopamine concentration: Insights in the polydopamine deposition mechanism*. Journal of Colloid and Interface Science, 2012. **386**(1): p. 366-372.
102. Andriukonis, E., V. Reinikovaite, and A. Ramanavicius, *Comparative study of polydopamine and polypyrrole modified yeast cells applied in biofuel cell design*. Sustainable Energy & Fuels, 2022.
103. Ceburnis, D., A. Masalaite, J. Ovadnevaite, A. Garbaras, V. Remeikis, W. Maenhaut, M. Claeys, J. Sciare, D. Baisnée, and C.D. O'Dowd, *Stable isotopes measurements reveal dual carbon pools contributing to organic matter enrichment in marine aerosol*. Scientific Reports, 2016. **6**: p. 36675.

104. Coplen, T.B., W.A. Brand, M. Gehre, M. Gröning, H.A. Meijer, B. Toman, and R.M. Verkouteren, *New guidelines for δ ¹³C measurements*. Analytical Chemistry, 2006. **78**(7): p. 2439-2441.
105. Garbariene, I., J. Sapolaite, A. Garbaras, Z. Ezerinskas, M. Pocevicus, L. Krikscikas, A. Plukis, and V. Remeikis, *Origin identification of carbonaceous aerosol particles by carbon isotope ratio analysis*. Aerosol and Air Quality Research, 2016. **16**(6): p. 1356-1365.
106. Ling, M., F. Merante, and B.H. Robinson, *A rapid and reliable DNA preparation method for screening a large number of yeast clones by polymerase chain reaction*. Nucleic Acids Research, 1995. **23**(23): p. 4924-4925.
107. Weng, B., R. Shepherd, J. Chen, and G.G. Wallace, *Gemini surfactant doped polypyrrole nanodispersions: an inkjet printable formulation*. Journal of Materials Chemistry, 2011. **21**(6): p. 1918-1924.
108. Wagner, B.A., S. Venkataraman, and G.R. Buettner, *The Rate of Oxygen Utilization by Cells*. Free radical biology & medicine, 2011. **51**(3): p. 700-712.
109. Robinson, J. and J.M. Cooper, *Method of determining oxygen concentrations in biological media, suitable for calibration of the oxygen electrode*. Analytical Biochemistry, 1970. **33**(2): p. 390-399.
110. Yan, H., M. Kajita, and N. Toshima, *Polymerization of Aniline Using Iron(III) Catalyst and Ozone, and Kinetics of Oxidation Reactions in the Catalytic System*. Macromolecular Materials and Engineering, 2002. **287**(8): p. 503-508.
111. Toshima, N. and O. Ihata, *Catalytic synthesis of conductive polypyrrole using iron (III) catalyst and molecular oxygen*. Synthetic Metals, 1996. **79**(2): p. 165-172.
112. Zagorska, M., A. Pron, S. Lefrant, Z. Kucharski, J. Suwalski, and P. Bernier, *Synthesis and spectroscopic characterization of polypyrrole containing ferrous cyanide anions*. Synthetic Metals, 1987. **18**(1): p. 43-48.
113. Dobson, K.D. and A. James McQuillan, *An in situ IR spectroscopic investigation of adsorption of hexa- and penta-cyanoferrates to metal oxides from aqueous solution*. Physical Chemistry Chemical Physics, 2000. **2**(22): p. 5180-5188.
114. Idemura, S., E. Suzuki, and Y. Ono, *Electronic state of iron complexes in the interlayer of hydrotalcite-like materials*. Clays and Clay Minerals, 1989. **37**(6): p. 553-557.
115. Zou, Y.J., J. Cheng, C.L. Xiang, H.L. Chu, S.J. Qiu, F. Xu, L.X. Sun, and L.J. Zheng, *Preparation, Characterization of Polypyrrole Encapsulated Prussian Blue Nanocomposite and Its Application for Biosensing*. International Journal of Electrochemical Science, 2015. **10**(6): p. 4626-4636.

116. Boutry, C.M., I. Gerber-Hörler, and C. Hierold, *Electrically conducting biodegradable polymer composites (polylactide-polypyrrole and polycaprolactone-polypyrrole) for passive resonant circuits*. *Polymer Engineering & Science*, 2013. **53**(6): p. 1196-1208.
117. Liebscher, J., R. Mrówczyński, H.A. Scheidt, C. Filip, N.D. Hädäde, R. Turcu, A. Bende, and S. Beck, *Structure of Polydopamine: A Never-Ending Story?* *Langmuir*, 2013. **29**(33): p. 10539-10548.
118. Zangmeister, R.A., T.A. Morris, and M.J. Tarlov, *Characterization of Polydopamine Thin Films Deposited at Short Times by Autoxidation of Dopamine*. *Langmuir*, 2013. **29**(27): p. 8619-8628.
119. Yuan, C., Q. Liu, H. Chen, and A. Huang, *Mussel-inspired polydopamine modification of supports for the facile synthesis of zeolite LTA molecular sieve membranes*. *RSC Advances*, 2014. **4**(79): p. 41982-41988.
120. Mercadé-Prieto, R., C. Thomas, and Z. Zhang, *Mechanical double layer model for Saccharomyces Cerevisiae cell wall*. *European Biophysics Journal*, 2013. **42**(8): p. 613-620.
121. Suchodolskis, A., V. Feiza, A. Stirke, A. Timonina, A. Ramanaviciene, and A. Ramanavicius, *Elastic properties of chemically modified baker's yeast cells studied by AFM*. *Surface and Interface Analysis*, 2011. **43**(13): p. 1636-1640.
122. Dague, E., R. Bitar, H. Ranchon, F. Durand, H.M. Yken, and J.M. Francois, *An atomic force microscopy analysis of yeast mutants defective in cell wall architecture*. *Yeast*, 2010. **27**(8): p. 673-84.
123. Bui, V.C., Y.U. Kim, and S.S. Choi, *Physical characteristics of Saccharomyces cerevisiae*. *Surface and Interface Analysis*, 2008. **40**(10): p. 1323-1327.
124. Wang, B., P. Liu, W. Jiang, H. Pan, X. Xu, and R. Tang, *Yeast cells with an artificial mineral shell: protection and modification of living cells by biomimetic mineralization*. *Angew Chem Int Ed Engl*, 2008. **47**(19): p. 3560-4.
125. Yu, M. and A. Ivanisevic, *Encapsulated cells: an atomic force microscopy study*. *Biomaterials*, 2004. **25**(17): p. 3655-62.
126. Svaldo-Lanero, T., S. Krol, R. Magrassi, A. Diaspro, R. Rolandi, A. Gliozzi, and O. Cavalleri, *Morphology, mechanical properties and viability of encapsulated cells*. *Ultramicroscopy*, 2007. **107**(10-11): p. 913-21.
127. Svaldo Lanero, T., O. Cavalleri, S. Krol, R. Rolandi, and A. Gliozzi, *Mechanical properties of single living cells encapsulated in polyelectrolyte matrixes*. *Journal of biotechnology*, 2006. **124**(4): p. 723-731.
128. Dague, E., D. Alsteens, J.-P. Latgé, and Y.F. Dufrière, *High-resolution cell surface dynamics of germinating Aspergillus fumigatus Conidia*. *Biophysical Journal*, 2008. **94**(2): p. 656-660.

129. Formosa, C., F. Pillet, M. Schiavone, R.E. Duval, L. Ressler, and E. Dague, *Generation of living cell arrays for atomic force microscopy studies*. Nat. Protocols, 2015. **10**(1): p. 199-204.
130. Dague, E., E. Jauvert, L. Laplatine, B. Viallet, C. Thibault, and L. Ressler, *Assembly of live micro-organisms on microstructured PDMS stamps by convective/capillary deposition for AFM bio-experiments*. Nanotechnology, 2011. **22**(39): p. 395102.
131. Wang, H., S.-T. Yang, A. Cao, and Y. Liu, *Quantification of Carbon Nanomaterials in Vivo*. Accounts of Chemical Research, 2013. **46**(3): p. 750-760.
132. Scott, J.H. and R. Schekman, *Lyticase: endoglucanase and protease activities that act together in yeast cell lysis*. J Bacteriol, 1980. **142**(2): p. 414-23.
133. Samukaite-Bubniene, U., A. Valiūnienė, V. Bucinskas, P. Genys, V. Ratautaite, A. Ramanaviciene, E. Aksun, A. Tereshchenko, B. Zeybek, and A. Ramanavicius, *Towards supercapacitors: Cyclic voltammetry and fast Fourier transform electrochemical impedance spectroscopy based evaluation of polypyrrole electrochemically deposited on the pencil graphite electrode*. Colloids and Surfaces A: Physicochemical and Engineering Aspects, 2021. **610**: p. 125750.

SANTRAUKA

Įvadas

Biokuro elementai, tai elektrocheminiai įrenginiai, kurie išgauna elektros energiją surenkant krūvininkus iš fermentinių reakcijų metu susidariusių produktų. Per pastaruosius tris dešimtmečius biokuro elementų tyrimų sritis tapo aktuali dėl sparčiai didėjančio globalaus energijos sunaudojimo ir populiarėjančių „žaliųjų“ technologijų. Pagrindinė biokuro elementų taikymo sritis išlieka vandens valymas tuo pat metu gaminant elektrą iš nuotekų, kurios pramoninių procesų metu buvo užterštos organiniais junginiais.

Biokuro elementai yra skirstomi pagal katalizatoriaus prigimtį: fermentinius arba mikrobinius. Pastarieji skiriasi tuo, kad vieni naudoja išgrynintus fermentus, kai kiti naudoja gyvus mikroorganizmus, kurie geba papildyti fermentų kiekį biokuro elemente. Dėl mikroorganizmų greitos reprodukcijos ir technologiskai brangaus, sudėtingo fermentų gryninimo, dažnai yra manoma, kad mikroorganizmų katalizuojami biokuro elementai yra pranašesni ir perspektyvesni už fermentinius. Tiek mikrobiniai biokuro elementai (MKE) tiek fermentiniai biokuro elementai gali veikti palyginus švelniomis sąlygomis. Tačiau MKE įprastai yra ženkliai paprasčiau pagaminama, nes reikiami mikroorganizmai gali būti išgauti iš daugybės natūralių šaltinių, kaip, pavyzdžiui, purvas ar dirvožemis. Tačiau nepaisant lengvo prieinamumo, MKE technologijos dar nėra plačiai taikomos dėl prastos elektros krūvio pernašos (KP) iš mikroorganizmo link MKE elektrodų. Kitaip tariant, mikroorganizmų elektrinis laidumas, per jų sienes ir membranas yra mažas. Įprastai ši problema yra sprendžiama naudojant elektrinį laidumą didinančias medžiagas arba naudojant specifinės fiziologijos mikroorganizmus, kurie geba atlikti tiesioginę elektronų pernašą į MKE elektrodą. Elektrinį laidumą gerinančių medžiagų, dar vadinamų mediatoriais, tarpe gausu: oksidacijos laipsnį lengvai keičiančių organinių junginių ar neorganinių druskų, elektrai laidžių nano dalelių, nano strypų ar polimerų. Priklausomai nuo pasirinkto mediatoriaus, pernaša gali gerėti skirtingose zonose: MKE užpildančiame skystyje, ties MKE elektrodų paviršiumi ar ties mikroorganizmų išoriniais sluoksniais. Literatūroje gausu skirtingų sistemų, kuriose KP gerinti yra naudojama net kelių pasirinktų mediatorių kombinacijos. Dažniausiai naudojamas metodas yra kombinuoti hidrofiliinį mediatorių su lipofiliiniu mediatoriumi, kad KP pagerėtų per mikroorganizmų membraną ir MKE užpildantį skystį. Kitas dažnai naudojamas metodas yra MKE elektrodų paviršiaus modifikavimas, kad pagerėtų tiek mikroorganizmų

adhezija tiek KP į elektrodą. Tačiau paminėti metodai yra klasikiniai, ir tik pastarajame dešimtmetyje atsirado naujas KP gerinantis metodas – ląstelių paviršiaus modifikavimas elektrolaidžiais polimerais.

Ši disertacija aprašo vienus pirmųjų ir pamatinius tyrimus susijusius su mikroorganizmų modifikavimu elektrolaidžiais polimerais. Taip pat, yra nagrinėjami polimerų formavimosi principai ant mikroorganizmų paviršiaus, susidariusių polimerų fizinės bei cheminės savybės ir modifikuotų mikroorganizmų mielių taikymas mikrobinuose kuro elementuose.

Tikslas ir uždaviniai

Šioje disertacijoje yra aprašomas atradimas bei susiję tyrimai apie elektrai laidžių polimerų sintezę ties mielių ląstelių paviršiumi. Darbo pagrindinis tikslas - ištirti mielių ląstelių ir elektrolaidžių polimerų kompozitus bei pritaikyti juos biokuro elementuose. Šiam tikslui pasiekti buvo iškelti uždaviniai:

i) Įvertinti polipirolo sintezę naudojant $K_3[Fe(CN)_6]$ skirtingų pH polimerizacijos tirpaluose. Charakterizuoti susidariusį polimerą optiniais metodais;

ii) Įvertinti polidopamino sintezę skirtingose pH sąlygose. Charakterizuoti susidariusį polimerą optiniais metodais;

iii) Sukurti mielių dengimo polipirolo bei polidopaminu metodikas;

iv) Charakterizuoti mielių ląstelių ir polipirolo kompozito struktūrą, sudėtį, jo chemines bei fizines savybes;

v) Pritaikyti modifikuotas mieles mikrobinų biokuro elementų kūrime ir įvertinti kompozitų elektrochemines savybes.

Svarbiausi rezultatai

Šiame skyriuje yra pristatomi svarbiausi atradimai ar įžvalgos susijusios su atliktais eksperimentais. Atradimai aprašomi tokia eilės tvarka, kad būtų lengviau sukurta „mokslinės minties“ vystymosi eiga.

Atradimas

Pastebėjus, kad polipirolo sintezė yra galima tirpaluose, kuriuose yra mielių ląstelės ir kompleksinė druska $K_3[Fe(CN)_6]$ (Fig. 3), buvo atlikta visa eilė eksperimentų aiškinančių procesus ar susidariusiu kompozitų savybes.

Polipirola sintezė, jos valdymas

$[\text{Fe}(\text{CN})_6]^{3-}$ inicijuota polipirola (Ppy) sintezė buvo tiriama UV-Vis spektrofotometru. Pirolo (Py) monomerai yra oksiduojami su $[\text{Fe}(\text{CN})_6]^{3-}$, susidaro polipirolas, o druska redukuojasi iki $[\text{Fe}(\text{CN})_6]^{4-}$. Tyrimų metu buvo analizuojami įvairių esminių komponentų mišiniai. Taipogi buvo atlikti polipirola susidarymo realiu laiku matavimai, tiek aerobinėmis (su atmosferiniu deguonimi), tiek anaerobinėmis sąlygomis (be atmosferinio deguonies). Taip pat buvo atliekami polipirola susidarymo kinetiniai tyrimai įvairaus rūgštingumo fosfatinio buferio tirpaluose. Naudojant tyrimų metu surinktus duomenis, buvo įvertinti polipirola susidarymo reakcijos greičio parametrai, bei kiti svarbūs aspektai.

Spektrofotometru buvo galima detektuoti kelis atskirus junginius vienu metu, nes jų spektrinės savybės skiriasi (Fig. 4). Kompleksinės druskos tik oksiduota $[\text{Fe}(\text{CN})_6]^{3-}$ forma turi aiškų sugerties maksimumą regimajame spektre ties 420 nm. O redukuota forma ($[\text{Fe}(\text{CN})_6]^{4-}$) regimojoje srityje jos neturi. Tuo tarpu Polipirolas pasižymi sugertimi ties 460 nm. Jo absorbcijos spektrai buvo užregistruoti naudojant skirtingose sąlygose susidariusį Ppy, norint įvertinti ar sugerties maksimumo padėtis yra pastovi. Tačiau artimos sugerties reikšmės netrukdyt optiškai atskirti ar įvertinti reaktantų koncentracijos ar kiekio kitimo laike, nes abiejų junginių vandeninis tirpalas pasižymėjo izobestiniu tašku ties 450 nm (Fig. 5a). Tai reiškia, kad atliekant vieną matavimą, galima buvo nustatyti šių dviejų skirtingai šviesą sugeriančių medžiagų koncentracijas bei jų kiekius realiu laiku.

Toliau buvo atlikti kinetiniai tyrimai, kurių metu buvo įvertinta, kaip $[\text{Fe}(\text{CN})_6]^{3-}$ ar $[\text{Fe}(\text{CN})_6]^{4-}$ dalyvauja reakcijoje su Py, esant anaerobinėms sąlygoms. Buvo tirta Py oksidacija naudojant $[\text{Fe}(\text{CN})_6]^{3-}$, kurios metu $[\text{Fe}(\text{CN})_6]^{3-}$ redukuojasi į $[\text{Fe}(\text{CN})_6]^{4-}$. Iš tyrimų paaiškėjo, kad jeigu nėra atmosferinio deguonies, $[\text{Fe}(\text{CN})_6]^{4-}$ negali būti paverstas iš redukuotos formos į oksiduotą, todėl negali vykti tolimesnė Py oksidacijos reakcija ir nesudaro Ppy (Fig. 5b). Jei yra naudojamas $[\text{Fe}(\text{CN})_6]^{3-}$ reakcijoje su Py ir yra atmosferinės deguonies, susidaręs $[\text{Fe}(\text{CN})_6]^{4-}$ sąveikoje su deguonimi yra pakartotinai oksiduojamas į $[\text{Fe}(\text{CN})_6]^{3-}$. Jei yra naudojamas $[\text{Fe}(\text{CN})_6]^{3-}$ reakcijoje su Py ir nėra atmosferinio deguonies, susidaręs $[\text{Fe}(\text{CN})_6]^{4-}$ nėra pakartotinai oksiduojamas ir $[\text{Fe}(\text{CN})_6]^{3-}$ oksidatoriaus kiekis mažėja šioje reakcijoje. Todėl esant atmosferiniam deguoniui $[\text{Fe}(\text{CN})_6]^{3-}/[\text{Fe}(\text{CN})_6]^{4-}$ dalyvauja redukcijos oksidacijos cikle, kurio metu yra gaminamas Ppy iš Py.

Nustačius, kad $[\text{Fe}(\text{CN})_6]^{4-}$ gali būti oksiduojamas su atmosferiniu deguonimi, buvo nuspręsta ištirti vykstančių procesų greičius skirtingo

rūgštingumo tirpaluose, tikintis surasti sąlygas, kuriose polimerizacijos procesas sulėtėja arba sustoja, net ir reakcijos mišinyje esant atmosferiniam deguoniui. Buvo tirtas polipirolas susidarymas naudojant $[\text{Fe}(\text{CN})_6]^{3-}$ ir atskirai naudojant $[\text{Fe}(\text{CN})_6]^{4-}$. Įvertinus kinetinius parametrus paaiškėjo, kad naudojant $[\text{Fe}(\text{CN})_6]^{3-}$ Ppy susidarymas yra lėčiausias neutraliame reakcijos mišinyje (pH 7, Fig. 6). Tačiau $[\text{Fe}(\text{CN})_6]^{4-}$ oksidacija su atmosferiniu deguonimi į aktyvią formą $[\text{Fe}(\text{CN})_6]^{3-}$ taip pat yra lėčiausia neutraliame tirpale. Iš šių duomenų buvo daroma išvada, kad neutraliuose mišiniuose, kurie turi $[\text{Fe}(\text{CN})_6]^{4-}$ ir Py, polimerizacijos reakciją galima sulėtinti iki $v = 9,35 \cdot 10^{-7} \Delta A \cdot s^{-1}$, nes $[\text{Fe}(\text{CN})_6]^{4-}$ pirmiausia turi oksiduotis iki aktyvios formos, kas yra limituojantis faktorius. Kadangi $[\text{Fe}(\text{CN})_6]^{3-}/[\text{Fe}(\text{CN})_6]^{4-}$ gali būti regeneruojamas oksidacijos metu, todėl šis Ppy sintezės metodas buvo pavadintas redukcijos oksidacijos ciklo polimerizacija.

Polidopamino sintezė, jos valdymas

Polidopaminas, kaip ir polipirolas, yra polimeras pasižymintis elektriniu laidumu. Dopamino monomeras, baziniuose tirpaluose, patiria vidumolekulinę reorganizaciją ir autopolimerizuojasi. Todėl buvo spektriniais metodais įvertinta PDA autopolimerizacija skirtingo rūgštingumo tirpaluose (UV-Vis, Fig. 9). Kaip ir buvo tikėtasi PDA visiškai nesusidaro rūgtiniuose tirpaluose. O įvairiuose šarminiuose tirpaluose susidariusio polimero spektrinės savybės yra analogiškos (FTIR, Fig. 10). Visiškas PDA nesusidarymas rūgtiniuose tirpaluose įgalina šios sintezės valdymą. Kitaip sakant, PDA nesusidarys kol tirpalas su dopaminu nebus paveiktas šarmu ir pH neviršys 7,5.

Mielės *Saccharomyces Cerevisiae* dengtos polipirolu

Polimerų sintezės, reguliuojamos tiek pH, tiek kinetiniais aspektais, yra patogios norint valdyti procesus. Polipirolas atveju, vykdytas ląstelių dengimas polimeru, procesą kontroliuojant reakcijos kinetiniais aspektais. Pasirinktose sąlygose pirolas monomeras buvo lėtai oksiduojamas į polipirolą, tačiau tuo pat metu dėl menko savo tirpumo tirpale jis įsigirdavo į ląstelių paviršinius sluoksnius. Reakcijos greičius taip pat lėtino mažas deguonies prieinamumas, nes pagrindinis deguonies vartotojas reakcijos mišinyje buvo mielės. Todėl vienintėlis galimas $[\text{Fe}(\text{CN})_6]^{4-}$ virtimas į $[\text{Fe}(\text{CN})_6]^{3-}$ buvo tik dėl šio junginio sąveikos su mielių ląstelėse esančiomis oksidoreduktazėmis. Ši prielaida buvo keliami dėl to, kad susidariusio Ppy pagrindiniai kiekiai buvo sukaupti ties

ląstelių paviršiumi, o tirpale susidariusios pavienės Ppy dalelės nebuvo stebimos.

Siekiant paaiškinti, kodėl susidaręs Ppy yra tik ant ląstelių paviršiaus buvo atliekami įvairūs tyrimai. Naudojant atominių jėgų mikroskopu (AFM) buvo vizualizuojamas mielių ląstelių dengtų Ppy paviršius ir jo morfologija, taip pat tiriamos mielių sienelės ir Ppy kompozito mechaninės savybės. Izotopų santykio masių spektroskopija buvo naudojama įvertinti susidariusio Ppy kiekį mielių ląstelių sienelėje, bei įvertinti susidarymo greitį. Buvo atliekami klasikiniai ir fluorescencinės mikroskopijos tyrimai aprašant ląstelių sąveiką su specifiniu žymėtu baltymu bei virškinimo fermentu.

AFM tyrimų metu buvo vizualizuotas modifikuotų ląstelių paviršius. Pastarasis lyginant su natūralių ląstelių paviršiumi buvo grublėtas ir pritaikius paviršiaus lyginimo algoritmus buvo stebimas grublėtumo išsidėstymas į diskretiškas sankaupas - salas (Fig. 11). Šie pastebėjimai sufleravo, kad Ppy gali būti išsidėstęs ar susiformavęs mažomis sankaupomis dėl lokalių nukleacijos ar polimerizacijos zonų. Buvo daroma prielaida, kad Py tirpdamas ląstelės sienelėje sudaro sankaupas, iš kurių polimerizacijos metu sudarydavo polimero salelės. Tolimesnių AFM tyrimu metu buvo tiriamas ląstelių sienelių elastingumas. Modifikuotos ląstelės Ppy jėgos artėjimo kreivėse išsiskyrė turinčios du skirtingus Jungo modulius (Fig. 12, Table 4). Kitaip sakant, stebimi rezultatai sutapo su „dvigubo sluoksnio sienelės“ teoriniu modeliu, kuris teigė jog mielių ląstelių sienelė elgiasi kaip dviejų sluoksnių struktūra, ir pastarieji turi skirtingas mechanines savybes. Šiuo atveju modifikacija Ppy leido išskirti šiuos sluoksnius. Taip pat, lyginant su kontrole buvo daromos išvados, jog Ppy minkština tankesnius ląstelių sluoksnius – Ppy elgiasi kaip plastifikatorius ir sienelės Ppy kompozitas tampa elastingesnis. O minkštesnius ar mažesnio tankio sluoksnius - sutvirtina su jais susirišdamas.

Toliau, kompleksinis objektas buvo tiriamas ir aprašomas izotopų santykio masių spektroskopiją naudojant ^{15}N izotopu žymėtą Py. Naudojant įvairaus izotopinio praturtinimo Py mišinius buvo paruošti ir ištirti Ppy modifikuotų mielių ląstelių mėginiai. Šis tyrimas leido įvertinti kelis aspektus: kiekybinę pirolų absorbciją ant ląstelės paviršiaus ir koks polipirolų kiekis buvo susidaręs nuo bendros ląstelių masės (Table 5). Taip pat tai leido įvertinti susidariusio žymėto polipirolų kiekio priklausomybę nuo naudotos $[\text{Fe}(\text{CN})_6]^{4-}$ koncentracijos. Tyrimai atskleidė, kad pirolų monomerai yra linkę įsiskverbti ar absorbuotis į mielių struktūras - procesas yra priklausomas nuo koncentracijos. O maksimali absorbcija vidutiniškai yra 2-3 %, nuo bendros kompozito masės. Vykstant polimerizacijos procesui yra pasiekiami didesni

polimero kiekiai nei monomero, savaiminės absorbcijos metu į mielių ląstelių sienelės struktūras (Fig. 13).

Mielių ir polipirolo kompozitas taip pat buvo chemiškai charakterizuojamas. Fluoresceino izotiocianatu (FITC) žymėtas konkavalino A baltymas buvo naudotas atlikti fluorescencinę mikroskopiją. Konkavalino A baltymas yra specifiškas mielių ląstelių paviršiaus polisacharidams ir chemiškai sąveikauja su jais prisikabindamas prie jų. Todėl baltymo dariniai konjuguoti su įvairiomis žymėmis yra naudojami mielių paviršiaus analizei. Buvo keliami hipotezė, kad polipirolo modifikuotos mielių ląstelės gali turėti polipirolo apvaskalą. Tačiau atlikus fluorescencinės mikroskopijos tyrimą paaiškėjo, kad FITC-konkavalionas A geba sąveikauti su mielių ląstelių paviršiuje esančiais polisacharidais ir kad polipirolo danga nėra vientisa arba yra susidariusi gilesniuose ląstelės sienelės sluoksniuose (Fig. 14).

Nagrinėjant šviesinės mikroskopijos atvaizdus buvo pastebėta, kad mielių ir polipirolo kompozitas sudaro diskretišką tamsų apvaskalą (Fig. 3), todėl reikėjo įrodyti jo lokalizaciją. Todėl buvo nuėsdintos mielių ląstelių sienelės naudojant fermentą litikazę. Tai yra fermentas, kuris pasižymi endogliukanaziniu ir proteaziniu aktyvumu, gebantis skaidyti/virškinti mielių ląstelių sienelės. Šis fermentas plačiai naudojamas verčiant mielių ląsteles į sferoplastus. Procesu metu fermentui suskaidžius mielių ląstelių sienelę, ląstelės išbrinksta ir išsipučia, nes nebeturi struktūriškai svarbaus apsauginio apvaskalo. Tad eksperimentų metu natyvios ląstelės išsipūsdavo, o Ppy modifikuotos ląstelės tik dalinai formavo sferoplastus (Fig. 15). Taip pat buvo atliktas izotopinis žymėjimas prieš sienelių skaidymo eksperimentus ir buvo surenkamos „apvirškintos“ ląstelės – sferoplastai. Lyginant su kontroliniais mėginiais buvo pastebėta, kad skaidymo metu nežymi dalis ^{15}N žymėto polipirolo atsilaisvina nuo mielių ir centrifugavimo metu nebuvo surenkama (Table 6), tačiau didžioji dalis lieka. Todėl buvo daroma išvada, kad Ppy yra įsipainiojęs į mielių sienelės struktūras ir padidina mielių ląstelių sienelės atsparumą litikazės fermentui.

Mielių ir polimerų kompozitų elektrocheminės savybės

Mielių ląstelių modifikacija polidopaminu kitaip nei polipirolo buvo iškart charakterizuojama elektrocheminiais metodais. Modifikavimo principai buvo adaptuoti pagal įžvalgas tiriant polipirolo modifikaciją, bei polidopamino cheminę sintezę. Todėl modifikacija polidopaminu buvo atskirta į du etapus: inkubacijos ir sintezės. Inkubacijos metu dopaminui buvo leidžiama

įsigerti/adsorbuotis į mielių ląstelių struktūras ribojant jo autopolimerizacija rūgštinėje terpėje. Toliau įdėjus žinomą kiekį analogiško šarminio fosfatinio buferio tirpalo (galutinis tirpalo pH 7,5), buvo inicijuojama dopamino autopolimerizacija. Po skirtingomis sąlygomis atliktos modifikacijos, chronoamperometriniu metodu, pratekančioje trijų elektrodų elektrocheminėje celėje, buvo matuojamas elektrinis krūvis išgaunamas iš mielių. Pratekanti elektrocheminė celė buvo sukursta specialiai šiems tyrimams, naudojant stereolitografijos 3D spausdinimą. Celės buvo sujungtos su atviro kodo peristaltinių pompų sistemą į daugybinių celių konfigūracija, su tikslu atlikti našius matavimus. Atlikus tyrimus, buvo nustatytos optimalios sąlygos mielių modifikavimui polidopaminu: 1 val. inkubacijos, 1 val (Fig. 16a ir b). Taip polidopaminu modifikuotos ląstelės toliau buvo taikomos mikrobiniame biokuro elemente.

Analogiškai, polipirolo modifikacija, pagal chronoamperometrinius tyrimus, buvo adaptuota taikymui mikrobiniam biokuro elementui. Modifikacija polipirolu buvo sutrumpinta nuo 24 iki 2 val (Fig. 16e). Trumpesnės modifikacijos metu buvo stebimas geriausias elektrinis sistemos atsakas – išgautos elektros srovės krūvis buvo didžiausias tarp tirtų mėginių. Rezultatai atskleidė, kad pratekančioje sistemoje abi modifikacijos pagerina sistemų elektrinį atsaką.

Optimizavus mielių modifikacijas polimerais buvo sukurti du klasikiniai dviejų elektrodų konstrukcijos mikrobiniai biokuro elementai. Eksperimentu metu buvo atliekami potenciometriniai matavimai atviros grandinės bei grandinės su apkrova principais. Rezultatai parodė, kad polidopamino mielių modifikacija yra tinkama mikrobinio biokuro elementui ir išgaunamos elektros galios tankis gali būti iki 5-6 kartų didesnis negu kontrolinių mėginių (Fig. 17). Modifikacija polipirolo vienareikšmiškų rezultatų neparodė, todėl buvo pripažinta netinkama naudojimui biokuro elementuose.

Išvados

Polipirolo ir polidopamino sintezė

$[\text{Fe}(\text{CN})_6]^{3-}$ inicijuota polipirolo sintezė bei polidopamino autopolimerizacija buvo ištirta ir pagrindinės išvados yra šios:

- Kai į polimerizacijos mišinį yra įdedamas $[\text{Fe}(\text{CN})_6]^{4-}$, dėl tirpaluose esančio ištirpusio deguonies, jis pirmiausia yra oksiduojamas į $[\text{Fe}(\text{CN})_6]^{3-}$. Tada susidaręs $[\text{Fe}(\text{CN})_6]^{3-}$ gali inicijuoti ar katalizuoti pirolo polimerizacijos reakciją.

- Polipirolo polimerizaciją atliekant su $[\text{Fe}(\text{CN})_6]^{3-}$, reakcijos greitį galima manipuliuoti keičiant reakcijos mišinio pH. Ir lėčiausiai reakcija vyksta neutraliame pH (pH 7,0).
- Polipirolo dalelės didėja jas legiruojuojant $[\text{Fe}(\text{CN})_6]^{4-}$ jonais ir stebėtas didesnis legiravimo efektyvumas rūgštiniuose sintezės tirpaluose.
- Polidopamino polimero sintezę galima kontroliuoti pakeičiant reakcijos mišinio pH iš 5,0 į 7,5.

Mielių ląstelių polimero kompozito pagerintas cheminis bei fizinis atsparumas

Darbe aprašomi rezultatai praplėtė supratimą apie mielių katalizuojamą polipirolo sintezę naudojant $[\text{Fe}(\text{CN})_6]^{3-/4-}$ redukcijos oksidacijos ciklą. Įvairūs metodai buvo pasitelkti įvertinant ir aprašant polipirolo ir mielių ląstelės kompozito susidarymą. Pagrindinės išvalgos yra šios:

- Atominių jėgų mikroskopija, žymėjimas konkovalinu A ir fermentinis skaidymas naudojant litikazę atskleidė, kad polipirolas mielių ląstelėse suformuoja mažus struktūrinius vienetus.
- Atominio jėgų mikroskopijos jėgos įgilinimo eksperimentai atskleidė, kad polipirolas keičia mechanines ląstelių sienelės savybes: gilesniuose ląstelės sienelės sluoksniuose susidaręs polipirolas sutrikdo normalią sienelės struktūrą, o išoriniuose sluoksniuose - sustiprina sienelės struktūras.
- Mielių ląstelės modifikuotos naudojant aukštesnės pirolo koncentracijas suformuoja tolygesnį polipirolo-mielių ląstelių sienelės kompozitą.
- Iš izotopinio žymėjimo eksperimentų paaiškėjo kad, polipirolo lokalizacija įvyksta dėl pradinės pirolo monomero absorbcijos į mielių ląstelių sienelės struktūras. Ko pasakoje polipirolas susidaro tik aplink mielių sienelių struktūras.
- Ląstelių sienelėje įkomponuotas polipirolas pagerina cheminį mielių ląstelių sienelių atsparumą, todėl polipirolo modifikuotos ląstelės tampa chemiškai atsparesnės tam tikriems aplinkos faktoriams.

Pakeistos mielių-polimerų kompozitų elektrinės savybės

Elektrocheminiai tyrimai atskleidė:

- Chronoamperometriniai tyrimai pratenkančioje trijų elektrodų celėje atskleidė, kad atlikus trumpas (2 val.) modifikacijas tiek polipirolo tiek polidopaminu, ląstelės generuoja daugiau elektros krūvio negu mėginiai ilgiau modifikuoti vienu ar kitu polimeru.

- Potenciometriniai tyrimai atskleidė, kad mielių ląstelės modifikuotos su elektrolaidžiais polimerais pagerina krūvio pernašą. Biokuro elemento paremto polidopamino modifikacija, maksimalus galios tankis padidėja iki $113 \mu\text{W}/\text{m}^2$ ties 21 mV kai kontrolės galios tankio maksimumas buvo $50 \mu\text{W}/\text{m}^2$ ties 14 mV. Tuo metu polipirolo modifikacija pagrįsta biokuro elemento galios tankis, lyginant su kontrole, padidėjo nuo $84 \text{mW}/\text{m}^2$ ties 18 mV iki $115 \text{mW}/\text{m}^2$ ties 21 mV.

Autoriaus indėlis

Autorius yra eksperimentatorius. Didžioji dalis eksperimentų bei matavimų buvo sugalvoti ir atlikti autoriaus. Visų pateiktų publikacijų pradiniai juodraščiai buvo sukurti autoriaus. Taip pat ženklus redagavimas ir formatavimas, grafinių elementų kūrimas buvo atliktas autoriaus. Detalesnis indėlis aprašomas žemiau publikacijų sąrašė.

PUBLICATION LIST AND OTHER PUBLICITY

I [29] Ramanavicius, A., **E. Andriukonis**, A. Stirke, L. Mikoliunaite, Z. Balevicius, and A. Ramanaviciene, *Synthesis of polypyrrole within the cell wall of yeast by redox-cycling of $[Fe(CN)_6]^{3-}/[Fe(CN)_6]^{4-}$* . Enzyme and Microbial Technology, 2016. 83: p. 40-47.

<http://dx.doi.org/10.1016/j.enzmictec.2015.11.009>

The author designed most of the experiments, performed all experiments and most of the measurements, constructed initial manuscript draft, performed extensive manuscript editing, formatting, generated all graphics, and prepared for publishing.

II [30] **Andriukonis, E.**, A. Ramanaviciene, and A. Ramanavicius, *Synthesis of Polypyrrole Induced by $Fe(CN)_6^{3-}$ and Redox Cycling of $Fe(CN)_6^{4-}/Fe(CN)_6^{3-}$* . Polymers, 2018. 10(7): p. 12.

<https://doi.org/10.3390/polym1007074>

The author designed and performed all experiments and almost all measurements. Constructed initial manuscript draft, performed extensive manuscript editing, formatting, generated all graphics, and prepared for publishing.

III [68] **Andriukonis, E.**, A. Stirke, A. Garbaras, L. Mikoliunaite, A. Ramanaviciene, V. Remeikis, B. Thornton, and A. Ramanavicius, *Yeast-assisted synthesis of polypyrrole: Quantification and influence on the mechanical properties of the cell wall*. Colloids and Surfaces B: Biointerfaces, 2018. 164: p. 224-231.

<https://doi.org/10.1016/j.colsurfb.2018.01.034>

The author designed most of the experiments, performed all experiments, and almost all measurements. Constructed initial manuscript draft, performed extensive manuscript editing, formatting, generated all graphics, and prepared for publishing.

IV [98] **Andriukonis, E.**, R. Celiesiute-Germaniene, S. Ramanavicius, R. Viter, and A. Ramanavicius, *From Microorganism-Based Amperometric Biosensors towards Microbial Fuel Cells*. Sensors, 2021. 21(7): p. 2442.

<https://doi.org/10.3390/s21072442>

The author constructed initial manuscript draft and wrote Sections 1,2,5, and 6, performed extensive manuscript editing, formatting, generated some graphics, and prepared for publishing.

V [102] Andriukonis, E., V. Reinikovaite, and A. Ramanavicius, *Comparative study of polydopamine and polypyrrole modified yeast cells applied in biofuel cell design*. Sustainable Energy & Fuels, 2022.
<https://doi.org/10.1039/D2SE00634K>

The author constructed initial manuscript draft, designed and constructed experimental tools, designed experiments, performed some experiments and measurements. Performed extensive manuscript editing, generated some graphics and prepare for publishing.

Copyrights to publishing

Publication I and III were published by Elsevier. Articles are not open access publications. However, authors retain rights to original material be used in theses, dissertation or other scholar purposes. Thus, full acknowledgements to original publication should be provided as requested by publisher. Detailed information can be found here:
<https://www.elsevier.com/about/policies/copyright#Author-rights>

Publications II and IV were published by MDPI. Articles are open access publications and are published under Creative Commons Attribution 4.0 International License (<http://creativecommons.org/licenses/by/4.0/>). Full official citations of these open access articles with active DOI link are provided.

Publication V was published by Royal Society Of Chemistry. This article is not an open access publication. However, authors retain rights to original material be used in theses, dissertation or other scholar purposes. Thus, full acknowledgements to original publication should be provided as requested by publisher. Detailed information can be found here:
<https://www.rsc.org/journals-books-databases/author-and-reviewer-hub/authors-information/licences-copyright-permissions/#acknowledgements>

International conferences


1. Open readings 2019, Vilnius, Lietuva, Hanna Yeliseyeva, **Eivydas Andriukonis**, Arūnas Stirkė „*Laccase II protein display with the ysd system aga1 - aga2*“;
2. Open readings 2021, Vilnius, Lietuva, **Eivydas Andriukonis**, Marius Butkevičius „*Hydrogel based micro Ag/AgCl reference electrodes. quick prototyping of reference electrodes*“;
3. Open readings 2021, Vilnius, Lietuva, Martynas Raila, **Eivydas Andriukonis**, Arūnas Ramanavičius „*SLA 3D printing application for fast electrochemical device prototyping*“;
4. Open readings 2022, Vilnius, Lietuva, Viktorija Reinikovaitė , **Eivydas Andriukonis**, Arūnas Ramanavičius „*Polydopamine and polypyrrole application in yeast biofuel cells: a short polymer synthesis for better function*“.

Patent

Eivydas Andriukonis, Arūnas Stirkė, Lina Mikoliūnaitė, Zigmas Balevičius, Almira Ramanavičienė, Arūnas Ramanavičius, “*Pyrrulo bio-polymerization using redox mediator*“ (liet. „*Pirola bio-polimerizacija naudojant redokso tarpininką*“, LT6239B, The State Patent Bureau of the Republic of Lithuania

Article

Synthesis of Polypyrrole Induced by $[\text{Fe}(\text{CN})_6]^{3-}$ and Redox Cycling of $[\text{Fe}(\text{CN})_6]^{4-}/[\text{Fe}(\text{CN})_6]^{3-}$

Eivydas Andriukonis ¹, Almira Ramanaviciene ² and Arunas Ramanavicius ^{1,3,*} 

¹ Department of Physical Chemistry, Faculty of Chemistry and Geosciences, Vilnius University, Naugarduko 24, LT-03225 Vilnius, Lithuania; eivydas.andriukonis@chgf.vu.lt

² NanoTechnas, Center of Nanotechnology and Materials Science, Faculty of Chemistry and Geosciences, Vilnius University, Naugarduko 24, LT-03225 Vilnius, Lithuania; almira.ramanaviciene@chgf.vu.lt

³ Laboratory of Nanotechnology, Center for Physical Sciences and Technology, State Research Institute, Sauletekio Ave. 3, LT-10257 Vilnius, Lithuania

* Correspondence: arunas.ramanavicius@chgf.vu.lt

Received: 11 June 2018; Accepted: 2 July 2018; Published: 6 July 2018



Abstract: Chemical synthesis of the conducting polymer polypyrrole induced by $[\text{Fe}(\text{CN})_6]^{3-}$ is reported. Reaction kinetics were characterized spectrophotometrically. Reaction rate was evaluated at several different pH levels in the presence of $[\text{Fe}(\text{CN})_6]^{3-}$ and $[\text{Fe}(\text{CN})_6]^{4-}$ ions. The formation of polypyrrole at aerobic and anaerobic conditions was evaluated. We report that at anaerobic conditions $[\text{Fe}(\text{CN})_6]^{4-}$ cannot initiate oxidative polymerization, while its oxidized form $[\text{Fe}(\text{CN})_6]^{3-}$ successfully initiates and maintains the pyrrole polymerization reaction. The formation of polypyrrole was also observed in the solution containing a pyrrole monomer, $[\text{Fe}(\text{CN})_6]^{4-}$ and dissolved oxygen due to re-oxidation (redox cycling) of $[\text{Fe}(\text{CN})_6]^{4-}$ into $[\text{Fe}(\text{CN})_6]^{3-}$ by dissolved oxygen. Experiments to determine the polymerization reaction rate were performed and showed the highest rate in the presence of 0.5 mM of $[\text{Fe}(\text{CN})_6]^{3-}$ at pH 9.0, while the polymerization reaction performed at pH 7.0 was determined as the slowest. This investigation opens new horizons for the application of $[\text{Fe}(\text{CN})_6]^{4-}/[\text{Fe}(\text{CN})_6]^{3-}$ -based redox cycling reactions in the synthesis of the conducting polymer polypyrrole and potentially in the formation of other conducting polymers which can be formed by oxidative polymerization.

Keywords: conducting polymers; polypyrrole; polymerization reaction; reaction kinetics; redox cycling; initiator of polymerization

1. Introduction

Conducting polymers have been a subject of great interest over the last 20 years. They are applied as conductors or semiconductors in many technological areas including the design of sensors and biosensors [1,2]. Among conducting polymers polypyrrole (Ppy) is one of the most widely investigated due to its excellent environmental and thermal stability, good electrical conductivity, useful optical properties, and insolubility in common organic solvents [3]. Polypyrrole has found attractive applications as one of the fundamental building materials in the design of various electronic analytical tools, solar cells, and light-weight batteries. It has attracted much interest in the development of biosensors based on immobilized biological substances in various fields such as health care, immunosensors, DNA sensors, biosensors, environmental monitoring, and food analysis [3,4]. In biosensors polypyrrole is used as an effective matrix for the immobilization of redox compounds [5,6], enzymes [7–10], DNA [11,12] or antibodies [11].

Synthesis of polypyrrole can be performed in many ways. The most efficient methods of conducting polymer synthesis are based on (i) chemical oxidative polymerization [6,12–16],

(ii) electrochemical polymerization [17], (iii) enzymatic polymerization [7–10], and (iv) UV-induced polymerization [18]. Significant differences between Ppy formed by the above mentioned synthesis methods allow the formation of a wide variety of different Ppy forms ranging from simple semi-conducting polymer films to polymeric nanoparticles [19,20]. It should be noted that using the listed methods not only polypyrrole but similar conducting polymers such as polyaniline [21] and polythiophene [22] can also be synthesized. However, among these conducting polymers Ppy is the most interesting due to its high biocompatibility and possible application in biomedicine [12,20,23].

Various oxidants including FeCl_3 , $(\text{NH}_4)_2\text{S}_2\text{O}_8$ and H_2O_2 are used as initiators of the chemical synthesis of polypyrrole [9,24–26]. These oxidants are mostly used for the chemical formation of Ppy. In the presence of the above mentioned oxidisers the formation of Ppy is very fast due to the relatively high oxidation potential of the oxidants. The polymerization reaction rate is very important for the control of particle size, shape, and some other properties [27]. In some particular cases the polymerization rate is controlled by the variation of temperature, but other parameters as size and shape are rarely controlled this way [28]. From a technological point of view it is important to determine relatively mild oxidative conditions suitable for the chemical synthesis of Ppy which will allow slower and better controlled formation of Ppy. $\text{K}_3[\text{Fe}(\text{CN})_6]$ was chosen as an oxidizer because it has smaller oxidation potential in water ($\sim +0.4$ V) compared to that of FeCl_3 or H_2O_2 (approximately $+0.7$ V).

All chemical and physical properties of $\text{K}_3[\text{Fe}(\text{CN})_6]/\text{K}_4[\text{Fe}(\text{CN})_6]$ are well known. Both oxidized and reduced forms of this redox-pair are easily traceable with optical and electrochemical techniques. This complex salt is able to act as a redox couple $[\text{Fe}(\text{CN})_6]^{3-}/[\text{Fe}(\text{CN})_6]^{4-}$ and is very often used as a soluble redox mediator in the design of amperometric biosensors [29] and biofuel cells [30–33]. In several studies this redox compound was applied as a dopant of a Ppy layer [34–36]. In most cases either other oxidizing agents were used as pyrrole polymerization initiators or an external potential had been applied to initiate the formation of Ppy. Up until now little research was dedicated to the application of $\text{K}_3[\text{Fe}(\text{CN})_6]$ in Ppy synthesis [6,37,38]. Therefore, not all aspects of $\text{K}_3[\text{Fe}(\text{CN})_6]$ -initiated Ppy synthesis were evaluated. Altogether Ppy synthesis induced by $\text{K}_3[\text{Fe}(\text{CN})_6]$ can be very promising and technologically useful due to direct synthesis and doping of the formed Ppy with $[\text{Fe}(\text{CN})_6]^{3-}$ or $[\text{Fe}(\text{CN})_6]^{4-}$ ions.

In this research we investigated the ability of $[\text{Fe}(\text{CN})_6]^{3-}$ to initiate the synthesis of Ppy. The possibility of exploiting the redox cycling of $[\text{Fe}(\text{CN})_6]^{3-}/[\text{Fe}(\text{CN})_6]^{4-}$ by dissolved oxygen during the synthesis of Ppy has been evaluated. The influence of pH on polymerization reaction kinetics has been investigated.

2. Methodology

2.1. Reagents and Materials

Potassium hexacyanoferrate (II) trihydrate ($\text{K}_4[\text{Fe}(\text{CN})_6]\cdot 3\text{H}_2\text{O}$, in further text depicted as $[\text{Fe}(\text{CN})_6]^{4-}$), was purchased from Carl Roth GmbH&Co (Karlsruhe, Germany). Pyrrole (Py) (98%) was purchased from Sigma-Aldrich (St. Luis, MO, USA) and Fluka Chemie GmbH (Buchs, Switzerland). Sodium phosphate dibasic and potassium hexacyanoferrate(III) $\text{K}_3[\text{Fe}(\text{CN})_6]$, depicted as $[\text{Fe}(\text{CN})_6]^{3-}$, were purchased from Sigma-Aldrich Laborchemikalien GmbH (Seelze, Germany).

2.2. Apparatus

The spectrophotometric measurements were performed with a Lambda 25 UV-VIS spectrophotometer and a Spectrum 100 Fourier transform infrared spectroscopy (FTIR) from Perkin Elmer (Waltham, MA, USA) using UV-cuvettes from semi-micro (Brand®) (Wertheim, Germany). Particles and aggregates were inspected with a Helios nanolap 650 focused ion beam scanning electron microscope (FIB SEM, Hillsboro, OR USA) and a Bruker Autoflex Max matrix-assisted laser desorption/ionization time of flight spectroscopy (MALDI ToF, Karlsruhe, Germany).

2.3. Evaluation of Ppy Synthesis Initiated by $[\text{Fe}(\text{CN})_6]^{3-}$

The standard solutions used in this research consisted of 0.1 M phosphate buffered saline (PBS) of different pHs with 0.04–0.1 M $[\text{Fe}(\text{CN})_6]^{3-}$ and/or $[\text{Fe}(\text{CN})_6]^{4-}$. Visual test of Ppy formation was performed at 0.04 M concentration of $[\text{Fe}(\text{CN})_6]^{3-}$ or $[\text{Fe}(\text{CN})_6]^{4-}$ with 0.5 M of pyrrole. Exact compositions of the solutions and visual evaluation of polymerization are indicated in Table 1. The same conditions were used to prepare Ppy for experiments with FTIR, matrix-assisted laser desorption/ionization time of flight (MALDI ToF), and focused ion beam scanning electron microscope (FIB SEM). The reaction was performed for 24 h with the reaction mixture mixed by an orbital shaker at 200 revolutions per minute at 30 °C. The synthesized polymer was centrifuged and supernatant (reaction mixture) was decanted. Collected sediments were washed multiple times using 1 mL of distilled water. Afterwards, the polymer was dried by being heated to 90 °C under a gentle stream of nitrogen gas. Dried samples were then analysed with an infrared spectrometer.

Table 1. Visual evaluation of Ppy (dark precipitant) formation in solutions with different compositions, performed at 0.04 M concentration of $[\text{Fe}(\text{CN})_6]^{3-}$ or $[\text{Fe}(\text{CN})_6]^{4-}$ with 0.5 M of pyrrole.

Sample No.	Compositions			Description of Result
	$[\text{Fe}(\text{CN})_6]^{3-}$	$[\text{Fe}(\text{CN})_6]^{4-}$	Pyrrole	
1	0.04 M	-	0.5 M	Ppy was formed instantly
2	-	0.04 M	0.5 M	Ppy distinctly appeared only after 1–2 days

The samples were prepared by mixing pre-calculated amounts of initial standard solutions directly before experiments. Reactions were performed in different pHs PBS solutions usually containing 0.5 mM $[\text{Fe}(\text{CN})_6]^{3-}$ or $[\text{Fe}(\text{CN})_6]^{4-}$ and a 0.5 M concentration of Py. The polymerization was studied at three different $[\text{Fe}(\text{CN})_6]^{4-}$ concentrations of 0.1, 0.5 and 1 mM and at two $[\text{Fe}(\text{CN})_6]^{3-}$ concentrations of 0.1 and 0.5 mM, at pH 3.0, 5.0, 7.0 and 9.0. The kinetics of the reactions were evaluated by measuring the absorption at 420 nm and 460 nm wavelengths, which are related to optical absorption of $[\text{Fe}(\text{CN})_6]^{3-}$ [39] (Figure 1a) and Ppy [9] (Figure 1b). The molar coefficient of optical extinction for $[\text{Fe}(\text{CN})_6]^{3-}$ is $1179 \text{ mol}^{-1} \cdot \text{dm}^3 \text{ cm}^{-1}$, determined experimentally, while other authors describe the slightly lower value of $1040 \text{ mol}^{-1} \cdot \text{dm}^3 \text{ cm}^{-1}$ [40]. $[\text{Fe}(\text{CN})_6]^{4-}$ did not show any significant absorption maximum in the visible light region (Figure 1a). These measurements were performed at aerobic conditions with oxygen from the ambient atmosphere dissolved in the reaction mixture, and at anaerobic conditions when oxygen was removed by argon gas. For the later experiments oxygen was removed from the standard solutions by purging with argon gas for 20 min, after which the solutions were tightly sealed for later use. Cuvettes were also filled with argon and then sealed. To ensure oxygen free reactions cuvette filling was performed under a gentle argon gas stream and sealed with a cuvette cap. All measurements were performed at least 3 times. Curves represented in graphs are average values of repeated measurements.

Samples for MALDI ToF and FIB SEM analysis after the synthesis were collected by filtering through Milipore polycarbonate filters (pore size 0.22 μm) and lyophilized prior to the analysis. For MALDI ToF measurements Ppy powder (7–10 mg/mL) was dissolved in methanol, tetrahydrofuran, and dimethyl sulphone mixture at a ratio of 49:49:2. To assist solvation samples were sonicated in an ultrasound bath for 1 h at 60 °C. It was observed that only a small part of Ppy had dissolved, possibly around 5% of the total mass. The obtained Ppy suspension was diluted with the matrix compound *trans*-2-[3-(4-*tert*-Butylphenyl)-2-methyl-2-propenylidene]malononitrile (DCTB, $M_r = 250.6 \text{ g/mol}$) methanol based solution (30 mg/mL) [41] up to a 1:10 ratio. Samples with diluted Ppy were then transferred on a MALDI ToF plate and left to crystallize before analysis. Using the linear MALDI ToF detector Ppy was sampled in all possible mass intervals from 500 Da to 210 kDa.

For FIB SEM images Ppy samples were suspended in methanol and suspension transferred on microscopic glass. Samples were coated with a thin chrome layer prior to visualization.

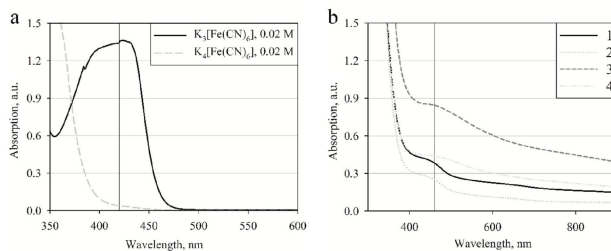


Figure 1. (a) Optical absorbance spectra of 0.02 M of $[\text{Fe}(\text{CN})_6]^{3-}$ and 0.02 M of $[\text{Fe}(\text{CN})_6]^{4-}$. The vertical line indicates the absorption maximum at 420 nm; (b) Optical absorbance spectra of Ppy synthesized under different conditions: (1) polymerization solution containing 0.5 M of pyrrole and 0.04 M of $[\text{Fe}(\text{CN})_6]^{3-}$, spectrum was registered after 24 h from the initialization of the polymerization reaction, (2) supernatant collected after 24 h of polymerization followed by centrifugation at 12,000 g for 10 min, (3) 0.375 M of pyrrole and 0.1 M of $[\text{Fe}(\text{CN})_6]^{3-}$ spectrum registered after 24 h of polymerization, (4) 1.5 M of pyrrole and 0.25 M of $[\text{Fe}(\text{CN})_6]^{3-}$ spectrum registered after 24 h of polymerization. All spectra were registered in a 0.1 M PBS, pH 7.0. The vertical line indicates poorly expressed absorption maximum at 460 nm.

3. Results and Discussion

Dissolved $[\text{Fe}(\text{CN})_6]^{3-}$ acted as an oxidant which induced the polymerization of pyrrole in both oxygen-containing and oxygen-free solutions. In the samples containing pyrrole and $[\text{Fe}(\text{CN})_6]^{4-}$ the formation of Ppy was observed only when oxygen was present in the solution. All the related experiments and kinetics of the polymerization of pyrrole are evaluated and described below.

3.1. Polypyrrole Formation

In the first part of this research the formation of Ppy was evaluated under different combinations of initial concentrations of compounds (Table 1). As expected $[\text{Fe}(\text{CN})_6]^{3-}$ acting as an oxidant resulted in much faster formation of Ppy (Table 1, sample No. 1) in comparison with the formation rate observed in $[\text{Fe}(\text{CN})_6]^{4-}$ solution (Table 1, sample No. 2). Ppy formation was much slower in the presence of $[\text{Fe}(\text{CN})_6]^{4-}$ because $[\text{Fe}(\text{CN})_6]^{4-}$ first needs to be oxidized into $[\text{Fe}(\text{CN})_6]^{3-}$ by dissolved oxygen. It is assumed that $[\text{Fe}(\text{CN})_6]^{4-}$ cannot initiate the polymerization of pyrrole before it is oxidized (Table 1, sample No. 2). To prove this assumption spectrophotometric evaluation of Ppy formation was conducted.

3.2. Spectrophotometric Evaluation of Ppy Formation Initiated by $[\text{Fe}(\text{CN})_6]^{3-}$

$[\text{Fe}(\text{CN})_6]^{3-}$ initiated Ppy formation was evaluated by UV-Vis spectrophotometry. Polymerization experiments were started by adding pyrrole into a reaction buffer containing $[\text{Fe}(\text{CN})_6]^{3-}$ or $[\text{Fe}(\text{CN})_6]^{4-}$.

Measurements were performed at wavelength ranges where selected compounds showed almost independent optical absorption. Spectra of $[\text{Fe}(\text{CN})_6]^{3-}$, $[\text{Fe}(\text{CN})_6]^{4-}$, and Ppy, which was formed using $[\text{Fe}(\text{CN})_6]^{3-}$, were measured in the range between 300 and 900 nm (Figure 1). $[\text{Fe}(\text{CN})_6]^{3-}$ has an absorption maximum at 420 nm (Figure 1a). $[\text{Fe}(\text{CN})_6]^{4-}$ does not show any distinct absorption maximum in the visible light region (Figure 1a). A poorly expressed optical absorption maximum of Ppy was recorded at 460 nm (Figure 1b) which is in line with data reported in other researches [9,42]. As is described in the literature this is a typical double bond absorption, which is measurable when

delocalized electrons are transferred from bonding orbitals to non-bonding orbitals (π - π^*), though this type of absorption is only characteristic of relatively short chains or small particles of Ppy [42]. Ppy spectra were recorded in different samples with varying concentrations of initial materials to evaluate if the absorption maximum of Ppy remained at a constant wavelength. Results show that the absorption maximum is constant and does not shift sideways, although some unspecific absorbance was observed. We presume that this absorption in a wide range of wavelengths appeared due to light scattering combined with other secondary effects induced by larger Ppy particles. In all these reactions no additional chemicals which can affect Ppy particle size were used, however due to a relatively high oxidizer ($[\text{Fe}(\text{CN})_6]^{3-}$) concentration the formation of Ppy particles of different size was observed.

Further changes of spectra during the course of polymerization initiated by $[\text{Fe}(\text{CN})_6]^{3-}$ were inspected. Polymerization was performed in 0.1 M PBS, pH 7.0, with 0.5 mM of $[\text{Fe}(\text{CN})_6]^{3-}$ and 0.5 M of pyrrole. Absorption spectra were registered at chosen time intervals (Figure 2a). In this experiment optical absorption at $\lambda = 420$ nm has decreased indicating that $[\text{Fe}(\text{CN})_6]^{3-}$ is involved in the reaction with pyrrole monomers and is reduced by pyrrole. The origin of optical absorbance increases in the range from 450 to 700 nm which is most probably related to the interconnection of shorter Ppy polymer chains. Such prolongation of conjugated double bond systems induces a bathochromic absorption shift. In this particular experiment the polymerization reaction initiated with 0.5 mM $[\text{Fe}(\text{CN})_6]^{3-}$ was relatively slow. In Figure 2a an isosbestic point at $\lambda = 450$ nm was observed. This indicates that during a time frame lasting up to 2 h from initialization of the polymerization reaction the spectra of $[\text{Fe}(\text{CN})_6]^{3-}$ and Ppy are still not overlaying one another. This allows spectrophotometric measurement of both $[\text{Fe}(\text{CN})_6]^{3-}$ and Ppy independently.

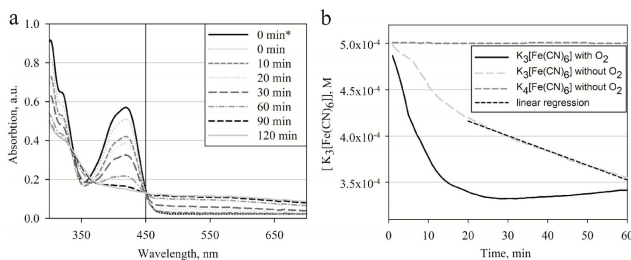
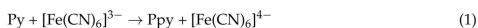


Figure 2. (a) Change of absorption spectra of a sample containing 0.5 mM $[\text{Fe}(\text{CN})_6]^{3-}$ and 0.5 M of pyrrole at different incubation periods; (b) evolution of absorption at 420 nm vs. incubation time in a solution consisting of 0.5 M of pyrrole with either 0.5 mM of $[\text{Fe}(\text{CN})_6]^{3-}$ or 0.5 mM of $[\text{Fe}(\text{CN})_6]^{4-}$ at pH 7.0, under aerobic and anaerobic conditions. Linear regression from $t = 20$ min was observed with $R^2 = 0.9933$; 0 min*, spectra registered before the addition of Py into reaction mixture.

Similar experiments were performed measuring optical absorption at $\lambda = 420$ nm while the reaction was performed at aerobic and anaerobic conditions. In these experiments the reduction of $[\text{Fe}(\text{CN})_6]^{3-}$ by pyrrole to $[\text{Fe}(\text{CN})_6]^{4-}$ was observed. In Figure 2b curves which indicate $[\text{Fe}(\text{CN})_6]^{3-}$ concentration changing in time at aerobic and anaerobic conditions are presented. In a reaction mixture which contained 0.5 M of pyrrole and 0.5 mM of $[\text{Fe}(\text{CN})_6]^{3-}$ at aerobic conditions the process reaches equilibrium during the 35th minute after the initialization of the polymerization reaction. The formed $[\text{Fe}(\text{CN})_6]^{4-}$ is re-oxidized back into $[\text{Fe}(\text{CN})_6]^{3-}$ by oxygen dissolved in the solution and the concentration of $[\text{Fe}(\text{CN})_6]^{3-}$ remains constant after this point. The concentration of dissolved oxygen in a reaction mixture of 0.1 M PBS, pH 7.0, at 25 °C is ~ 250 μM [43,44]. Alternatively under anaerobic conditions $[\text{Fe}(\text{CN})_6]^{3-}$ reacts slowly with pyrrole and the concentration of $[\text{Fe}(\text{CN})_6]^{3-}$ steadily

decreases. The decrease of $[\text{Fe}(\text{CN})_6]^{3-}$ concentration from the 20th minute after the initialization of polymerization reaction can be approximated using a linear function with regression coefficient $R^2 > 0.99$. This suggests that during polymerization the formed $[\text{Fe}(\text{CN})_6]^{4-}$ is not oxidized back into $[\text{Fe}(\text{CN})_6]^{3-}$. From this graph it is possible to determine that at anaerobic conditions with an excess of pyrrole the polymerization reaction is terminated when all $[\text{Fe}(\text{CN})_6]^{3-}$ is consumed or has reached its lowest thermodynamically favorable concentration. At aerobic conditions the cycling of oxidation and reduction reactions take place, which only stop when all pyrrole has been polymerized into polypyrrole. In both reactions Ppy formation was observed, however this is not represented in figures. In anaerobic conditions the reaction between $[\text{Fe}(\text{CN})_6]^{4-}$ and pyrrole was also inspected and no transition or oxidation from $[\text{Fe}(\text{CN})_6]^{4-}$ to $[\text{Fe}(\text{CN})_6]^{3-}$ or formation of Ppy was observed (Figure 2b). Constant oxidation of $[\text{Fe}(\text{CN})_6]^{4-}$ into $[\text{Fe}(\text{CN})_6]^{3-}$ at aerobic conditions without Py was also observed, although the data is not presented. The experiment described here proves that the re-oxidation step of $[\text{Fe}(\text{CN})_6]^{4-}$ is essential in order to produce Ppy efficiently at relatively low initial concentrations of $[\text{Fe}(\text{CN})_6]^{3-}$. This shows that the $[\text{Fe}(\text{CN})_6]^{3-}/[\text{Fe}(\text{CN})_6]^{4-}$ is reusable in the initiation of Ppy polymerization reactions. Few studies have pointed out that iron compounds such as FeCl_3 and Fe_2O_3 can be regenerated and reused in Ppy and polyaniline synthesis when they are coupled with an oxidation cycle by oxygen [45,46].

As the above shows, the re-oxidation of $[\text{Fe}(\text{CN})_6]^{4-}$ into $[\text{Fe}(\text{CN})_6]^{3-}$ has been performed by oxygen dissolved in PBS under standard conditions. To control this process it is important to find conditions where the influence of dissolved oxygen on the reaction is the lowest or has no impact at all. In Figure 3 graphs represent both the variation rate of $[\text{Fe}(\text{CN})_6]^{3-}$ concentration and the rate of Ppy formation at different pH values measured at 420 and 460 nm. Measurements were performed in a 0.1 M PBS of different pHs. 0.5 M of pyrrole was present in all these reaction mixtures and 0.5 mM of $[\text{Fe}(\text{CN})_6]^{3-}$ or 0.5 mM of $[\text{Fe}(\text{CN})_6]^{4-}$ were added into the polymerization solution. At different pH values we observed polymerization of Ppy using $[\text{Fe}(\text{CN})_6]^{3-}$ according to reaction Equation (1).



In this polymerization reaction (Equation (1)), the rate of $[\text{Fe}(\text{CN})_6]^{3-}$ concentration change through time was evaluated and is represented in Figure 3a. The Ppy formation rate was evaluated and is represented in Figure 3c. The other two graphs represent kinetic parameters of the subsequent cascade of reactions (Equation (2)):

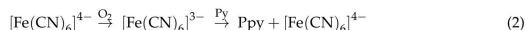


Figure 3b represents the rate of change of $[\text{Fe}(\text{CN})_6]^{3-}$ concentration and Figure 3d addresses the formation rate of Ppy. In Figure 3b the represented rates correspond to changes of overall $[\text{Fe}(\text{CN})_6]^{3-}$ concentration. During the experiment a constant increase of $[\text{Fe}(\text{CN})_6]^{3-}$ concentration was observed, illustrating that the oxidation of $[\text{Fe}(\text{CN})_6]^{4-}$ to $[\text{Fe}(\text{CN})_6]^{3-}$ is faster than the reduction of $[\text{Fe}(\text{CN})_6]^{3-}$ by Ppy. In Figure 3a, the rates of $[\text{Fe}(\text{CN})_6]^{3-}$ concentration decrease ($v = 1.75 \times 10^{-7} \text{ mol}\cdot\text{s}^{-1}$ and $v = 4.74 \times 10^{-7} \text{ mol}\cdot\text{s}^{-1}$) indicate that the reaction is faster at neutral pH (pH 7.0) and at basic conditions (pH 9.0). In Figure 3b the formation of $[\text{Fe}(\text{CN})_6]^{3-}$ from $[\text{Fe}(\text{CN})_6]^{4-}$ due to oxidation by dissolved ambient oxygen is represented. The slowest oxidation of $[\text{Fe}(\text{CN})_6]^{4-}$ into $[\text{Fe}(\text{CN})_6]^{3-}$ occurs at pH 7.0 with a reaction rate of $v = 3.10 \times 10^{-9} \text{ mol}\cdot\text{s}^{-1}$. This process is approximately two orders of magnitude slower than that described above. Figure 3c,d represent Ppy formation rates in the presence of $[\text{Fe}(\text{CN})_6]^{3-}$ and $[\text{Fe}(\text{CN})_6]^{4-}$ respectively. In both cases polypyrrole particles are formed the slowest at pH 7.0. In the presence 0.5 mM of $[\text{Fe}(\text{CN})_6]^{3-}$ the reaction rate was $v = 2.24 \times 10^{-6} \Delta\text{A}\cdot\text{s}^{-1}$, and in the presence 0.5 mM of $[\text{Fe}(\text{CN})_6]^{4-}$ it was equal to $v = 9.35 \times 10^{-7} \Delta\text{A}\cdot\text{s}^{-1}$. From these results it can be estimated that if $[\text{Fe}(\text{CN})_6]^{4-}$ is in the same reaction mixture with Py at aerobic conditions and at pH 7.0 then the oxidation process (Equation (2)) is the rate determining step for the whole polymerization process. Consequently, the variation of pH can be exploited to control reaction kinetics.

Differences in Ppy formation rates determined at different pH values suggest that the polymer might undergo polymerization under two different mechanisms. According to the detailed Ppy synthesis mechanism proposed in [15] there are few steps during the prolongation of Ppy chains when formed Ppy undergoes deprotonation. In the basic pH range hydroxyl ions might promote this deprotonation process. However, in an acidic medium deprotonation is slower, therefore the velocity of Ppy prolongation is also slower than the initiation of Ppy chain formation where protonation is important, therefore short Ppy oligomers are formed more rapidly. This could be the reason why reaction rates were almost 4 times higher in basic solutions than those in acidic solutions (Figure 3c). In the case of Ppy chain prolongation longer Ppy chains absorb visible light mostly at 460 nm. The increased acidity facilitates the polymerization initiation step during which short Ppy oligomer chains appear more rapidly than the long ones.

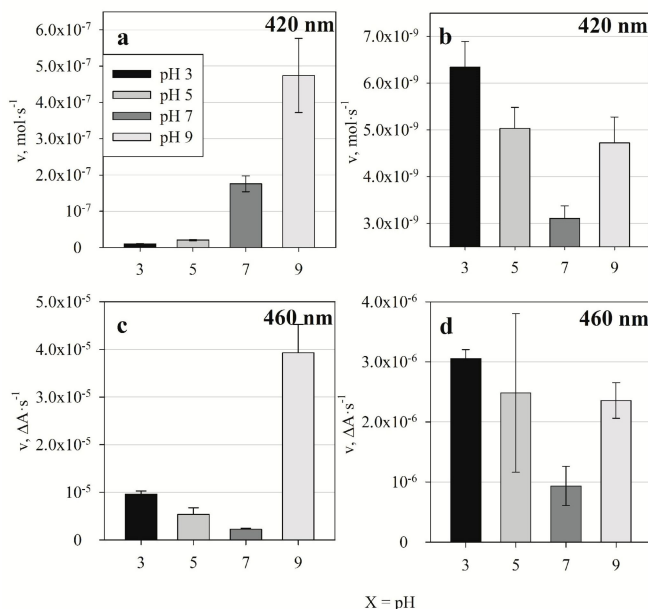


Figure 3. Reaction rates at different pH values: (a) $[\text{Fe}(\text{CN})_6]^{3-}$ concentration decrease rate was measured at 420 nm in the presence of $[\text{Fe}(\text{CN})_6]^{3-}$ and pyrrole due to the formation of Ppy; (b) $[\text{Fe}(\text{CN})_6]^{3-}$ concentration increase rate due to the re-oxidation of $[\text{Fe}(\text{CN})_6]^{4-}$ by dissolved oxygen was measured at $\lambda = 420$ nm; (c) Ppy polymerization rate in the presence of $[\text{Fe}(\text{CN})_6]^{3-}$ measured at $\lambda = 460$ nm; (d) Ppy polymerization rate in the presence of $[\text{Fe}(\text{CN})_6]^{4-}$ at 460 nm. In all samples 0.5 M of pyrrole and either 0.5 mM of $[\text{Fe}(\text{CN})_6]^{3-}$ or 0.5 mM of $[\text{Fe}(\text{CN})_6]^{4-}$ was used. All reactions were performed in aerobic conditions. Error bars indicates standard deviation of the calculated reaction rate.

3.3. Ppy Doping in Acidic Medium and Characterization of Aggregates

The polypyrrole powders prepared at different pH values were analysed by FTIR. All Ppy samples were synthesized using $K_3[Fe(CN)_6]$ in PBS at pH values of 3.0, 5.0, 7.0 and 9.0. FTIR spectra (Figure 4) showed main characteristics peaks at 774, 1039, 1183, 1563, and 1690 cm^{-1} and a broad band at ~ 3100 – 3500 cm^{-1} . These peaks were observed in all samples. A variable peak at 2071 cm^{-1} has been observed in Ppy which was formed in an acidic polymerization solution. The main FTIR characteristic peaks are in good agreement with that presented by other researchers [38]. The bands at 774 cm^{-1} and 1684 cm^{-1} , which are ascribed to C-N bond, and 1563 cm^{-1} correspond to fundamental vibrations of the polypyrrole ring. The band at 1039 cm^{-1} is based on the =C-H in-plane vibrations, and the band at 1196 cm^{-1} corresponds to the C-N stretching vibrations. The peak at ~ 3100 – 3500 cm^{-1} corresponds to the N-H bond. The band at 2071 cm^{-1} corresponds to C-N stretching of $K_3[Fe(CN)_6]$. The absorption band for $[Fe(CN)_6]^{3-}$ varies between 2040–2120 cm^{-1} [47]. It is most likely that this band represents $[Fe(CN)_6]^{4-}$ [48]. These FTIR spectra suggests that $[Fe(CN)_6]^{4-}$ remains in the Ppy layer as a dopant if Ppy is synthesized in an acidic medium. This is a common feature for doping of Ppy in an acidic medium because Ppy becomes positively charged and can incorporate negative ions in its structure [47]. Consequently, the efficiency of Ppy doping by $[Fe(CN)_6]^{4-}$ can be controlled by the varying the pH of the polymerization solution.

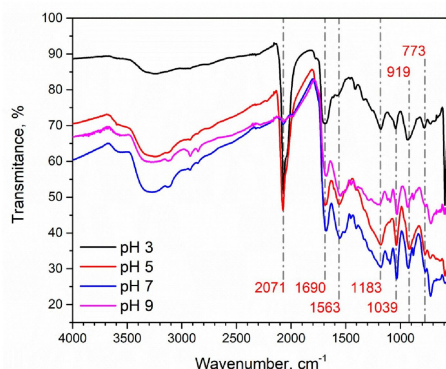


Figure 4. FTIR spectra of Ppy synthesized at different pH values. 0.5 M of Py and 0.04 M of $K_3[Fe(CN)_6]$ were used for Ppy synthesis in 0.1 M PBS buffers of four different pH's: 3.0, 5.0, 7.0 and 9.0.

Analysis of FTIR spectra reveals that it is possible to achieve doping with $[Fe(CN)_6]^{4-}$ directly without using an additional oxidizer or an external electric stimulus, and to produce the Ppy/ $[Fe(CN)_6]^{4-}$ composite in one step, which corresponds to results published in [49], where additional oxidizer was used. This finding corresponds to that presented in other research, which reports that in acidic mediums anions tends to remain within the Ppy matrix [50].

Synthesized Ppy was also inspected with a focused ion beam scanning electron microscope (FIB SEM) and matrix-assisted laser desorption/ionization time of flight (MALDI ToF). It was determined that Ppy, which was prepared in basic or neutral conditions, is only partially soluble in organic solvents. This is most probably due to Ppy having a neutral nature at this pH, meaning that the Ppy polymeric-backbone was not in an ionic state and thus was partially soluble. From MALDI ToF results (Figure 5a) it was determined that particles with molecular mass between 550 to 1000 Da

are highly abundant. This suggests that only Ppy oligomers tend to dissolve and form co-crystals with *trans*-2-[3-(4-*tert*-Butylphenyl)-2-methyl-2-propenyldene]malononitrile (DCTB). High molecular mass Ppy was also observed with molecular mass around 160 kDa (Figure 5b). According to [51] polymers such as Ppy cannot have their molecular mass determined using MALDI ToF due to the fact that these type of polymers are insoluble in any type of solvents. However, according to [41] it is possible to measure polythiophenes, similar class to Ppy polymers, using DCTB as a supporting matrix compound. Using DTCB as a matrix we were only able to determine with confidence Ppy with low molecular mass. According to our best knowledge, no other studies provided any convincing evidence where Ppy molecular mass was determined using MALDI ToF.

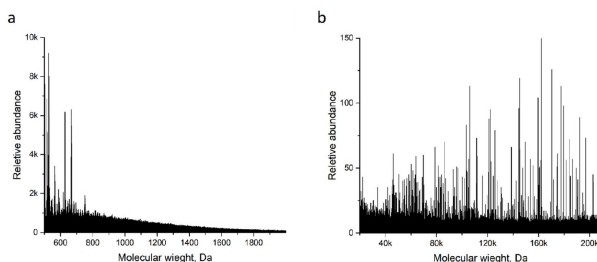


Figure 5. MALDI ToF spectra in different mass ranges. Spectra were registered in a DCTB matrix using a linear detector. Only those mass ranges in which some particle abundance was observed are represented here. (a) mass range of 500–2000 Da, (b) mass range of 20k–210k Da.

FIB SEM images revealed that commonly reported Ppy aggregates constituted from smaller spherical shaped units (Figure 6). Upon further inspection variation among spherical unit size was detected, which was altered by pH value. Ppy prepared at different pHs (3.0, 5.0, 7.0 and 9.0) were formed respectively of 152 ± 12 nm, 76 ± 26 nm, 52 ± 15 nm and 54 ± 14 nm size base units. Thus, Ppy synthesized in more acidic conditions tended to form larger Ppy units. On the other hand, the Ppy unit size was lower at neutral and basic conditions. FIB SEM study in agreement with FTIR data suggests that the incorporation of $[\text{Fe}(\text{CN})_6]^{4-}$ into the Ppy structure increases its porosity. This is possible because formed $\text{Ppy}(\text{H}^+)/[\text{Fe}(\text{CN})_6]^{4-}$ ion pairs in acidic medium, in accordance with FTIR results, might be hydrated and yield larger constituent units of Ppy.

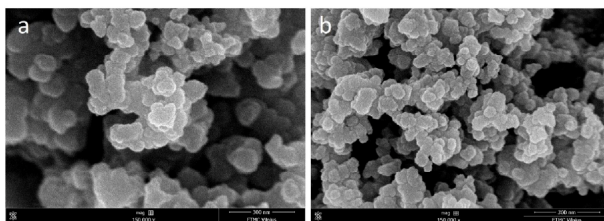


Figure 6. FIB SEM images of Ppy aggregates synthesized using 0.5 M Py and 0.04 M $\text{K}_3[\text{Fe}(\text{CN})_6]$. (a) Synthesis was performed in 0.1 M PBS, pH 3.0; (b) synthesis was performed in 0.1 M PBS, pH 9.0. Both images were obtained using 150k magnification.

4. Conclusions

In this research we report the evaluation of polymerization of pyrrole initiated by $[\text{Fe}(\text{CN})_6]^{3-}$. It was determined that if $[\text{Fe}(\text{CN})_6]^{4-}$ is initially added into a bulk polymerization solution then it can be oxidized into $[\text{Fe}(\text{CN})_6]^{3-}$ by dissolved oxygen. The formed $[\text{Fe}(\text{CN})_6]^{3-}$ then acts as the initiator of the pyrrole polymerization reaction. On the other hand using $[\text{Fe}(\text{CN})_6]^{3-}$ the polymerization rate of pyrrole can be controlled by varying the pH value of the polymerization bulk solution. There is some evidence that Ppy-based particle size increases by doping with $[\text{Fe}(\text{CN})_6]^{4-}$ and such doping is more efficient in an acidic medium. The slowest Ppy formation rate was observed when the reaction was performed at neutral pH (pH 7.0).

Author Contributions: Conceptualization, E.A., A.R. (Almira Ramanaviciene) and A.R. (Arunas Ramanavicius); Methodology, E.A.; Experiment Execution and Data Analysis, E.A.; Writing-Original Draft Preparation, E.A.; Contribution to Writing & Editing, E.A., A.R. (Almira Ramanaviciene) and A.R. (Arunas Ramanavicius); Visualization, E.A.; Supervision, A.R. (Almira Ramanaviciene) and A.R. (Arunas Ramanavicius).

Funding: This research was funded by a grant (No. S-LAT-17-1) from the Research Council of Lithuania.

Acknowledgments: Support by Viktoras Masevicius in the determination of molecular weight of Ppy is acknowledged.

Conflicts of Interest: The authors declare no conflicts of interest.

References

1. Das, T.K.; Prusty, S. Review on conducting polymers and their applications. *Polym. Plast. Technol. Eng.* **2012**, *51*, 1487–1500. [[CrossRef](#)]
2. Ravichandran, R.; Sundarajan, S.; Venugopal, J.R.; Mukherjee, S.; Ramakrishna, S. Applications of conducting polymers and their issues in biomedical engineering. *J. R. Soc. Interface* **2010**, *7*, S559–S579. [[CrossRef](#)] [[PubMed](#)]
3. Oh, E.J.; Jang, K.S.; MacDiarmid, A.G. High molecular weight soluble polypyrrole. *Synth. Met.* **2001**, *125*, 267–272. [[CrossRef](#)]
4. Njagi, J.; Andreescu, S. Stable enzyme biosensors based on chemically synthesized Au–polypyrrole nanocomposites. *Biosens. Bioelectron.* **2007**, *23*, 168–175. [[CrossRef](#)] [[PubMed](#)]
5. Feng, C.H.; Ma, L.; Li, F.B.; Mai, H.J.; Lang, X.M.; Fan, S.S. A polypyrrole/anthraquinone-2,6-disulphonic disodium salt (PPy/AQDS)-modified anode to improve performance of microbial fuel cells. *Biosens. Bioelectron.* **2010**, *25*, 1516–1520. [[CrossRef](#)] [[PubMed](#)]
6. Torres-Gomez, G.; Gomez-Romero, P. Conducting organic polymers with electroactive dopants. Synthesis and electrochemical properties of hexacyanoferrate-doped polypyrrole. *Synth. Met.* **1998**, *98*, 95–102. [[CrossRef](#)]
7. Mazur, M.; Krywko-Cendrowska, A.; Krysinski, P.; Rogalski, J. Encapsulation of laccase in a conducting polymer matrix: A simple route towards polypyrrole microcontainers. *Synth. Met.* **2009**, *159*, 1731–1738. [[CrossRef](#)]
8. Ramanaviciene, A.; Schuhmann, W.; Ramanavicius, A. AFM study of conducting polymer polypyrrole nanoparticles formed by redox enzyme—Glucose oxidase—Initiated polymerisation. *Colloids Surf. B Biointerfaces* **2006**, *48*, 159–166. [[CrossRef](#)] [[PubMed](#)]
9. Ramanavicius, A.; Kausaite, A.; Ramanaviciene, A.; Acaite, J.; Malinauskas, A. Redox enzyme—Glucose oxidase—Initiated synthesis of polypyrrole. *Synth. Met.* **2006**, *156*, 409–413. [[CrossRef](#)]
10. Song, H.K.; Palmore, G.T.R. Conductive polypyrrole via enzyme catalysis. *J. Phys. Chem. B* **2005**, *109*, 19278–19287. [[CrossRef](#)] [[PubMed](#)]
11. Riccardi, C.D.; Yamanaka, H.; Josowicz, M.; Kowalik, J.; Mizaikoff, B.; Kranz, C. Label-free DNA detection based on modified conducting polypyrrole films at microelectrodes. *Anal. Chem.* **2006**, *78*, 1139–1145. [[CrossRef](#)] [[PubMed](#)]
12. Balint, R.; Cassidy, N.J.; Cartmell, S.H. Conductive polymers: Towards a smart biomaterial for tissue engineering. *Acta Biomater.* **2014**, *10*, 2341–2353. [[CrossRef](#)] [[PubMed](#)]
13. Ansari, R. Polypyrrole Conducting Electroactive Polymers: Synthesis and Stability Studies. *J. Chem.* **2006**, *3*, 186–201. [[CrossRef](#)]

14. Bjorklund, R.B. Kinetics of pyrrole polymerisation in aqueous iron chloride solution. *J. Chem. Soc. Faraday Trans. Phys. Chem. Condens. Phases* **1987**, *83*, 1507–1514. [[CrossRef](#)]
15. Tan, Y.; Ghandi, K. Kinetics and mechanism of pyrrole chemical polymerization. *Synth. Met.* **2013**, *175*, 183–191. [[CrossRef](#)]
16. Ballav, N.; Biswas, M. Oxidative polymerization of aniline and pyrrole by isopolymetallates of vanadium. *J. Appl. Polym. Sci.* **2005**, *96*, 1483–1486. [[CrossRef](#)]
17. Chen, J.H.; Huang, Z.P.; Wang, D.Z.; Yang, S.X.; Li, W.Z.; Wen, J.G.; Ren, Z.F. Electrochemical synthesis of polypyrrole films over each of well-aligned carbon nanotubes. *Synth. Met.* **2001**, *125*, 289–294. [[CrossRef](#)]
18. Wei, Y.Y.; Li, L.; Yang, X.M.; Pan, G.L.; Yan, G.P.; Yu, X.H. One-Step UV-Induced Synthesis of Polypyrrole/Ag Nanocomposites at the Water/Ionic Liquid Interface. *Nanoscale Res. Lett.* **2010**, *5*, 433–437. [[CrossRef](#)] [[PubMed](#)]
19. Chougule, M.A.; Pawar, S.G.; Godse, P.R.; Mulik, R.N.; Sen, S.; Patil, V.B. Synthesis and Characterization of Polypyrrole (PPy) Thin Films. *Soft Nanosci. Lett.* **2011**, *1*, 6–10. [[CrossRef](#)]
20. Vaitkuviene, A.; Kasetas, V.; Voronovic, J.; Ramanauskaite, G.; Bizileviciene, G.; Ramanaviciene, A.; Ramanavicius, A. Evaluation of cytotoxicity of polypyrrole nanoparticles synthesized by oxidative polymerization. *J. Hazard. Mater.* **2013**, *250*, 167–174. [[CrossRef](#)] [[PubMed](#)]
21. Kausaite, A.; Ramanaviciene, A.; Ramanavicius, A. Polyaniline synthesis catalysed by glucose oxidase. *Polymer* **2009**, *50*, 1846–1851. [[CrossRef](#)]
22. Krikstolaityte, V.; Kuliesius, J.; Ramanaviciene, A.; Mikoliunaite, L.; Kausaite-Minkstimiene, A.; Oztekin, Y.; Ramanavicius, A. Enzymatic polymerization of polythiophene by immobilized glucose oxidase. *Polymer* **2014**, *55*, 1613–1620. [[CrossRef](#)]
23. Ramanaviciene, A.; Kausaite, A.; Tautkus, S.; Ramanavicius, A. Biocompatibility of polypyrrole particles: An in vivo study in mice. *J. Pharm. Pharmacol.* **2007**, *59*, 311–315. [[CrossRef](#)] [[PubMed](#)]
24. Henry, M.C.; Hsueh, C.-C.; Timko, B.P.; Freund, M.S. Reaction of Pyrrole and Chlorauric Acid A New Route to Composite Colloids. *J. Electrochem. Soc.* **2001**, *148*, D155–D162. [[CrossRef](#)]
25. Ramanavicius, A.; Kaušaitė, A.; Ramanavičienė, A. Polypyrrole-coated glucose oxidase nanoparticles for biosensor design. *Sens. Actuators B Chem.* **2005**, *111*, 532–539. [[CrossRef](#)]
26. Leonavicius, K.; Ramanaviciene, A.; Ramanavicius, A. Polymerization model for hydrogen peroxide initiated synthesis of polypyrrole nanoparticles. *Langmuir* **2011**, *27*, 10970–10976. [[CrossRef](#)] [[PubMed](#)]
27. Kobayashi, D.; Endo, Y.; Takahashi, T.; Otake, K.; Shono, A. New method for the synthesis of polypyrrole particle using water/oil emulsion. *J. Chem. Eng. Jpn.* **2013**, *46*, 550–555. [[CrossRef](#)]
28. Shanthala, V.S.; Shobha Devi, S.N.; Murugendrappa, M.V. Synthesis, characterization and DC conductivity studies of polypyrrole/copper zinc iron oxide nanocomposites. *J. Asian Ceram. Soc.* **2017**, *5*, 227–234. [[CrossRef](#)]
29. Wang, J. Electrochemical glucose biosensors. *Chem. Rev.* **2008**, *108*, 814–825. [[CrossRef](#)] [[PubMed](#)]
30. Rawson, F.J.; Downard, A.J.; Baronian, K.H. Electrochemical detection of intracellular and cell membrane redox systems in *Saccharomyces cerevisiae*. *Sci. Rep.* **2014**, *4*, 9. [[CrossRef](#)] [[PubMed](#)]
31. Heiskanen, A.; Yakovleva, J.; Spegel, C.; Taboryski, R.; Koudelka-Hep, M.; Emneus, J.; Ruzgas, T. Amperometric monitoring of redox activity in living yeast cells: Comparison of menadiene and menadiene sodium bisulfite as electron transfer mediators. *Electrochem. Commun.* **2004**, *6*, 219–224. [[CrossRef](#)]
32. Heiskanen, A.; Coman, V.; Kostesha, N.; Sabourin, D.; Haslett, N.; Baronian, K.; Gorton, L.; Dufva, M.; Emneus, J. Bioelectrochemical probing of intracellular redox processes in living yeast cells-application of redox polymer wiring in a microfluidic environment. *Anal. Bioanal. Chem.* **2013**, *405*, 3847–3858. [[CrossRef](#)] [[PubMed](#)]
33. Nagamine, K.; Takahashi, Y.; Ino, K.; Shiku, H.; Matsue, T. Influence of tip size on single yeast cell imaging using scanning electrochemical microscopy. *Electroanalysis* **2011**, *23*, 1168–1174. [[CrossRef](#)]
34. Dong, S.; Lian, G. Redox reactions of $\text{Fe}(\text{CN})_6^{3-/4-}$ in polypyrrole films: Accumulation and removal of cations. *J. Electroanal. Chem. Interfacial Electrochem.* **1990**, *291*, 23–39. [[CrossRef](#)]
35. Michalska, A.; Ivaska, A.; Lewenstam, A. Modeling potentiometric sensitivity of conducting polymers. *Anal. Chem.* **1997**, *69*, 4060–4064. [[CrossRef](#)] [[PubMed](#)]
36. Goel, S.; Mazumdar, N.A.; Gupta, A. Synthesis and characterization of polypyrrole nanofibers with different dopants. *Polym. Adv. Technol.* **2010**, *21*, 205–210. [[CrossRef](#)]

37. Toshima, N.; Hara, S. Direct synthesis of conducting polymers from simple monomers. *Prog. Polym. Sci.* **1995**, *20*, 155–183. [[CrossRef](#)]
38. Zagorska, M.; Pron, A.; Lefrant, S.; Kucharski, Z.; Suwalski, J.; Bernier, P. Synthesis and spectroscopic characterization of polypyrrole containing ferrous cyanide anions. *Synth. Met.* **1987**, *18*, 43–48. [[CrossRef](#)]
39. Chakrabarti, M.H.; Roberts, E.P.L. Analysis of Mixtures of Ferrocyanide and Ferricyanide using UV-Visible Spectroscopy for Characterisation of a Novel Redox Flow Battery. *J. Chem. Soc. Pak.* **2008**, *30*, 817–823.
40. Appleby, C.A.; Morton, R.K. Lactic dehydrogenase and cytochrome b(2) of baker's yeast. Purification and crystallization. *Biochem. J.* **1959**, *71*, 492–499. [[CrossRef](#)] [[PubMed](#)]
41. De Winter, J.; Deshayes, G.; Boon, F.; Coulembier, O.; Dubois, P.; Gerbaux, P. MALDI-ToF analysis of polythiophene: Use of *trans*-2-[3-(4-*t*-butyl-phenyl)-2-methyl-2-propenyldiene]malononitrile-DCTB-as matrix. *J. Mass Spectrom. JMS* **2011**, *46*, 237–246. [[CrossRef](#)] [[PubMed](#)]
42. Weng, B.; Shepherd, R.; Chen, J.; Wallace, G.G. Gemini surfactant doped polypyrrole nanodispersions: An inkjet printable formulation. *J. Mater. Chem.* **2011**, *21*, 1918–1924. [[CrossRef](#)]
43. Wagner, B.A.; Venkataraman, S.; Buettner, G.R. The rate of oxygen utilization by cells. *Free Radic. Biol. Med.* **2011**, *51*, 700–712. [[CrossRef](#)] [[PubMed](#)]
44. Robinson, J.; Cooper, J.M. Method of determining oxygen concentrations in biological media, suitable for calibration of the oxygen electrode. *Anal. Biochem.* **1970**, *33*, 390–399. [[CrossRef](#)]
45. Yan, H.; Kajita, M.; Toshima, N. Polymerization of Aniline Using Iron(III) Catalyst and Ozone, and Kinetics of Oxidation Reactions in the Catalytic System. *Macromol. Mater. Eng.* **2002**, *287*, 503–508. [[CrossRef](#)]
46. Toshima, N.; Ihata, O. Catalytic synthesis of conductive polypyrrole using iron(III) catalyst and molecular oxygen. *Synth. Met.* **1996**, *79*, 165–172. [[CrossRef](#)]
47. Dobson, K.D.; James McQuillan, A. An in situ IR spectroscopic investigation of adsorption of hexa- and penta-cyanoferrates to metal oxides from aqueous solution. *Phys. Chem. Chem. Phys.* **2000**, *2*, 5180–5188. [[CrossRef](#)]
48. Idemura, S.; Suzuki, E.; Ono, Y. Electronic state of iron complexes in the interlayer of hydrotalcite-like materials. *Clays Clay Miner.* **1989**, *37*, 553–557. [[CrossRef](#)]
49. Zou, Y.J.; Cheng, J.; Xiang, C.L.; Chu, H.L.; Qiu, S.J.; Xu, F.; Sun, L.X.; Zheng, L.J. Preparation, characterization of polypyrrole encapsulated Prussian blue nanocomposite and its application for biosensing. *Int. J. Electrochem. Sci.* **2015**, *10*, 4626–4636.
50. Boutry, C.M.; Gerber-Hörlner, I.; Hierold, C. Electrically conducting biodegradable polymer composites (polylactide-polypyrrole and polycaprolactone-polypyrrole) for passive resonant circuits. *Polym. Eng. Sci.* **2013**, *53*, 1196–1208. [[CrossRef](#)]
51. Wu, K.J.; Odom, R.W. Peer Reviewed: Characterizing Synthetic Polymers by MALDI MS. *Anal. Chem.* **1998**, *70*, 456A–461A. [[CrossRef](#)] [[PubMed](#)]



© 2018 by the authors. Licensee MDPI, Basel, Switzerland. This article is an open access article distributed under the terms and conditions of the Creative Commons Attribution (CC BY) license (<http://creativecommons.org/licenses/by/4.0/>).

Review

From Microorganism-Based Amperometric Biosensors Towards Microbial Fuel Cells

Eivydas Andriukonis ^{1,2,3}, Raimonda Celiesiute-Germaniene ^{1,4}, Simonas Ramanavicius ^{1,2,3}, Roman Viter ^{1,5,6*} and Arunas Ramanavicius ^{1,2,3,*}

¹ NanoTechnas-Center of Nanotechnology and Material Science, Faculty of Chemistry and Geosciences, Vilnius University, LT-03225 Vilnius, Lithuania; eivydas.andriukonis@chgf.vu.lt (E.A.); raimonda.celiesiute@fmc.lt (R.C.-G.); simonas.ramanavicius@fmc.lt (S.R.)

² Department of Physical Chemistry, Faculty of Chemistry and Geosciences, Vilnius University, LT-03225 Vilnius, Lithuania

³ Laboratory of Nanotechnology, State Research Institute Center for Physical Sciences and Technology, LT-10257 Vilnius, Lithuania

⁴ Laboratory of Bioelectrics, State Research Institute Center for Physical Sciences and Technology, LT-10257 Vilnius, Lithuania

⁵ Center for Collective Use of Scientific Equipment, Sumy State University, 40018 Sumy, Ukraine

⁶ Institute of Atomic Physics and Spectroscopy, University of Latvia, LV-1004 Riga, Latvia

* Correspondence: roman.viter@lu.lv (R.V.); Arunas.Ramanavicius@chf.vu.lt (A.R.)

Citation: Andriukonis, E.; Celiesiute-Germaniene, R.; Ramanavicius, S.; Viter, R.; Ramanavicius, A. From Microorganism-Based Amperometric Biosensors Towards Microbial Fuel Cells. *Sensors* **2021**, *21*, 2442. <https://doi.org/10.3390/s21072442>

Academic Editor: Felipe Conzuelo, Jesús M. Corres

Received: 28 February 2021

Accepted: 29 March 2021

Published: 1 April 2021

Publisher's Note: MDPI stays neutral with regard to jurisdictional claims in published maps and institutional affiliations.



Copyright: © 2021 by the authors. Licensee MDPI, Basel, Switzerland. This article is an open access article distributed under the terms and conditions of the Creative Commons Attribution (CC BY) license (<http://creativecommons.org/licenses/by/4.0/>).

Abstract: This review focuses on the overview of microbial amperometric biosensors and microbial biofuel cells (MFC) and shows how very similar principles are applied for the design of both types of these bioelectronics-based devices. Most microorganism-based amperometric biosensors show poor specificity, but this drawback can be exploited in the design of microbial biofuel cells because this enables them to consume wider range of chemical fuels. The efficiency of the charge transfer is among the most challenging and critical issues during the development of any kind of biofuel cell. In most cases, particular redox mediators and nanomaterials are applied for the facilitation of charge transfer from applied biomaterials towards biofuel cell electrodes. Some improvements in charge transfer efficiency can be achieved by the application of conducting polymers (CPs), which can be used for the immobilization of enzymes and in some particular cases even for the facilitation of charge transfer. In this review, charge transfer pathways and mechanisms, which are suitable for the design of biosensors and in biofuel cells, are discussed. Modification methods of the cell-wall/membrane by conducting polymers in order to enhance charge transfer efficiency of microorganisms, which can be potentially applied in the design of microbial biofuel cells, are outlined. The biocompatibility-related aspects of conducting polymers with microorganisms are summarized.

Keywords: microbial biofuel cells; yeast; direct electron transfer; extracellular electron transfer; cell membrane/wall modifications; conducting polymers; enzyme-based biofuel cells; bioelectronics; microbial biosensors; whole cell-based biosensors

1. Introduction

A biofuel cell (BFC) is a bioelectrochemical system or device, which can produce electricity from organic materials by enzymatic catalysis or metabolic processes running in bacteria and/or other living cells. Recently this research topic has attracted increasing attention as a prospective 'green' technology. The most intriguing aspect of biofuel cell application is waste water treatment by simultaneous production of electricity followed by the degradation of organic-waste. BFCs can be driven by enzymes or microorganisms. Microorganism-driven biofuel cells, which are often called microbial biofuel cells (MFCs), are the most prospective because microorganisms are capable of reproducing themselves

and there is no need for the purification of enzymes [1–5], which is otherwise a very important and costly procedure required for the development of enzymatic biofuel cells (EBFCs) [6]. Both microbial biofuel cells (MFCs) and EBFCs operate at ambient temperatures, but MFCs are cheaper and can be designed from bacteria populating sludge, soil and many other natural environments. However, the main obstacle for their wide application is a low electrical conductivity of the cell wall and cell membrane, which limits charge transfer (CT) ability and efficiency. The improvement of the electron transfer from the living cells to the anode during oxidation of organic matter is considered to be the main challenge for the enhancement of biofuel cell efficiency. Thus, researchers try to use various methods to increase the charge transfer from living cells. The extracellular electron transport towards the anode of microbial-biosensor and/or MFC is performed by internal/external electron transfer mediators, which very often are membrane-bound compounds capable of transferring electrons, or by electrode modifications that enable charge transfer to be improved [6]. The most commonly microorganisms used in direct electron transfer based biosensors and fuel cells are *Shewanella putrefaciens*, *Geobacter sulfurireducens*, *Aeromonas hydrophila*, *Geobacter metallic reducens* and *Rhodoferrax ferrireducens*. Their catalytic activity and electron transfer route have been relatively well investigated; therefore, it is thought that physical contact between electrode and outer-membrane cytochromes or/and conductive pili of microorganisms can enable direct ‘wiring’. Catalytic activity and possible CT pathways and mechanism from eukaryotic microorganisms such as *Saccharomyces cerevisiae* is under intensive investigation [7–9]. It should be noted that *S. cerevisiae* recently are considered as a prospective ‘biocatalyst’ suitable for MFCs due to its broad substrate spectrum, easy and fast mass cultivation, reasonable cost and non-pathogenic material. For efficient performance of *S. cerevisiae* in MFCs, exogenous mediators are still required, because these microorganisms do not produce redox mediators indigenously [7–11]. It was determined that higher conversion efficiencies are observed using microorganisms capable of generating compounds that are able to act as redox mediators if compared to these microorganisms, which are not producing any redox compounds with redox mediating properties [6,12]. Therefore, MFCs, using eukaryotic yeast cells are still very rare. MFCs, based on *S. cerevisiae* extract the energy using the nicotinamide adenine dinucleotide (NADH/NAD⁺) redox cycle from anaerobic glycolysis, which takes place in the cytosol of the cell. Thus, NADH is easily accessible to a mediator molecule attached to the cell membrane. Then NADH is re-oxidized back into NAD⁺ while a redox mediator is reduced; in this way the energy extraction process in the fuel cell does not disrupt the natural metabolism of the yeast cell. In order to improve *S. cerevisiae*-based MFCs performance, various modifications are being investigated and applied, such as electrode, cell wall or membrane modifications [7,13–15].

The aim of this review is to overview common principles that are applied in the development of amperometric biosensors, which can be easily adapted for the design of biofuel cells.

2. Whole Cell-Based Biosensors

Nowadays, electrochemical (bio)sensors are of great significance in many areas [16] providing information on various analytes of interest [17]. Typically, biosensors are categorized according to their bio-recognition elements, which can be antibodies [18], receptors [19], enzymes [20], DNA [21] or living cells [22]. Whole-cell biosensors are based on microbial or other type cells acting as their bio-recognition elements. Microbial biosensors are ideally suited for the analysis of extracellular chemicals, their main advantages are: (i) ability to detect a wide variety of substrates, (ii) rather cheap and basic mass production, and (iii) easier genetic modification compared to other types of sensors and biosensors [16]. Moreover, microorganisms are able to adapt towards adverse conditions and to develop the capability to consume different chemicals over time. However, some limitations of whole-cell and microorganism-based sensors still remain, one of them being that very precise determination of target compounds is still not possible, due to the relatively poor

sensitivity and selectivity. Another intrinsic limitation of microbial biosensors is their rather slow response caused by moderated diffusion of substrates into the cell through natural cell barriers such as the membrane or cell wall [17].

To overcome these drawbacks of the microbial biosensors numerous techniques are applied, such as genetic engineering in order to block undesired or induce desired metabolic pathways in the cells [23]; micro- and nano-technologies with the goals for miniaturization, high-throughput screening, enhanced sensitivity, increased selectivity and more efficient immobilization of microorganisms [17]. Attempts to overcome barriers of the cells applying various techniques include physical (freezing and thawing), chemical (dissolving within organic solvents/detergents), enzymatic (treatment by lysozyme, papain) [24] and electroporation [25] based approaches. All of these cell modification methods have some disadvantages, e.g., reduced cells viability after treatment with electric pulses [25].

During the development of whole cell biosensors, selection of the immobilization method on the electrode surface is of great importance. An ideal matrix for the cell immobilization should function at ambient temperature; enable to maintain high cell activity; prevent the cells from leakage to the buffer; allow the influx of nutrients, oxygen, and analytes as well as the removal of the resulting metabolites from the cells; and ensure electron transfer from the cell to the electrode. Entrapment into polymers of natural origin prepared from alginate/pectate, κ -carrageenan, collagen, gelatin, chitosan and agar (agarose) was performed under mild conditions with high viability of entrapped cells [22]. However, these matrices can be easily destroyed by chelating agents, which could be present in a sample, because they are formed by an ionotropic gelation in the presence of Ca^{2+} or K^{+} ions [22]. The synthetic polymers such as polyvinylalcohol, polyacrylamide, and polyurethane (PU) are more stable, but in many cases, they can induce the decrease of cell viability. The major limitation of cells entrapped within polymeric matrices is a creation of an additional diffusion barrier, which slows down the response of the biosensor [26].

A novel 'cells-on-beads' immobilization strategy is providing a fast and simple fabrication method suitable for the construction of viable whole-cell biosensor chip [27]. The proposed immobilization method is based on the modification of polyacrylamide porous beads with positively charged groups, which favors good *Escherichia coli* cell adsorption to the surface of gold. This amperometric biochip yielded a signal within the range of tens of nanoamperes, which was linearly dependent on the concentration of aniline [27].

A whole-cell amperometric biosensor based on 'bioelectrochemical wire' consisting of riboflavin-cytochrome C proteins between cells of *Shewanella oneidensis* MR-1 and working electrode was developed for riboflavin detection by using fumarate as the electron acceptor. A linear calibration curve with extremely wide riboflavin concentration (5 nM to 10 μM) was obtained, with the limit of detection (LOD) of 2.2 nM. [28]. In other study, reproducible microbial electrochemical cell-based biosensor for the determination of cyclohexane carboxylic acid in water samples was developed with cyclohexane carboxylic acid concentrations ranging from 50 to 250 mg chemical oxygen demand (COD) L^{-1} . The biosensor could be used as a bioanalytical tool for monitoring naphthenic acids concentrations in oil sands process-affected water [29].

Some kinds of whole cell sensor can match requirements of enzymatic sensors due to applied genetic modifications of enzymes coding DNA sequences that are fused with DNA sequences of proteins, which are expressed on the surface of living cells [30]. Using this technology, it is possible to create cells containing enzymes of interest that are bound to the surface of the cell. This technology prevents enzyme leakage and the expressed enzymes possess high response rate, sensitivity and specificity. These systems can be based on various types of cell, including bacteria, fungi or yeast [31]. The main drawback of such systems that not all DNA sequences of enzymes can be genetically fused with that of native cells' extracellular surface proteins and they do not always retain normal catalytic activity because the fusion of proteins can disrupt their normal folding procedure.

3. Electrode Modifications for the Improvement of Charge Transfer in Biosensors and Microbial Biofuel Cells

The characteristics of anode material play a critical role in amperometric biosensors and MFC, because the nature of material is among the key factors, which significantly affects charge transfer efficiency from biomaterials, and it is one of the major reasons causing the rather low efficiency of some MFC prototypes. In order to maintain the viability of immobilized microorganisms the most efficient anode material should be biocompatible with these microbes, should have a high surface area for biomaterial to adhere to, and should be susceptible to robust microbial cell attachment. At the same time, materials used for the modification of anode should facilitate electron transfer, which is a limiting factor for the sensitivity of amperometric biosensor or the efficiency of MFCs. The adhesion of microorganisms on the electrode surface plays one of a key roles in the electron transfer process and generated power density [12]. The most popular MFC design is based on two-compartment cell with microorganisms enclosed in an anode compartment and/or sometimes even in a cathode compartment. Between compartments, the ion uptake is required and, therefore, components should be divided by semipermeable membrane, which enables the exchange of some ions. The extracellular charge transfer from microorganisms towards the anode is facilitated by internal or external electron mediators or membrane-bound compounds, which are capable of electron transfer [6] (Figure 1).

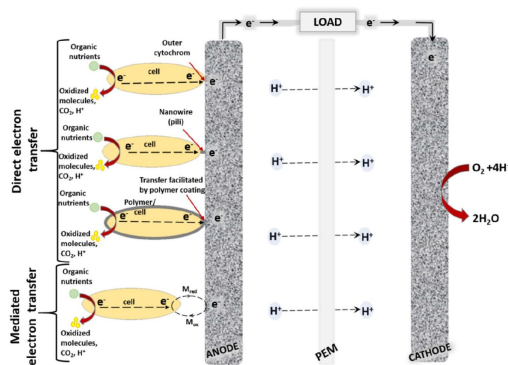


Figure 1. General scheme of microbial biofuel cell with direct and mediated electron transfer.

Commercially available state-of-the-art membranes suitable for MFC are often modified by perfluorosulfonic acid (Nafion) layer, which exhibit a high proton conductivity and chemical stability and are the most popular for the application in MFCs. However, despite numerous advantages Nafion membranes significantly increase the cost of the system in comparison to those based on other types of membranes or membrane-less MFCs. In addition, Nafion-based membranes become fouled during the action of MFCs and, therefore, researchers are attempting to substitute them by other material-based membranes [32,33].

The most commonly utilized anode material in the MFCs are carbon-based materials, because they have high conductivity, they are chemically stable, and relatively cheap.

Nevertheless, carbon materials are intrinsically hydrophobic, which is unfavorable for robust attachment of living cells, resulting in non-efficient charge transfer. To resolve this problem, various chemical and physical modifications were involved to enhance the properties of carbon-based materials. However, the effect of modifications makes it important to compromise between low cost and biocompatibility, while supporting strong attachment of microbes and facilitating charge transfer towards electrodes, which are extremely important for optimal MFC performance. In addition, modifications should also provide good electrical conductivity with low resistance, large surface area, anti-corrosion and anti-degradation properties, suitable mechanical strength and toughness [34]. The most common modifications of electrodes are based on the functionalization with carbon nanomaterials [35–38], metal oxide nanoparticles or their nanocomposites, conducting polymers or the formation of various nanocomposites based on conducting polymers [34,39].

Carbonaceous nanomaterials provide a large surface area and extraordinary electron transfer properties. Carbon felt (CF) is commonly used as a low-cost anode material, which is very suitable for MFCs design due to a good electronic conduction, high surface area and porosity enabling sufficient mechanical stability to be provided and, therefore, carbon felt seems to be a favorable material for biofilm formation [40,41]. However, highly hydrophobic nature of carbon felt makes their application more complicated in aqueous electrolyte medium and for the population of this structure with living cells. To overcome this drawback, many modification methods have been developed and used resulting into a new and benefiting composites. Chemical modifications change the hydrophobic surface of bare felts to hydrophilic. For example, polyethylenimine has a high positive charge density and can interact through its abundant amine groups with the carbon-based materials [42]. This material is commonly used for the modification of carbon felt anodes employed in MFCs [43,44]. Carbon nanotubes (CNTs) have shown controversial characteristics towards living cells [45] thus, the anode modifications of the MFCs often go together with biocompatible polymers, such as polyurethane (PU) [20], or polyaniline (PANI) [46–48].

The influence of polyurethane on biocompatibility and adhesion-activity of carbon anode with the composite of polyurethane/carbon nanotubes composite was investigated [14]. Polyurethane is known as a biocompatible material [46], thus the composites with CNTs have less effect on the biological activity of living cells used in amperometric biosensors and MFCs. The porous polyurethane sponge provided a vast surface area for physical CNTs adsorption as well as for cell biofilm formation. Daily substitution of analyte allowed the MFC to operate at 70% of maximum power (100 mW m^{-2}) for long periods. Thus, this MFC has a prospect as a low-cost energy generating device [14]. To separate anode and cathode chambers, the aforementioned ion exchange separator based on (polystyrene-polyvinyl alcohol)/(phosphoric acid) membrane was applied in the design of this MFC. This membrane proved to enhance proton conductivity in dehydrated as well as hydrated states, with an estimated ion transfer number in order of 0.97 as well as had an antifouling effect [14] unlike the usually used Nafion membranes [32] (Table 1). In order to avoid the application of ion exchange separators, membrane-less BFCs are designed [49]. Stability and compatibility of membraneless MFC based on yeast/CNT catalyst were investigated and catalytic activity of this MFC was evaluated [49]. In this study, carbon nanotubes and poly(ethylenimine) were selected as a supporting material for the immobilization of the yeast cells based on hydrophobic interactions between CNTs and yeast cells followed by the cross-linking technique. It was proved that yeast/CNTs induced excellent catalytic activities and MFC performance (344 mW m^{-2}) with MFC stability of 86% from its initial value after eight days (Table 1) [49].

Strategy for anode modification with multiple bilayers of CNTs/PANI decorated indium tin oxide (ITO) electrode with a nanoporous network exhibited superior biocatalytic properties with a maximal current density of $6.98 \mu\text{A cm}^{-2}$ and maximum power of 34.51 mW m^{-2} (Table 1) [47]. The layers of PANI were graft-polymerized via covalent bonding

while the CNTs were assembled applying layer-by-layer deposition technique, which ensured low CT resistance. The modified electrode had more than seven times higher maximum power density in comparison to that registered by the unmodified ITO electrode. This result indicates that CNTs/PANI conductive films greatly increases the area of electrode surface and the number of sites that are involved in charge transfer from bacteria. In addition, the toxicity of the CNTs toward the *Shewanella loihica* cells was minimized by modification with biocompatible polymer-PANI [47]. The genus of *Shewanella* is known as metal-reducing bacteria and, therefore this type of MCFs could be applied for the control of chromium ion-based pollution as well as the production of chromium-based nanoparticles [50] that can be harvested from formed sediment.

Facilitation of charge transfer from biological objects by redox polymers is discussed in the work of Coman et al. [51]. In this study researchers explored the applicability of flexible osmium polymers (poly(1-vinylimidazole)₂-[Os-(4,4'-dimethyl-2,2'-bipyridyl)₂Cl₂]^{0/2+} (I) and poly(vinylpyridine)-[Os-(N,N'-methylated-2,2'-biimidazole)]^[2+/3+] as a matrix material and for electron transfer between the cells and the electrode. *Bacillus subtilis* were suspended in dried polymer, thus wiring them through the polymer matrix to the electrode (Table 1). Wired bacteria managed to reach 5 $\mu\text{A cm}^{-2}$ current density supplied with 0.3 mM succinate using an aldrithiol-modified gold electrode. A stability test showed slightly decreased current response over time and they reached approximately 73% of the initial response after 6 h.

New strategies for the modification of the anode of a MFC with alginate film were proposed by another group of researchers [52]. Neutral red (NR) was used as a mediator in this electrochemical system. The anode was modified with yeast by drop-coating method, and yeast film was formed by physical adsorption using immersion of carbon felt into yeast-alginate suspension. To determine anode performance, electrochemical characterization was performed, which proved that the deposit of an alginate film entrapping yeast cells is an efficient way to promote glucose oxidation and to transfer electron. Performance of the MFC were evaluated in terms of maximum power generation (0.326 A m^{-2}) at the load of 1 $\text{k}\Omega$. Such MFC had operational stability for a period of 44 days. The current of MFC partially decreased due to the reduced activity and viability of immobilized cells. It was stated that another approach when yeast cells were entrapped within alginate-NR microbeads, then current was limited by obstruction of the NR reduced form, which was exiting the matrix gel layer towards the electrode surface [52].

To improve carbon-based anode materials, the performance of conductivity, electrocatalytic activity, various noble metal and metal-based materials are utilized to modify carbon materials. Nanoparticles act as the bridge for electron transfer between bacteria and anode. In contrary to carbon nanomaterials, metal nanoparticles are not very widely applied because of their corrosiveness [53] and cytotoxicity [54]. However, gold nanoparticles (AuNPs) and their composites are considered as suitable for electrode modification in bioelectrochemical devices due to their wide array of beneficial properties, such as biocompatibility, high surface-to-volume ratio, and enhanced conductivity [55].

Biogenic golden nanoparticles (BioAu) and the composite with multivalued CNTs (BioAu/MWCNT) was used for the modification of carbon cloth anodes for MFC construction [56]. Biologically produced AuNPs are known for their low toxicity, high purity and biocompatibility thus allowing the aforementioned general drawbacks of metal-based nanoparticles to be minimized. The biofilm was constituted mostly from the classes of *Gammaproteobacteria* and *Negativicutes*, which increased after anode modification. The MFCs with the bioAu/MWCNT electrode had the highest power density of $178.34 \pm 4.79 \text{ mW m}^{-2}$ and operation time of shorter than 7 days (Table 1), which in the term of power density was 56% higher and in the term of operation time was 142% shorter compared with these characteristics of unmodified control electrode showing the strong affinity between the electrode surface and materials used for the modification [56]. Authors in this study attempted to investigate the electrochemical MFC performance and microbial community behavior affected by novel anode modification based on biogenic Au nanoparticles.

Duarte et al. developed and characterized golden nanostructures grown on a polyethyleneimine functionalized carbon felt substrate as an anode material of MFC. The gold nanoparticles growth process utilized surface-bound seeds. The developed widespread gold nano-flower structures had an irregular shape, which proved to be very beneficial for the physical adhesion and inhabitation of the yeast cells. The maximum power density achieved was $2771 \pm 569 \text{ mW m}^{-2}$ for the polyethyleneimine-modified carbon felt with gold nanoparticles prepared with $715 \mu\text{M}$ 4-mercaptobenzoic acid after only 30 min after preparation (Table 1). The higher power density, which was achieved by this approach was affected by AuNPs that bridge the external cellular wall of the yeast cells and the surface of carbon fibers. The contribution of AuNPs for direct electron transfer enabled 'local harvesting of more electrons' and the accumulation of charge on the CF electrode [44]. The same authors later developed metal composite nanostructures, namely manganese oxide-decorated iron oxide nanoflowers on the same anode material- polyethyleneimine functionalized carbon felt. A very efficient electrochemical interface between the yeast biofilm, metallic nanoflowers, and carbon felt fibers was constructed, further enhanced by the inclusion of the anionic surfactant mediator, sodium dodecylbenzenesulfonate (SDBS). Biofilm formation was performed by physical attachment of yeast cells on the anode material. When SDBS was used, the nanostructures stayed firmly attached to the carbon felt fibers due to the additional anionic interactions strengthening the entrapment bonds of the polyethyleneimine-coated fibers. This is supported by the increased surface coverage activity of the samples containing SDBS. Extracellular polysaccharides of the yeasts cell wall directly influenced the direct electron transfer properties of the yeast and, thus, the functionality of the MFC. The external nutrient-enriched and highly electrochemically responsive extracellular polysaccharide matrix reached out around the individual FeMnNPs on the electrode surface and created a strong electrochemical bridging effect between the yeast cells and nanostructures. The best power density of $5.83 \pm 0.61 \text{ W m}^{-2}$ was achieved (Table 1) [43].

In the work of Christwardana et al. [57], the quorum-sensing molecules, which are employed by microorganisms as a major means of communication and biofilm formation [58] were used for MFC anode functionalization to ascertain the suitable surface for microbial attachment, to enhance the biofilm formation, activity, and conductivity for the electron transfer and electron-electrode interaction in MFCs [59]. This scheme of the anode functionalization proved to be rather efficient, as the maximum power density of the MFC were $159.46 \pm 10.68 \text{ mW m}^{-2}$ and $156.57 \pm 5.84 \text{ mW m}^{-2}$, using different quorum sensing molecules phenylethanol and tryptophol, respectively. The third quorum sensing molecule, tyrosol was slightly less effective (Table 1). As seen from the Table 1, the constructed MFC did not have well-expressed maximum power density, however the idea of using quorum-sensing molecules was promising because of the possibility to speed natural formation of the biofilm. The presence of extracellular polysaccharide in a biofilm did enhance the direct electron transfer between yeast cells and working electrode surface. The improvements by using microbial consortiums, electrode surface modifications and other methods for the sophistications that could be applied are suggested by authors [59].

Table 1. The description of microbial biofuel cells (MFCs) anode modification method and MFC performance. Abbreviations provided below the table.

Electricigen	Anode modification method	Anode material	Electron donor	PD, mW m ⁻²	Other remarks	Ref.
<i>Saccharomyces cerevisiae</i>	Physical adsorption of CNTs, followed by physical adhesion of the cells	PU	Glucose/MB	100	After first 24 h PD reduces to 70% of the maximum, and remains constant with continuous substitution of glucose/MB for long periods.	[14]
<i>Sheewanella loihica</i>	Graft-polymerization of PANI and layer by layer self-assembly of carbon nanotubes	APTES/ITO	Sodium lactate	34.5	Maximal current density was 6.98 $\mu\text{A cm}^{-2}$, 26 times higher than plain ITO electrode.	[47]
<i>Saccharomyces cerevisiae</i>	Dip-coating of PEI and seed-mediated green synthesis growth of AuNPs followed by the biofilm formation during 72 h	CF	Glucose	2771	The single chamber architecture played a role in reducing the number of chemicals and costs.	[44]
<i>Saccharomyces cerevisiae</i>	Physical adsorption of alginate film with entrapped yeast cells	CF	Glucose	-	Current density was 0.326 A m^{-2} (CF-Yeast-algae electrode) and 0.185 A m^{-2} (CF-Yeast-Neutral Red beads electrode). Operation time was 44 days.	[52]
Classes of <i>Gammmaproteobacteria</i> and <i>Negativicutes</i>	MWCNTs blended with biogenic Au and evenly spreading the paste followed by the biofilm formation	CF	Sludge	178	Start-up time 6.75 days.	[56]
<i>Saccharomyces cerevisiae</i>	Dip coating of PEI, SDBS mediated chemical growth of FeMnNPs followed by the biofilm formation	CF	Glucose	5838	Controlled FeMnNP surfactant-mediated growth was performed within a single vial under ambient conditions. Relationship between the surfactant-mediated FeMnNPs and yeast biofilm development was revealed.	[43]
<i>Saccharomyces cerevisiae</i>	Dip coating of PEI followed by dipcoating of one of the QS molecules (phenylethanol, tryptophol and tyrosol). Biofilm growth.	CF	Glucose	159* 156 135	Start-up time 3 days	[57]
<i>Scedosporium dehoogii</i>	Electrochemical deposition of the biofilm	CF	APAP	6.5	A mature biofilm was obtained at day 7	[60]
<i>Scedosporium dehoogii</i>	Electrochemical deposition of the biofilm	CF	APAP Lignin	50 16	A mature biofilm was obtained at day 7. The power density in presence of lignin of 16 mW m^{-2} lasted 200 h.	[61]
<i>Saccharomyces cerevisiae</i>	Cross-linking and hydrophobic interaction of yeast, PEI and CNTs	CNTs	Glucose	344	Membraneless MFC. MPD was maintained to 86% of initial value even after 8 days	[49]
<i>Saccharomyces cerevisiae</i>	Drop coating of PQ and drop coating of MWCNTs	Graphite	Glucose	1.13 10^{-4}	The application of MWCNTs in anode of biofuel cell increased generated power by 69 times and generated voltage by 8 times.	[7]
<i>Bacillus subtilis</i>	Self-assembly of aldrithiol monolayer, drop coating of OsRP solution, drop coating	Gold Graphite	Succinate	-	The maximum current density response was $-5 \mu\text{A cm}^{-2}$. Stability test showed slight decrease response in current with	[51]

of <i>B. subtilis</i> suspension followed by dialysis membrane fixing on the gold electrode. Drop coating of OsRP solution and drop coating of <i>B. subtilis</i> suspension on the graphite electrode	time and reached approximately 73% of the initial response after 6 h.
--	---

*-power densities for MFCs based on phenylethanol, tryptophol and tyrosol, respectively. APAP-acetaminophen. APTES- γ -aminopropyltriethoxysilane. CF-carbon felt. ITO-indium tin oxide. MB-methylene blue. MWCNTs-multi-walled carbon nanotubes. NPs-nanoparticles. OsRP-osmium redox polymer. PANI-polyaniline. PD-power density. PEI-polyethyleneimine. PU-polyurethane. PQ-9,10-phenanthrenequinone. QS-quorum sensing.

Another group of authors presented a biofilm of fungi *Scedosporium dehoogii*, which was used for the modification of the CF anode in a MFC for potential bioremediation of a toxic pharmaceutical compound para-aminophenol from wastewater [60,61]. *S. dehoogii* is a fungus able to use aromatic hydrocarbons as an energy source; thus, it can be simultaneously applied for two purposes: bioremediation of waste water from toxic contaminants as well as for energy production. The cathode of MFC was a CF electrochemically modified by electrodeposition of a poly-Ni (II) tetrasulphonated phthalocyanine (poly-NiTSPc) film, which replaced the classical Pt/Air cathode by the modification of carbon felt surface with poly-NiTSPc. This kind of modification aimed to increase the intensity of O_2 reduction, leading to an increased performance of the MFC [60,61]. Waste waters generally contain low concentrations of pharmaceutical compounds and thus cannot allow a MFC to attain a high-power density. Therefore, the additional source of electron donor cellulose-based fuel was evaluated. It showed a maximum power density of 16 mW m^{-2} for a time of 200 h (Table 1).

As the conductance of the conductive polymers themselves is relatively low, other materials, such as carbon nanotubes, are researched for the modifications of anode surface to promote effective direct electron transfer [7]. It was determined that at lowest explored concentration ($2 \mu\text{g mL}^{-1}$) of MWCNTs and at rather short-lasting exposure of MWCNTs do not significantly affect the viability and other properties of yeast cells. The results obtained from electrochemical characterization showed MWCNTs being a very good candidate for the development of MFCs, as the application of MWCNTs in the anode of the biofuel cell increased generated power by 69 times (113 nW cm^{-2}) (Table 1). Therefore, authors suggest, that MWCNTs can be applied for the modification of the electrode in order to improve electrical CT through the yeast cell membrane and/or cell wall. Evaluations based on fluorescence microscopy and cell count revealed that the viability of the cells was not affected by MWCNTs when the concentration was of $2 \mu\text{g mL}^{-1}$ [7].

As seen from the Table 1, the highest maximum power density was achieved using CF anodes, which were decorated with golden nanoparticles [44] or manganese oxide decorated iron oxide nano-flowers [43] and then modified by *S. cerevisiae*, and in both cases the extracellular polysaccharide matrix of *S. cerevisiae* interacted with NPs, which were deposited on the electrode surface, and created a strong electrochemical bridging between the yeast cells and applied nanostructures. A very advantageous surface of the carbon felt anodes providing a high surface area as well as good physical surface characteristics for microbial attachment and direct electron transfer was achieved in both cases [43,44]. The Nafion membranes were used in most cases for the separation of ion exchange. The different strategy was developed by de Oliveira et al. [14], which enabled to achieve more stable membrane. Biomaterials such as algae [52] and quantum sensing molecules [57] were employed for better microorganism entrapment to the electrode surface, and in the alginate case the extraordinary stability for 44 days was achieved most likely owing to biocompatible environment provided by algae preventing the cells from leakage to the buffer.

The applicability of the constructed MFCs is rarely discussed in the reviewed papers due to them still being in an early stage of development. Thus improvements for generated power density, stability and other properties still needed. The *S. dehoogii* based MFCs showed organic micropollutant para-aminophenol as an efficient model fuel for this MFC, which could be applied for the bioremediation of this toxic pharmaceutical compound. Moreover, the aforementioned devices were stable for more than 8 days [60,61]. *S. loihica* is known to reduce metals, thus the MFC based on this microorganism [47] could be applied as an environmentally friendly and nontoxic approach for the production of chromium nanoparticles as well as for the remediation of chromium and its contamination [50]. MFCs based on classes of *Gamma*proteobacteria and *Negativicutes* were applied for bioremediation and energy generation from sludge [56]. In many cases the main focus of the researches were on the electrode surface modifications with various materials as the guide for better strategy in order to develop the devices with better performance [7,14,43,44,49,51,57] rather than a MFC ready for applications. In many of the aforementioned cases *S. Cerevisiae* was used as a model microorganism.

4. Electrochemically Deposited Conducting Polymers for Better Biocompatibility of MFCs

Electrochemical deposition of conducting polymers is rather simple method for the modification of electrode surface. This method is frequently applied during the development of bioelectronic-based devices. The number of electrical characteristics (such as electrochemical technique, working electrode potentials that are required for the initiation of monomer polymerization, etc.) can be varied and easily adapted during the formation conducting polymer layer with required physicochemical performance [62,63]. Therefore, the physical characteristics of formed layers such as layer thickness, density, ion-permeability can be adjusted by the adaptation of optimal electrochemical conditions required for polymerization reaction. Moreover, many chemical parameters including solvents, polymerizable monomers, polymerization bulk composition, and pH are strongly affecting characteristics of formed CP layers. During the course of electrochemical polymerization some biologically active materials such as proteins [64–67], DNA [21,68] and even living cells and bacteria can be entrapped within the conducting polymer-based layer when they are added into a polymerization solution. The scheme of electrochemical deposition of Ppy layers with entrapped protein molecules [69] is presented in Figure 2.

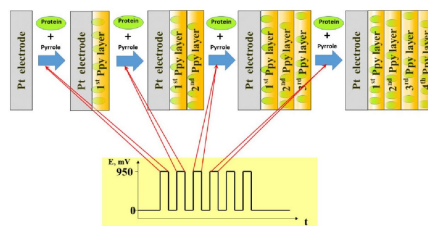


Figure 2. Electrochemical deposition of conducting polymer-polyppyrole and entrapment of proteins within formed Ppy layer, while potential pulses are applied. Adapted from [62].

The application of suitable electrodeposition conditions enables the efficiently of conducting polymer layers to be adapted in the design of bioelectronics-based devices [70–72]. The diffusion rate of the nutrients, which are acting as microbial biofuel is a very

important factor for the performance of MFCs. Therefore, sometimes it is reasonable to change the porosity of the formed CP-based layer by the incorporation of some organic-based ‘spacers’, which are interlinking different polymeric chains [73]. The conductivity of CPs-based layers is also very important for the efficiency of MFCs. Here the achievements of some research groups in the evaluation of synthesis parameters on electrical conductivity of electrochemically deposited Ppy films [74] and PANI-based layers [75] (Figure 3) [69] as well as mathematical model, which was derived by our team [76] can be exploited.

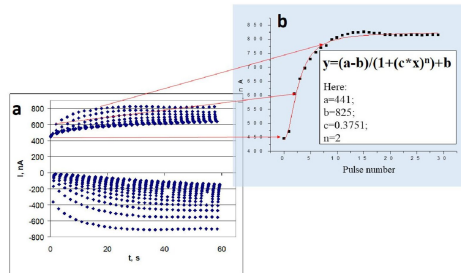


Figure 3. a) Chrono-amperogram, which was registered during electrodeposition of Ppy, using pulsed-potential-based mode. b) Dependence of anodic peaks, which are presented in Figure 3a, on the pulse number during electrochemical deposition. Adapted according to data presented in [69].

The concentration and viability of entrapped cells are also very important for the performance of amperometric biosensors and biofuel cells. Therefore, the compatibility of conducting polymers with microorganisms play a very important role for the performance and application of these bioelectronics-based devices. Such bioelectronics-based devices find new application areas in biomedicine including that in biomedical implants [77], which need suitable long-lasting power sources [78]. In this context, the most suitable power sources for such devices could be enzymatic or catalytic biofuel cells, because they can use unlimited resource of biofuel (e.g., glucose) from our organisms (Figure 4).

Despite diverging opinions regarding the applicability of biofuel cells [79,80], advantages of them were demonstrated by the implantation of BFCs into plants [81,82], animals such as rabbits [83], rats [84–87], clams [88], insects [89], snails [90], and even the human body [91,92]. Therefore, the demand for BFCs is constantly increasing, but many specific challenges are arising in this area of technology [93]. Biofuel cells can be implanted together with powered device, but biocompatibility of implanted BFC is the most important issue, because the electrodes of BFCs differently from many other parts of the device should be in direct contact with body liquids, otherwise the BFC will not operate. Hence, a very important issue is the biocompatibility of materials that are in direct contact with body tissues. If the materials that are contacting with body liquids [94] lacks biocompatibility then allergic and inflammatory reactions can be induced [95,96]. Therefore, the selection of proper materials capable to retain sufficient functionality of immobilized biomaterial is the most important for the development of bioelectronics-based devices [97,98]. CPs are among such materials that can effectively cover surfaces of electrodes with layers modified by biological objects, therefore, numerous research works evaluated some aspects of CPs’ biocompatibility with proteins [1], DNA and stem cells [99,100]. Despite

these studies, just limited number of researches have been dedicated for the investigation of CPs' influence on immune system of laboratory animals [101]. Our research team has conducted research in this direction by the evaluation of effect towards more advanced 'biological systems' such as living stem cells [99,100] and on immune system of laboratory mice [101]. It was demonstrated that Ppy only slightly affects the immune system of these laboratory animals [101]; some influence of Ppy on bone marrow-derived stem cells was determined when higher concentration of Ppy nanoparticles was applied, and by contrast, if a low concentration of polypyrrole nanoparticles was used, then the toxicity towards mouse hepatoma (MH-22A), human T lymphocyte Jurkat, and primary mouse embryonic fibroblast cells was not observed at all [99]. Hence, these investigations revealed that Ppy is biocompatible with evaluated cell-lines [99,100] and immune system of laboratory animals [101]. In addition to Ppy, some aspects of biocompatibility of another conducting polymer—polyaniline (PANI) were also investigated [48]. It is interesting that electric field based stimulation induces the differentiation of nerve cells, which were deposited on a hetero-structure based on polypyrrole/poly (2-methoxy-5 aniline sulfonic acid) [102]. If necessary, the biocompatibility of CP-based structures can be advanced by mixing them with biocompatible polymer—chitosan [103–105] or forming water-rich hydrogel-based structures [106,107]. CP/gel-based structures can be used as scaffolds for growing cells that are used for tissue engineering [108,109], and transplantation [110] or in other biomedical applications [111,112]. Superior biocompatibility of Ppy with biomaterials enables the application of Ppy in the design of various BFCs that potentially can be integrated and implanted together with other biomedical devices.

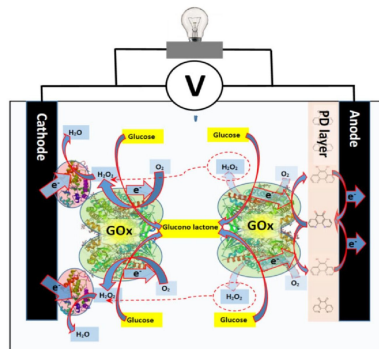


Figure 4. Enzymatic biofuel cell powered by glucose, cathode of this biofuel cell is based on co-immobilized horseradish peroxidase (HRP) and glucose oxidase (GOx) and anode is based on immobilized glucose oxidase. On anode electrons from GOx are transferred to the electrode via redox mediator power density (PD) and in cathode hydrogen peroxide created during enzymatic reaction of GOx is consumed by HRP and electrons from cathode are transferred directly to HRP.

5. Modifications of Microorganisms to Improve MFCs Performance

Different microorganisms [113,114] and living cells of mammals, namely lymphocytes [115] and erythrocytes [116] can be used in the development of BFCs, but the electron transfer from microorganisms to the electrode is very rarely observed, therefore, it is a significant challenge when these bioelectronics devices are designed. The involvement of

microorganism metabolic processes in the polymerization processes of conducting polymers is a very attractive strategy, which is useful during the modification of microorganisms [10,11,117,118], because conducting polymers can improve electron transfer efficiency of microorganisms, which were modified in such way. In our previous works it has been shown that stem cells [99,100] and some microorganisms [10,119] after the modification by CPs can retain viability and still can perform metabolic processes, which can be applied in the generation of electrical current by biofuel cells. The formation of CPs inside of microorganisms seems very innovative and the application of such modified microorganisms in biofuel cells and biosensors is more progressive, because living cells remain biocatalytically active for a longer time [120] when compared with the activity of conducted polymer modified enzymes [121,122]. For this reason, several types of cells [15], bacteria [123] fungi [117] and yeast [11] were engaged in the formation of various polymers, including conducting polymers.

An alternative way to improve MFCs' performance is to target microorganism charge transfer via cell wall and/or membrane. Until now the preferred method has been based on the application of redox compounds capable to assist charge transfer, these redox compounds can be suspended or dissolved in cell suspension and not anchored to electrodes. These molecules are commonly known as redox mediators and are well investigated in numerous researches [7–9,122,124]. Redox mediators can be assigned into few groups: (i) hydrophilic and (ii) lipophilic mediators, (iii) nanoparticles of various origin [124,125], and (iv) conducting and/or redox polymer-based matrices [119,126,127]. If redox mediators are properly applied in the design of biofuel cells, they are able 'to wire cells with electrodes' and are providing more efficient at charge transfer from cell cytoplasm. Hydrophilic mediators usually enhances MFC performance by interaction with cell transplasma membrane redox system [128]. This interaction is thought to occur between mediator and redox enzymes that are located in the cytoplasm. The most common examples are various membrane bound cytochromes [129]. Cytochromes typically possess a redox active center, a functional group, a co-enzyme or a whole cascade of them [130]. Usually, it is thought that hydrophilic enzymes cannot pass through the membrane. Hence, here lipophilic mediators play their role in the charge transfer trough cell membrane. These redox mediators are capable of dissolving into plasma membrane and thus can easily transport charge from cell internals to the cell membrane's outer surface. Lipophilic mediators charge transfer/migration perform via redox capable functional groups. Nonetheless, the most commonly lipophilic mediators are used in tandem with hydrophilic ones. Thus, significant improvements of charge transfer are achieved [128].

On the other hand, various types, shapes or origin nanomaterials are often implied in MFCs. The most often carbon based nanomaterials or metallic nanoparticles play major role for improving charge transfer from redox enzymes [7,131,132]. Modification involves preparation of suspension [133] or either attachment of nanoparticles to cell surface in order to create electrical pathway from cells to electrodes. By contrast with electrode modifications, the cells are conjugated with nanoparticles rather than anchored to electrodes itself [134]. The aforementioned cell modification methodologies can be considered 'traditional'. Recently, self-encapsulation of cells with polymers has emerged. By contrast with other methods, polymer matrices can be prepared in situ with cell culture or sometimes even produced by metabolic/chemical processes that are running inside of cells. Currently, the application of Ppy rises in the field [118]. Very first study, which is reporting Ppy bio-assisted polymer synthesis, to our best knowledge was published in 2016 by our research group [123]. It was reported that bacteria *Streptomyces* spp. are able to catalyze spherical Ppy particles formation without any additional chemicals, because bacteria *Streptomyces* spp. are able to secrete redox-enzymes (e.g., phenol-oxidase) to extracellular media. These enzymes are capable to initiate polymerization of different phenol-based monomers such as Ppy. Thus, it was demonstrated that phenol-oxidases can be exploited for the synthesis of polypyrrole. After 6 days of growing *Streptomyces* spp. bacteria were able to create favorable conditions for the formation of hollow Ppy microspheres. Hollow

microspheres where of 10–20 μm in size. Researchers discussed that particle shape were influenced by organic compounds present in growth medium. Later on, it was reported that it is possible to coat yeast *S. cerevisiae* cells with Ppy [10,135]. In this case, we have used yeast cells to cycle redox mediator $[\text{Fe}(\text{CN})_6]^{3-}/[\text{Fe}(\text{CN})_6]^{4-}$ and thus to perform Ppy synthesis in situ, in a controlled manner (Figure 5). We have suggested some insight into the possible formation mechanism and documented cell viability and Ppy effects on cells and possible locations of the formed polymer. In further studies we have evaluated mechanical properties of Ppy coated cells. Additionally applying isotope ratio mass spectroscopy and non-radioactive isotopic monomer label, we were able to evaluate amounts of Ppy, which forms intercalating matrix in cell wall [11,135]. After the modification by Ppy, the microorganism remained viable, which is very important for the development of long lasting microbial biofuel cells. It was also observed that formed Ppy structures were intergrowing through yeast cell-walls and were strongly affecting physical and chemical properties of modified cells, because cell walls became resistant to yeast wall lysis enzymes [11]. At the same time it was shown that using iron nitride iron (III) nitrate nonahydrate it was possible to form similar Ppy structures based on various bacteria: *Shewanella oneidensis* MR-1, *Escherichia coli*, *Ochrobacterium anthropic* or *Streptococcus thermophilus* [136]. During the preparation, bacterial cells were soaked with iron (III) nitrite nonahydrate, which was located in cell outer layers and further upon introduction of pyrrole performed polymerization of Ppy. It was reported that bacterial cells remain viable and coating procedure does not affect proliferation. Considering the electrical properties, the modification with conducting polymer-Ppy-has improved power density by 14.1 times compared to that of unmodified *S. oneidensis* (147.9 $\mu\text{W cm}^{-2}$). Similar self-encapsulation of microorganisms with the Ppy technique also were performed and analyzed for MFC application using *Aspergillus niger* and *Rhizoctonia sp.* [117,119,137]. For MFC evaluation, scanning electrochemical microscopy (SECM) was applied [118]. The study reported that during electrochemical probing over immobilized modified cell culture current output ($I_{\text{max}} = 0.86 \text{ nA}$) was up 3 times greater when compared to that ($I_{\text{max}} = 0.30 \text{ nA}$) of control group [118]. Results were determined by the registration of surface approach curves. These experiments also showed how charge transfer efficiency, which is crucial for current generation in MFC, depends on several factors: (i) the distance between ultra-micro electrode of SECM and cells and (ii) surface modification of the microorganism. Nominal current output when the ultra-micro electrode was 20 μm apart from test sample was 0.47 nA, which was 1.5 times greater than that of the control sample. White-rot fungal strains belonging to *Trametes spp.* were also modified with Ppy [118]. Researchers pointed out that Ppy formation in fungal hyphae were achieved using laccase enzyme, which is produced and secreted to growth medium by *Trametes spp.* fungi. Polymerization of pyrrole in crude enzyme extract and with cell culture in growth medium was observed. Bio-assisted polymer synthesis at that time was very innovative [138] and, according to our best knowledge, it was one of the first studies that facilitated practical application of enzyme-assisted formation of conducting polymers [70,138–141], and later led towards polymer-based coating formation in cell culture [10,11,117,118]. Thus, it was demonstrated that cells modified with conducting polymer have advanced electron transfer ability, which enables to use these microorganisms in microbial biofuel cells (MFCs) [119] and biosensors [137,142].

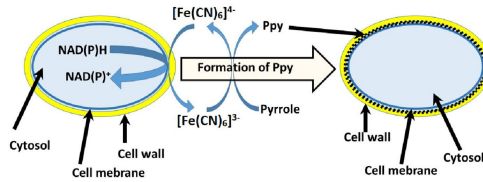


Figure 5. Schematic representation of Ppy synthesis in cell wall of yeast [10]; Redox enzymes that are located in plasma membrane are oxidizing $[\text{Fe}(\text{CN})_6]^{4-}$ into $[\text{Fe}(\text{CN})_6]^{3-}$ that is inducing polymerization reaction of pyrrole [135].

The most interesting application of living cell-induced Ppy formation was demonstrated by the modification/coating of mammalian cells by Ppy [143]. Researchers have applied the synthesis method, which was proposed in our earlier research [10] (Figure 5), and they were able to produce Ppy using suspension of the leukemia cell line, K562 cells. They determined that previous suggested pyrrole polymerization mechanism could be driven by cell exudate molecules, not by plasma membrane oxido-reductase systems differently from the mechanism, which is presented in Figure 5. During the polymerization of pyrrole they observed cancer cell death, which provides another application of this pyrrole polymerization mechanism as ‘reverse pro drug’ systems, meaning that cytotoxic pyrrole after cell death tends to polymerize, which yields biocompatible conducting polymer–polypyrrole [101] that is black-colored and, therefore, can also be used as optical indicator of dead cells. Following this, it was reported that implementing FeCl_3 compound with metal reduction-capable bacteria: *Cupriavidus metallidurans*, *Escherichia coli* and *Clostridium sporogenes*, could initiate atom transfer radical polymerization (ATRP) of various monomers (poly (ethylene glycol methyl ether methacrylate); hydroxyethyl methacrylate; N-hydroxyethyl acrylamide; 2-acrylamido-2-methyl-1-propanesulfonic sodium; 2-(methacryloyloxy) ethyl dimethyl-(3- sulfopropyl) ammonium hydroxide [144]. Researchers suggested interesting approach for designing cell-assisted polymerization. Synthesis not capable Fe (III) compound is reduced into Fe (II) in controlled way and thus initiates the polymerization of monomers that are not toxic to cells, which are engaged in redox processes of Fe (II)/Fe (III). After ATRP polymerization, cells still maintain high viability.

In addition to Ppy some other polymers are also used for cell modification in order to increase their performance in designed MFC. In similar fashion *S. xiamenensis* were coated by polydopamine (PDA) [145]. Selected bacteria can adhere to PDA during their formation via oxidative polymerization in aerobic, slightly alkali (pH 8) conditions. Researchers report PDA modified bacteria *S. xiamenensis* cells were able to generate 452.8 mW m^{-2} power density, which was 6.1 times greater than that for electrodes based on non-modified cells (74.7 mW m^{-2}). Conducting PDA additives were formed within 3 h, which is rather fast, and it seems also that bacteria modification just barely influence cell viability, which dropped only by 2–3%. Rather, popular bacteria for MFC design is *Shewanella oneidensis* MR-1, which was also coated with PDA. In study [146], Yu et.al. report that it is possible to use cell-assisted synthesis for the formation of conducting PDA or using the same bacteria exploit bio mineralization of FeS nanoparticles. Results show that different interfaces wire up cells at different levels and thus their electric/electrochemical properties are different. They also showed that by polysulfide reductase mineralized FeS nanoparticles interface increase the efficiency of MFC anodes up to 3.2 W m^{-2} , which was 14.5 times higher than that of anodes modified by native *S. oneidensis* cells (0.2 W m^{-2}), while for PDA-coated anodes current density was of -0.6 W m^{-2} .

An alternative method was demonstrated in some other research [147,148]. Researchers managed to feed or internalize pre-synthesized carbon dots (CD, carbon nanoparticles) into *S. oneidensis* and *Shewanella xiamenensis*, accordingly [147,148]. Both studies showed remarkable effects of carbon dots, because they are highly biocompatible. Also, carbon dots are able to enhance metabolic activity, because internal adenosine triphosphate (ATP) levels were significantly elevated. It was hypothesized that facilitated metabolism could also produce unwanted reactive oxygen species, but it was not the case. Also, carbon dots form photoactive particles, which promote lactate consumption together with current generation upon illumination. With *Shewanella oneidensis* MR-1 maximum current density achieved was 1.23 A m^{-2} while control was 0.19 A m^{-2} . Meanwhile, the maximum power density of the MFC with carbon dots were 0.491 W m^{-2} , which was by 6.46 folds higher in comparison to that of the control based with not modified same microorganisms (0.076 W m^{-2}). *Shewanella xiamenensis* upon illumination conditions and sole lactate carbon source were able to reach the density of $329.4 \mu\text{A cm}^{-2}$, which was by 4.8 times higher than that of the control electrode ($68.1 \mu\text{A cm}^{-2}$). Osmium redox polymers are also applied in the development of MFC [51,149–151]. In study [149], cells were trapped and wired to electrode surface via [Osmium (2,2'-bipyridine)(poly-vinylimidazole)_nCl] Cl. The pre-synthesized polymer was used as co-mediator and as a conductive binding matrix for *Gluconobacter oxydans* bacterial cells. Electrodes were designed via the drop coating methodology onto glassy carbon paste electrode. Researchers achieved maximum charge density of $15.079 \text{ mA cm}^{-2}$ and open circuit potential value of 176 mV.

Here we explored and overviewed emerging technologies and methodologies for enhanced performance of MFC by introduction of a modification agent into cells themselves or covering them. Summarizing these technologies, they can be classified as cell surface engineering, internalization, or artificial biofilm film formation (Figure 6). The most promising cell modification technologies involve polymeric coating formation and the internalization of living cells. While there is clear evidence of such modification-based impact on charge transfer [119], there still are some drawbacks. As some modifications are quite complex, their application in 'real life' MFCs could be troublesome. Main drawbacks circles around microorganism viability and proliferation as newly formed cells in MFC either should inherit or undergo the modification. Overall, cell surface modifications in tandem with other listed methodologies in this review should yield synergetic effects on the output of electricity from MFCs.

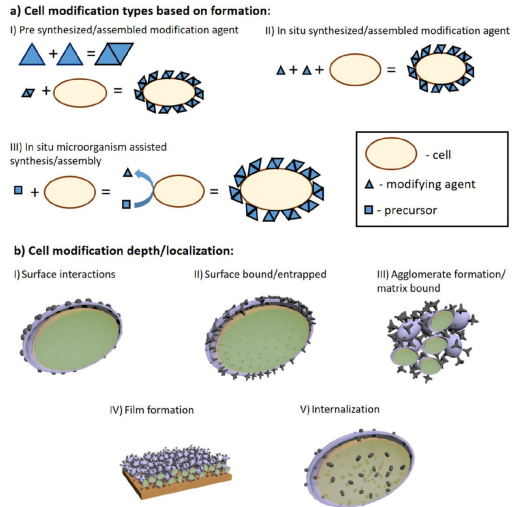


Figure 6. (A) Schematic representation of cell modification by agent formation principle. Cells can be modified using pre-synthesized compounds (I), assembled/ synthesized in situ with living cells are present (II) and in situ when cell assists/catalyzes synthesis assembly of modification agent; (B) schematic representation of modifying agent localization in MFC applications: (I) surface interactions as adsorption, electrostatic interactions etc.; (II) modifying agent is either covalently bonded or forms interlacing and inseparable structures with cell walls or other similar structures; (III) when modifying agent forms aggregates from its matrix and cells; (IV) higher agglomerate organization onto surfaces; (V) internalization of modification agent.

6. Conclusions and Future Aspects

The design of whole cell biosensors requires an optimal matrix for cell immobilization ensuring good cell performance, cell leakage prevention and electron transfer enhancement. Nevertheless, the microorganism-based biosensors show rather poor specificity and slow response because charge transfer from the cell to the electrode is delayed due to natural cell barriers (membrane and cell wall) and the cells are affected by the wide variety of chemicals. But this disadvantage can be very efficiently exploited in the design of microbial biofuel cells, as the immobilized cells can use various materials as the fuel for the generation of electrical energy.

Microbial fuel cells (MFCs) are a promising emerging technology suitable for the generation of 'green' electricity and bioremediation as the increase of fossil fuels causes the global energy crisis and further increases attention to environmental problems. Nevertheless, the power produced in the MFCs is still rather low for practical applications, thus the need for MFC performance improvements is of great importance. The anode as well as current-generating microorganisms are two critical components of the MFC setup. The anode provides the support for microorganism attachment, meanwhile the living cells are responsible for bacteria-electrode charge transfer mechanisms. Poor performance of the anode in MFC is still a most significant obstacle for its proper applications, therefore, efficient anode modifications are supposed to increase the surface area and efficient attachment of biofilm, which subsequently increases the electrical power production of the MFC. Another obstacle to overcome is the slow electron transfer between bacterial cells and electrode. Various chemical modifications of the cell wall or membrane are applied in order to remarkably improve the electron transfer rate and thus the power density of MFCs. Therefore, materials such as carbon nanotubes, conducting polymers, metal nanoparticles and some other metal-based nanostructures have been employed for the modification of anode and/or bacteria cell wall/membrane in order to improve the efficiency of MFCs.

The biocompatibility issues of the implantable MFCs could be resolved by electrochemically coating electrodes of BFCs with conducting polymers such as PPy or PANI or mixes of conducting polymers with chitosan or hydrogels. Various characteristics of the layers formed could be easily controlled by choosing optimal chemical and electrochemical parameters for effective electrode modifications in order to prevent inflammatory reactions while in contact with body tissues.

Author Contributions: Conceptualization-A.R. and E.A.; validation-S.R., R.V., R.C.-G. and A.R.; resources-A.R., R.C.-G., A.R. and S.R.; writing-original draft preparation-R.C.-G. and E.A.; writing-review and editing E.A., R.C.-G., A.R., R.V. and S.R.; visualization-E.A., R.C.-G., A.R.; supervision-A.R. All authors have read and agreed to the published version of the manuscript

Funding: This research was funded by a grant (No. S-MIP-20-18) from the Lithuanian Research Council.

Institutional Review Board Statement: This is review paper, therefore, the study did not require any institutional approval.

Informed Consent Statement: This is review paper, therefore, the study did not require ethical approval

Data Availability Statement: This is review paper, data available in referred papers.

Conflicts of Interest: The authors declare no conflict of interest.

References

1. Ramanavicius, A.; Kausaitė, A.; Ramanavičienė, A. Biofuel cell based on direct bioelectrocatalysis. *Biosens. Bioelectron.* **2005**, *20*, 1962–1967.
2. Ramanavicius, A.; Kausaitė, A.; Ramanavičienė, A. Enzymatic biofuel cell based on anode and cathode powered by ethanol. *Biosens. Bioelectron.* **2008**, *24*, 761–766.
3. Ramanavicius, A.; Ramanavičienė, A. Hemoproteins in Design of Biofuel Cells. *Fuel Cells* **2009**, *9*, 25–36.

4. Krikstoliaitė, V.; Orztek, Y.; Kuliesius, J.; Ramanavičienė, A.; Yazıcıgil, Z.; Ersoz, M.; Okumus, A.; Kausaite-Minkstimiene, A.; Kilić, Z.; Solak, A.O.; et al. Biofuel Cell Based on Anode and Cathode Modified by Glucose Oxidase. *Electroanalysis* **2013**, *25*, 2677–2683.
5. Ramanavičius, A.; Kausaite-Minkstimiene, A.; Morkvenaite-Vilkonciene, I.; Genys, P.; Mikhailova, R.; Semashko, T.; Voronovic, J.; Ramanavičienė, A. Biofuel cell based on glucose oxidase from *Penicillium funiculosum* 46.1 and herringfish peroxidase. *Chem. Eng. J.* **2015**, *264*, 165–173.
6. Slate, A.J.; Whitehead, K.A.; Brownson, D.A.C.; Banks, C.E. Microbial fuel cells: An overview of current technology. *Renew. Sustain. Energy Rev.* **2019**, *101*, 60–81.
7. Bruzaite, I.; Rozene, J.; Morkvenaite-Vilkonciene, I.; Ramanavičius, A. Towards Microorganism-Based Biofuel Cells: The Viability of *Saccharomyces cerevisiae* Modified by Multiwalled Carbon Nanotubes. *Nanomaterials* **2020**, *10*, 954.
8. Rozene, J.; Morkvenaite-Vilkonciene, I.; Bruzaite, I.; Dziedzickis, A.; Ramanavičius, A. Yeast-based microbial biofuel cell mediated by 9,10-phenanthrenequinone. *Electrochim. Acta* **2021**, *373*, 137918.
9. Rozene, J.; Morkvenaite-Vilkonciene, I.; Bruzaite, I.; Zinovičius, A.; Ramanavičius, A. Baker's Yeast-Based Microbial Fuel Cell Mediated by 2-Methyl-1,4-Naphthoquinone. *Membranes* **2021**, *11*, 182.
10. Ramanavičius, A.; Andriukonis, E.; Stirke, A.; Mikoliūnaitė, L.; Balevičius, Z.; Ramanavičienė, A. Synthesis of polypyrrole within the cell wall of yeast by redox-cycling of [Fe(CN)₆]³⁻/[Fe(CN)₆]⁴⁻. *Enzym. Microb. Technol.* **2016**, *83*, 40–47.
11. Andriukonis, E.; Stirke, A.; Garbaras, A.; Mikoliūnaitė, L.; Ramanavičienė, A.; Remeikis, V.; Thornton, B.; Ramanavičius, A. Yeast-assisted synthesis of polypyrrole: Quantification and influence on the mechanical properties of the cell wall. *Colloids Surf. B Biointerfaces* **2018**, *164*, 224–231.
12. Yang, Y.; Xu, M.; Guo, J.; Sun, G. Bacterial extracellular electron transfer in bioelectrochemical systems. *Process. Biochem.* **2012**, *47*, 1707–1714.
13. Gal, I.; Schlesinger, O.; Amir, L.; Alfonta, L. Yeast surface display of dehydrogenases in microbial fuel-cells. *Bioelectrochemistry* **2016**, *112*, 53–60.
14. De Oliveira, A.H.P.; Alcaraz-Espinoza, J.J.; da Costa, M.M.; Nascimento, M.L.F.; Swager, T.M.; de Oliveira, H.P. Improvement of Baker's yeast-based fuel cell power output by electrodes and proton exchange membrane modification. *Mater. Sci. Eng. C* **2019**, *105*, 110082.
15. Niu, J.; Lunn, D.J.; Pusuluri, A.; Yoo, J.I.; O'Malley, M.A.; Mitragotri, S.; Soh, H.T.; Hawker, C.J. Engineering live cell surfaces with functional polymers via cytochrome-controlled radical polymerization. *Nat. Chem.* **2017**, *9*, 537–545.
16. Bousse, L. Whole cell biosensors. *Sens. Actuators B Chem.* **1996**, *34*, 270–275.
17. Su, L.; Jia, W.; Hou, C.; Lei, Y. Microbial biosensors: A review. *Biosens. Bioelectron.* **2011**, *26*, 1788–1799.
18. Sharma, S.; Byrne, H.; O'Kennedy, R.J. Antibodies and antibody-derived analytical biosensors. *Essays Biochem.* **2016**, *60*, 9–18.
19. Kozitsina, A.N.; Svalova, T.S.; Malysheva, N.N.; Okhokhonin, A.V.; Vidrevich, M.B.; Brainina, K.Z. Sensors Based on Bio and Biomimetic Receptors in Medical Diagnostic, Environment, and Food Analysis. *Biosensors* **2018**, *8*, 35.
20. Nguyen, H.H.; Lee, S.H.; Lee, U.J.; Fermin, C.D.; Kim, M. Immobilized Enzymes in Biosensor Applications. *Materials* **2019**, *12*, 121.
21. Ramanavičienė, A.; Ramanavičius, A. Pulsed amperometric detection of DNA with an ssDNA/polypyrrole-modified electrode. *Anal. Bioanal. Chem.* **2004**, *379*, 287–293.
22. Plochanova, Y.V.; Reshetilov, A.N. Microbial Biosensors for the Determination of Pesticides. *J. Anal. Chem.* **2019**, *74*, 1159–1173.
23. Lim, J.W.; Ha, D.; Lee, J.; Lee, S.K.; Kim, T. Review of Micro/Nanotechnologies for Microbial Biosensors. *Front. Bioeng. Biotechnol.* **2015**, *3*, 61.
24. Dolatabadi, S. Microbial Biosensors and Bioelectronics. *Res. J. Biotechnol.* **2012**, *7*, 102–108.
25. Simonis, P.; Garjonyte, R.; Stirke, A. Mediated amperometry as a prospective method for the investigation of electroporation. *Sci. Rep.* **2020**, *10*, 19094.
26. Tkáč, J.; Štefca, V.; Gemeiner, P. Biosensors with Immobilised Microbial Cells Using Amperometric and Thermal Detection Principles. In *Applications of Cell Immobilisation Biotechnology*; Nedović, V., Willaert, R., Eds. Springer Netherlands: Dordrecht, The Netherlands, 2005; pp. 549–566.
27. Yoetz-Kopelman, T.; Dror, Y.; Shacham-Diamand, Y.; Freeman, A. "Cells-on-Beads": A novel immobilization approach for the construction of whole-cell amperometric biosensors. *Sens. Actuators B Chem.* **2016**, *232*, 758–764.
28. Si, R.-W.; Yang, Y.; Yu, Y.-Y.; Han, S.; Zhang, C.-L.; Sun, D.-Z.; Zhai, D.-D.; Liu, X.; Yong, Y.-C. Writing Bacterial Electron Flow for Sensitive Whole-Cell Amperometric Detection of Riboflavin. *Anal. Chem.* **2016**, *88*, 11222–11228.
29. Chung, T.H.; Meshref, M.N.A.; Dhar, B.R. Microbial electrochemical biosensor for rapid detection of naphthenic acid in aqueous solution. *J. Electroanal. Chem.* **2020**, *873*, 114405.
30. Tanaka, M.; Nakata, Y.; Mori, T.; Okamura, Y.; Miyasaka, H.; Takeyama, H.; Matsunaga, T. Development of a Cell Surface Display System in a Magnetotactic Bacterium, "Magnetospirillum magneticum" AMB-1. *Appl. Environ. Microbiol.* **2008**, *74*, 3342.
31. Park, M. Surface Display Technology for Biosensor Applications: A Review. *Sensors* **2020**, *20*, 2775.
32. Flimban, S.G.A.; Hassan, S.H.A.; Rahman, M.M.; Oh, S.-E. The effect of Nafion membrane fouling on the power generation of a microbial fuel cell. *Int. J. Hydrogen Energy* **2020**, *45*, 13643–13651.
33. Christgen, B.; Scott, K.; Dolfing, J.; Head, I.M.; Curtis, T.P. An Evaluation of the Performance and Economics of Membranes and Separators in Single Chamber Microbial Fuel Cells Treating Domestic Wastewater. *PLoS ONE* **2015**, *10*, e0136108.
34. Hindatu, Y.; Annuar, M.S.M.; Gumel, A.M. Mini-review: Anode modification for improved performance of microbial fuel cell. *Renew. Sustain. Energy Rev.* **2017**, *73*, 236–248.

35. Taufiq Musa, M.; Shaari, N.; Kamarudin, S.K. Carbon nanotube, graphene oxide and montmorillonite as conductive fillers in polymer electrolyte membrane for fuel cell: An overview. *Int. J. Energy Res.* **2021**, *45*, 1309–1346.
36. Liu, J.; Qiao, Y.; Guo, C.X.; Lim, S.; Song, H.; Li, C.M. Graphene/carbon cloth anode for high-performance mediatorless microbial fuel cells. *Bioresour. Technol.* **2012**, *114*, 275–280.
37. Wu, Y.; Wang, L.; Jin, M.; Kong, F.; Qi, H.; Nan, J. Reduced graphene oxide and biofilms as cathode catalysts to enhance energy and metal recovery in microbial fuel cell. *Bioresour. Technol.* **2019**, *283*, 129–137.
38. Guo, W.; Chen, M.; Liu, X.; Cheng, F.; Lu, X. Mo2C/Reduced Graphene Oxide Composites with Enhanced Electrocatalytic Activity and Biocompatibility for Microbial Fuel Cells. *Chem. Eur. J.* **2021**, *27*, 4291–4296.
39. Gopalan, A.L.; Muthuchamy, N.; Komathi, S.; Lee, K.P. A novel multicomponent redox polymer nanobead based high performance non-enzymatic glucose sensor. *Biosens. Bioelectron.* **2016**, *84*, 53–63.
40. Huong Le, T.X.; Bechelany, M.; Cretin, M. Carbon felt based-electrodes for energy and environmental applications: A review. *Carbon* **2017**, *122*, 564–591.
41. Moubib, M.; Antonucci, A.; Reggente, M.; Amirjani, A.; Gillen, A.J.; Boghossian, A.A. Enhancing bioelectricity generation in microbial fuel cells and biophotovoltaics using nanomaterials. *Nano Res.* **2019**, *12*, 2184–2199.
42. Correia, A.; Oliveira, R.; Sousa, C.; Morais, S.; Lima-Neto, P. Polyethylenimine-Multi-Walled Carbon Nanotubes/Glassy Carbon Electrode as an Efficient Sensing Platform for Promethazine. *J. Electrochem. Soc.* **2020**, *167*, 107506.
43. Duarte, K.D.Z.; Kwon, Y. Enhanced extracellular electron transfer of yeast-based microbial fuel cells via one pot substrate-bound growth iron-manganese oxide nanoflowers. *J. Power Sources* **2020**, *474*, 228496.
44. Duarte, K.D.Z.; Frattini, D.; Kwon, Y. High performance yeast-based microbial fuel cells by surfactant-mediated gold nanoparticles grown atop a carbon felt anode. *Appl. Energy* **2019**, *256*, 113912.
45. Yuan, X.; Zhang, X.; Sun, L.; Wei, Y.; Wei, X. Cellular Toxicity and Immunological Effects of Carbon-based Nanomaterials. *Part. Fibre Toxicol.* **2019**, *16*, 18.
46. Uscátegui, Y.L.; Diaz, L.E.; Valero, M.F. In vitro and in vivo biocompatibility of polyurethanes synthesized with castor oil polyols for biomedical devices. *J. Mater. Res.* **2019**, *34*, 519–531.
47. Wu, W.; Niu, H.; Yang, D.; Wang, S.; Jiang, N.; Wang, J.; Lin, J.; Hu, C. Polyaniline/Carbon Nanotubes Composite Modified Anode via Graft Polymerization and Self-Assembling for Microbial Fuel Cells. *Polymers* **2018**, *10*, 759.
48. Humpolicek, P.; Kasparikova, V.; Saha, P.; Stejskal, J. Biocompatibility of polyaniline. *Synth. Met.* **2012**, *162*, 722–727.
49. Christwardana, M.; Kwon, Y. Yeast and carbon nanotube based biocatalyst developed by synergetic effects of covalent bonding and hydrophobic interaction for performance enhancement of membraneless microbial fuel cell. *Bioresour. Technol.* **2017**, *225*, 175–182.
50. Wang, W.; Zhang, B.; Liu, Q.; Du, P.; Liu, W.; He, Z. Biosynthesis of palladium nanoparticles using *Shewanella loihica* PV-4 for excellent catalytic reduction of chromium(vi). *Environ. Sci. Nano* **2018**, *5*, 730–739.
51. Coman, V.; Gustavsson, T.; Finkelstein, A.; von Wachenfeldt, C.; Hägerhall, C.; Gorton, L. Electrical Wiring of Live, Metabolically Enhanced *Bacillus subtilis* Cells with Flexible Osmium-Redox Polymers. *J. Am. Chem. Soc.* **2009**, *131*, 16171–16176.
52. Mardiana, U.; Innocent, C.; Cretin, M.; Setyanto, H.; Nurpalah, R.; Kusmiati, M. Applicability of Alginate Film Entrapped Yeast for Microbial Fuel Cell. *Russ. J. Electrochem.* **2019**, *55*, 78–87.
53. Liu, Y.; Zhang, X.; Zhang, Q.; Li, C. Microbial Fuel Cells: Nanomaterials Based on Anode and Their Application. *Energy Technol.* **2020**, *8*, 2000206.
54. Bahadar, H.; Maqbool, F.; Niaz, K.; Abdollahi, M. Toxicity of Nanoparticles and an Overview of Current Experimental Models. *Iran. Biomed. J.* **2016**, *20*, 1–11.
55. Guo, S.; Wang, E. Synthesis and electrochemical applications of gold nanoparticles. *Anal. Chim. Acta* **2007**, *598*, 181–192.
56. Wu, X.; Xiong, X.; Owens, G.; Brunetti, G.; Zhou, J.; Yong, X.; Xie, X.; Zhang, L.; Wei, P.; Jia, H. Anode modification by biogenic gold nanoparticles for the improved performance of microbial fuel cells and microbial community shift. *Bioresour. Technol.* **2018**, *270*, 11–19.
57. Christwardana, M.; Frattini, D.; Duarte, K.D.Z.; Accardo, G.; Kwon, Y. Carbon felt molecular modification and biofilm augmentation via quorum sensing approach in yeast-based microbial fuel cells. *Appl. Energy* **2019**, *238*, 239–248.
58. Albuquerque, P.; Casadevall, A. Quorum sensing in fungi—A review. *Med. Mycol.* **2012**, *50*, 337–345.
59. Angellaalincy, M.J.; Navanietha Krishnaraj, R.; Shakambari, G.; Ashokkumar, B.; Kathiresan, S.; Varalakshmi, P. Biofilm Engineering Approaches for Improving the Performance of Microbial Fuel Cells and Bioelectrochemical Systems. *Front. Energy Res.* **2018**, *6*, 63.
60. Mbokou, S.F.; Tontle, I.K.; Pontié, M. Development of a novel hybrid biofuel cell type APAP/O2 based on a fungal bioanode with a *Scedosporium dehoogii* biofilm. *J. Appl. Electrochem.* **2017**, *47*, 273–280.
61. Pontié, M.; Jaspard, E.; Frattini, C.; Kilani, J.; Fix-Tailleur, A.; Innocent, C.; Chery, D.; Mbokou, S.F.; Somrani, A.; Cagnon, B.; et al. A sustainable fungal microbial fuel cell (FMFC) for the bioremediation of acetaminophen (APAP) and its main by-product (PAP) and energy production from biomass. *Biocatal. Agric. Biotechnol.* **2019**, *22*, 101376.
62. Ramanavicius, A.; Oztekin, Y.; Ramanaviciene, A. Electrochemical formation of polypyrrole-based layer for immunosensor design. *Sens. Actuators B Chem.* **2014**, *197*, 237–243.
63. Long, Y.-Z.; Li, M.-M.; Gu, C.; Wan, M.; Duvail, J.-L.; Liu, Z.; Fan, Z. Recent advances in synthesis, physical properties and applications of conducting polymer nanotubes and nanofibers. *Prog. Polym. Sci.* **2011**, *36*, 1415–1442.

64. Rahman, M.A.; Kumar, P.; Park, D.-S.; Shim, Y.-B. Electrochemical Sensors Based on Organic Conjugated Polymers. *Sensors* **2008**, *8*, 118–141.
65. Bredas, J.L.; Street, G.B. Polarons, bipolarons, and solitons in conducting polymers. *Acc. Chem. Res.* **1985**, *18*, 309–315.
66. Srilalitha, S.; Jayaveera, K.N.; Madhuvendhra, S.S. The effect of dopant, temperature and band gap on conductivity of conducting polymers. *Int. J. Innov. Res. Sci. Eng. Technol.* **2013**, *2*, 2694–2696.
67. Le, T.-H.; Kim, Y.; Yoon, H. Electrical and Electrochemical Properties of Conducting Polymers. *Polymers* **2017**, *9*, 150.
68. Ratautaitė, V.; Topkaya, S.N.; Mikoliūnaitė, L.; Oszos, M.; Oztekin, Y.; Ramanaviciene, A.; Ramanavicius, A. Molecularly Imprinted Polypyrrole for DNA Determination. *Electroanalysis* **2013**, *25*, 1169–1177.
69. Ramanavicius, S.; Ramanavicius, A. Charge Transfer and Biocompatibility Aspects in Conducting Polymer-Based Enzymatic Biosensors and Biofuel Cells. *Nanomaterials* **2021**, *11*, 371.
70. Ramanavicius, A.; Kausaitė, A.; Ramanaviciene, A. Self-encapsulation of oxidases as a basic approach to tune the upper detection limit of amperometric biosensors. *Analyst* **2008**, *133*, 1083–1089.
71. Bai, S.; Hu, Q.; Zeng, Q.; Wang, M.; Wang, L. Variations in Surface Morphologies, Properties, and Electrochemical Responses to Nitro-Analyte by Controlled Electropolymerization of Thiophene Derivatives. *ACS Appl. Mater. Interfaces* **2018**, *10*, 11319–11327.
72. Stewart, S.; Ivy, M.A.; Anshyn, E.V. The use of principal component analysis and discriminant analysis in differential sensing routines. *Chem. Soc. Rev.* **2014**, *43*, 70–84.
73. Jiang, J.-X.; Su, F.; Trewin, A.; Wood, C.D.; Campbell, N.L.; Niu, H.; Dickinson, C.; Ganin, A.Y.; Rosseinsky, M.J.; Khimiy, Y.Z.; et al. Conjugated Microporous Poly(aryleneethynylene) Networks. *Angew. Chem. Int. Ed.* **2007**, *46*, 8574–8578.
74. Patois, T.; Lakard, B.; Martin, N.; Fievet, P. Effect of various parameters on the conductivity of free standing electro synthesized polypyrrole films. *Synth. Met.* **2010**, *160*, 2180–2185.
75. Lete, C.; Lakard, B.; Hihm, J.-Y.; del Campo, F.J.; Lupu, S. Use of sinusoidal voltages with fixed frequency in the preparation of tyrosinase based electrochemical biosensors for dopamine electroanalysis. *Sens. Actuators B Chem.* **2017**, *240*, 801–809.
76. Leonavicius, K.; Ramanaviciene, A.; Ramanavicius, A. Polymerization Model for Hydrogen Peroxide Initiated Synthesis of Polypyrrole Nanoparticles. *Langmuir* **2011**, *27*, 10970–10976.
77. Joung, Y.-H. Development of Implantable Medical Devices: From an Engineering Perspective. *Int. Neuronal J.* **2013**, *17*, 98–106.
78. Holmes, C.F.; Owens, B.B. Batteries for Implantable Biomedical Applications. In *Wiley Encyclopedia of Biomedical Engineering*; Wiley: Hoboken, NJ, USA, 2006.
79. Shleev, S.; Bergel, A.; Gorton, L. Biological fuel cells: Divergence of opinion. *Bioelectrochemistry* **2015**, *106*, 1–2.
80. Katz, E.; MacVittie, K. Implanted biofuel cells operating in vivo—Methods, applications and perspectives—Feature article. *Energy Environ. Sci.* **2013**, *6*, 2791–2803.
81. Mano, N.; Mao, F.; Heller, A. Characteristics of a Miniature Compartment-less Glucose-O₂ Biofuel Cell and Its Operation in a Living Plant. *J. Am. Chem. Soc.* **2003**, *125*, 6588–6594.
82. MacVittie, K.; Conlon, T.; Katz, E. A wireless transmission system powered by an enzyme biofuel cell implanted in an orange. *Bioelectrochemistry* **2015**, *106*, 28–33.
83. El Ichi-Ribault, S.; Alcaraz, J.-P.; Boucher, F.; Boutaud, B.; Dalmolin, R.; Boutonnat, J.; Cinquin, P.; Zebda, A.; Martin, D.K. Remote wireless control of an enzymatic biofuel cell implanted in a rabbit for 2 months. *Electrochim. Acta* **2018**, *269*, 360–366.
84. Miyake, T.; Haneeda, K.; Nagai, N.; Yatagawa, Y.; Onami, H.; Yoshino, S.; Abe, T.; Nishizawa, M. Enzymatic biofuel cells designed for direct power generation from biofluids in living organisms. *Energy Environ. Sci.* **2011**, *4*, 8008–8012.
85. Castorena-Gonzalez, J.A.; Foote, C.; MacVittie, K.; Halámek, J.; Halámková, L.; Martínez-Lemus, L.A.; Katz, E. Biofuel Cell Operating in Vivo in Rat. *Electroanalysis* **2013**, *25*, 1579–1584.
86. Zebda, A.; Cosnier, S.; Alcaraz, J.P.; Holzinger, M.; Le Goff, A.; Gondran, C.; Boucher, F.; Giroud, F.; Gorgy, K.; Lamraoui, H.; et al. Single Glucose Biofuel Cells Implanted in Rats Power Electronic Devices. *Sci. Rep.* **2013**, *3*, 1516.
87. Andoralov, V.; Falk, M.; Suyatin, D.B.; Granmo, M.; Sotres, J.; Ludwig, R.; Popov, V.O.; Schouenborg, J.; Blum, Z.; Shleev, S. Biofuel Cell Based on Microscale Nanostructured Electrodes with Inductive Coupling to Rat Brain Neurons. *Sci. Rep.* **2013**, *3*, 3270.
88. Szczupak, A.; Halámek, J.; Halámková, L.; Bocharova, V.; Alfonta, L.; Katz, E. Living battery—Biofuel cells operating in vivo in clams. *Energy Environ. Sci.* **2012**, *5*, 8891–8895.
89. Falk, M.; Narváez Villarrubia, C.W.; Babanova, S.; Atanassov, P.; Shleev, S. Biofuel Cells for Biomedical Applications: Colonizing the Animal Kingdom. *ChemPhysChem* **2013**, *14*, 2045–2058.
90. Halámková, L.; Halámek, J.; Bocharova, V.; Szczupak, A.; Alfonta, L.; Katz, E. Implanted Biofuel Cell Operating in a Living Snail. *J. Am. Chem. Soc.* **2012**, *134*, 5040–5043.
91. Calabrese Barton, S.; Gallaway, J.; Atanassov, P. Enzymatic Biofuel Cells for Implantable and Microscale Devices. *Chem. Rev.* **2004**, *104*, 4867–4886.
92. Cosnier, S.; Le Goff, A.; Holzinger, M. Towards glucose biofuel cells implanted in human body for powering artificial organs: Review. *Electrochem. Commun.* **2014**, *38*, 19–23.
93. Zebda, A.; Alcaraz, J.-P.; Vadgama, P.; Shleev, S.; Minter, S.D.; Boucher, F.; Cinquin, P.; Martin, D.K. Challenges for successful implantation of biofuel cells. *Bioelectrochemistry* **2018**, *124*, 57–72.
94. Falk, M.; Andoralov, V.; Blum, Z.; Sotres, J.; Suyatin, D.B.; Ruzgas, T.; Arnebrant, T.; Shleev, S. Biofuel cell as a power source for electronic contact lenses. *Biosens. Bioelectron.* **2012**, *37*, 38–45.
95. Huang, L.; Zhuang, X.; Hu, J.; Lang, L.; Zhang, P.; Wang, Y.; Chen, X.; Wei, Y.; Jing, X. Synthesis of Biodegradable and Electroactive Multiblock Poly(lactide and Aniline Pentamer Copolymer for Tissue Engineering Applications. *Biomacromolecules* **2008**, *9*, 850–858.

96. Guo, Y.; Li, M.; Mylonakis, A.; Han, J.; MacDiarmid, A.G.; Chen, X.; Lelkes, P.I.; Wei, Y. Electroactive Oligoaniline-Containing Self-Assembled Monolayers for Tissue Engineering Applications. *Biomacromolecules* **2007**, *8*, 3025–3034.
97. Lakard, B.; Herlem, G.; Lakard, S.; Antoniou, A.; Fahys, B. Urea potentiometric biosensor based on modified electrodes with urease immobilized on polyethylenimine films. *Biosens. Bioelectron.* **2004**, *19*, 1641–1647.
98. Lakard, B.; Magnin, D.; Deschaume, O.; Vanlancker, G.; Glinel, K.; Demoustier-Champagne, S.; Nysten, B.; Jonas, A.M.; Bertrand, P.; Yunus, S. Urea potentiometric enzymatic biosensor based on charged biopolymers and electrodeposited polyaniline. *Biosens. Bioelectron.* **2011**, *26*, 4139–4145.
99. Vaitkuvienė, A.; Kaseta, V.; Voronovic, J.; Ramanauskaitė, G.; Bizulevičienė, G.; Ramanavičienė, A.; Ramanavičius, A. Evaluation of cytotoxicity of polypyrrole nanoparticles synthesized by oxidative polymerization. *J. Hazard. Mater.* **2013**, *250–251*, 167–174.
100. Vaitkuvienė, A.; Ratautaitė, V.; Mikoliūnaitė, L.; Kaseta, V.; Ramanauskaitė, G.; Bizulevičienė, G.; Ramanavičienė, A.; Ramanavičius, A. Some biocompatibility aspects of conducting polymer polypyrrole evaluated with bone marrow-derived stem cells. *Colloids Surf. A Physicochem. Eng. Asp.* **2014**, *442*, 152–156.
101. Ramanavičienė, A.; Kausaitė, A.; Tautkus, S.; Ramanavičius, A. Biocompatibility of polypyrrole particles: An in-vivo study in mice. *J. Pharm. Pharmacol.* **2007**, *59*, 311–315.
102. Liu, X.; Gilmore, K.J.; Moulton, S.E.; Wallace, G.G. Electrical stimulation promotes nerve cell differentiation on polypyrrole/poly (2-methoxy-5-aniline sulfonic acid) composites. *J. Neural Eng.* **2009**, *6*, 065002.
103. Zhao, X.; Li, P.; Guo, B.; Ma, P.X. Antibacterial and conductive injectable hydrogels based on quaternized chitosan-graft-polyaniline/oxidized dextran for tissue engineering. *Acta Biomater.* **2015**, *26*, 236–248.
104. El Ichi, S.; Zebda, A.; Alcaraz, J.P.; Laaroussi, A.; Boucher, F.; Boutonnat, J.; Reverdy-Bruas, N.; Chaussy, D.; Belgacem, M.N.; Cinquin, P.; et al. Bioclectrodes modified with chitosan for long-term energy supply from the body. *Energy Environ. Sci.* **2015**, *8*, 1017–1026.
105. El Ichi-Ribault, S.; Zebda, A.; Tingry, S.; Petit, M.; Suherman, A.L.; Boualam, A.; Cinquin, P.; Martin, D.K. Performance and stability of chitosan-MWCNTs-laccase bioanode: Effect of MWCNTs surface charges and ionic strength. *J. Electroanal. Chem.* **2017**, *799*, 26–33.
106. Zhao, F.; Bae, J.; Zhou, X.; Guo, Y.; Yu, G. Nanostructured Functional Hydrogels as an Emerging Platform for Advanced Energy Technologies. *Adv. Mater.* **2018**, *30*, 1801796.
107. Shi, Y.; Wang, M.; Ma, C.; Wang, Y.; Li, X.; Yu, G. A Conductive Self-Healing Hybrid Gel Enabled by Metal-Ligand Supramolecule and Nanostructured Conductive Polymer. *Nano Lett.* **2015**, *15*, 6276–6281.
108. Xu, Y.; Cui, M.; Patsis, P.A.; Günther, M.; Yang, X.; Eckert, K.; Zhang, Y. Reversibly Assembled Electroconductive Hydrogel via a Host-Guest Interaction for 3D Cell Culture. *ACS Appl. Mater. Interfaces* **2019**, *11*, 7715–7724.
109. Mawad, D.; Stewart, E.; Officer, D.L.; Romeo, T.; Wagner, P.; Wagner, K.; Wallace, G.G. A Single Component Conducting Polymer Hydrogel as a Scaffold for Tissue Engineering. *Adv. Funct. Mater.* **2012**, *22*, 2692–2699.
110. Dong, R.; Zhao, X.; Guo, B.; Ma, P.X. Self-Healing Conductive Injectable Hydrogels with Antibacterial Activity as Cell Delivery Carrier for Cardiac Cell Therapy. *ACS Appl. Mater. Interfaces* **2016**, *8*, 17138–17150.
111. Ginting, M.; Pasaribu, S.P.; Masmur, I.; Kaban, J. Self-healing composite hydrogel with antibacterial and reversible restorability conductive properties. *RSC Adv.* **2020**, *10*, 5050–5057.
112. Bhat, A.; Amanor-Boadu, J.M.; Guiseppe-Elie, A. Toward Impedimetric Measurement of Acidosis with a pH-Responsive Hydrogel Sensor. *Sens. Cans.* **2020**, *5*, 800–809.
113. Pankratova, G.; Hederstedt, L.; Gorton, L. Extracellular electron transfer features of Gram-positive bacteria. *Anal. Chim. Acta* **2019**, *1076*, 32–47.
114. Pankratova, G.; Pankratov, D.; Milton, R.D.; Minter, S.D.; Gorton, L. Extracellular Electron Transfer: Following Nature: Bioinspired Mediation Strategy for Gram-Positive Bacterial Cells. *Adv. Energy Mater.* **2019**, *9*, 1970055.
115. Güven, G.; Lozano-Sanchez, P.; Güven, A. Power Generation from Human Leukocytes/Lymphocytes in Mammalian Biofuel Cell. *Int. J. Electrochem.* **2013**, *2013*, 706792.
116. Ayato, Y.; Sakurai, K.; Fukunaga, S.; Suganuma, T.; Yamagiwa, K.; Shiroishi, H.; Kuwano, J. A simple biofuel cell cathode with human red blood cells as electrocatalysts for oxygen reduction reaction. *Biosens. Bioelectron.* **2014**, *55*, 14–18.
117. Apetrei, R.-M.; Carac, G.; Bährim, G.; Ramanavičienė, A.; Ramanavičius, A. Modification of *Aspergillus niger* by conducting polymer, Polypyrrole, and the evaluation of electrochemical properties of modified cells. *Bioelectrochemistry* **2018**, *121*, 46–55.
118. Apetrei, R.-M.; Carac, G.; Ramanavičienė, A.; Bährim, G.; Tanase, C.; Ramanavičius, A. Cell-assisted synthesis of conducting polymer—Polypyrrole—For the improvement of electric charge transfer through fungal cell wall. *Colloids Surf. B Biointerfaces* **2019**, *175*, 671–679.
119. Kisielute, A.; Popov, A.; Apetrei, R.-M.; Cîrâc, G.; Morkvenaite-Vilkonciene, I.; Ramanavičienė, A.; Ramanavičius, A. Towards microbial biofuel cells: Improvement of charge transfer by self-modification of microorganisms with conducting polymer—Polypyrrole. *Chem. Eng. J.* **2019**, *356*, 1014–1021.
120. Magenlis, E.P.; Fernandez-Trillo, F.; Sui, C.; Spain, S.G.; Bradshaw, D.J.; Churchley, D.; Mantovani, G.; Winzer, K.; Alexander, C. Bacteria-instructed synthesis of polymers for self-selective microbial binding and labelling. *Nat. Mater.* **2014**, *13*, 748–755.
121. German, N.; Ramanavičienė, A.; Ramanavičius, A. Formation and Electrochemical Evaluation of Polyaniline and Polypyrrole Nanocomposites Based on Glucose Oxidase and Gold Nanostructures. *Polymers* **2020**, *12*, 3026.
122. Van der Zee, F.P.; Cervantes, F.J. Impact and application of electron shuttles on the redox (bio)transformation of contaminants: A review. *Biotechnol. Adv.* **2009**, *27*, 256–277.
123. Shirke, A.; Apetrei, R.-M.; Kirsynite, M.; Dedelaite, L.; Bondarenka, V.; Jusulaitiene, V.; Pucetaite, M.; Selskis, A.; Carac, G.; Bährim, G.; et al. Synthesis of polypyrrole microspheres by *Streptomyces* spp. *Polymer* **2016**, *84*, 99–106.

124. Zhou, M.; Yang, J.; Wang, H.; Jin, T.; Hassett, D.J.; Gu, T. Chapter 9—Bioelectrochemistry of Microbial Fuel Cells and their Potential Applications in Bioenergy. In *Bioenergy Research: Advances and Applications*; Gupta, V.K., Tuohy, M.G., Kubicek, C.P., Saddler, J., Xu, F., Eds.; Elsevier: Amsterdam, The Netherlands, 2014; pp. 131–152.
125. Ramanaviciene, A.; Nasitajute, G.; Snitka, V.; Kausaite, A.; German, N.; Barauskas-Memenas, D.; Ramanavicius, A. Spectrophotometric evaluation of gold nanoparticles as red-ox mediator for glucose oxidase. *Sens. Actuators B Chem.* **2009**, *137*, 483–489.
126. Rudra, R.; Pattanayak, P.; Kundu, P. Conducting Polymer-Based Microbial Fuel Cells. In *Enzymatic Fuel Cells: Materials and Applications*; Materials Research Forum LLC: Millersville, PA, USA, 2019; pp. 173–187.
127. Oztekin, Y.; Ramanaviciene, A.; Yazicigil, Z.; Solak, A.O.; Ramanavicius, A. Direct electron transfer from glucose oxidase immobilized on polyphenanthroline-modified glassy carbon electrode. *Biosens. Bioelectron.* **2011**, *26*, 2541–2546.
128. Rawson, F.J.; Downard, A.J.; Baronin, K.H. Electrochemical detection of intracellular and cell membrane redox systems in *Saccharomyces cerevisiae*. *Sci. Rep.* **2014**, *4*, 5216.
129. Holmes, D.E.; Ueki, T.; Tang, H.-Y.; Zhou, J.; Smith, J.A.; Chaput, G.; Lovley, D.R. A Membrane-Bound Cytochrome Enables “Methanosarcina acetivorans” To Conserve Energy from Extracellular Electron Transfer. *mBio* **2019**, *10*, e00789-19.
130. Okamoto, A.; Kalathil, S.; Deng, X.; Hashimoto, K.; Nakamura, R.; Nealon, K.H. Cell-secreted Flavins Bound to Membrane Cytochromes Dictate Electron Transfer Reactions to Surfaces with Diverse Charge and pH. *Sci. Rep.* **2014**, *4*, 5628. Jiang, X.; Hu, J.; Lieber, A.M.; Jackan, C.S.; Biffinger, J.C.; Fitzgerald, L.A.; Ringeisen, B.R.; Lieber, C.M. Nanoparticle Facilitated Extracellular Electron Transfer in Microbial Fuel Cells. *Nano Lett.* **2014**, *14*, 6737–6742.
131. Sharma, T.; Mohana Reddy, A.L.; Chandra, T.S.; Ramaprabhu, S. Development of carbon nanotubes and nanofluids based microbial fuel cell. *Int. J. Hydrogen Energy* **2008**, *33*, 6749–6754.
132. Zhao, C.-c.; Chen, J.; Ding, Y.; Wang, V.B.; Bao, B.; Kjelleberg, S.; Cao, B.; Loo, S.C.J.; Wang, L.; Huang, W.; et al. Chemically Functionalized Conjugated Oligoelectrolyte Nanoparticles for Enhancement of Current Generation in Microbial Fuel Cells. *ACS Appl. Mater. Interfaces* **2015**, *7*, 14501–14505.
133. Cui, Q.; Wang, X.; Yang, Y.; Li, S.; Li, L.; Wang, S. Binding-Directed Energy Transfer of Conjugated Polymer Materials for Dual-Color Imaging of Cell Membrane. *Chem. Mater.* **2016**, *28*, 4661–4669.
134. Andriukonis, E.; Ramanaviciene, A.; Ramanavicius, A. Synthesis of Polypyrrole Induced by Fe(CN)₆³⁻ and Redox Cycling of Fe(CN)₆⁴⁻/Fe(CN)₆³⁻. *Polymers* **2018**, *10*, 12.
135. Song, R.-B.; Wu, Y.; Lin, Z.-Q.; Xie, J.; Tan, C.H.; Loo, J.S.C.; Cao, B.; Zhang, J.-R.; Zhu, J.-J.; Zhang, Q. Living and Conducting; Coating Individual Bacterial Cells with In Situ Formed Polypyrrole. *Angew. Chem. Int. Ed.* **2017**, *56*, 10516–10520.
136. Apetrei, R.-M.; Cărac, G.; Bahrim, G.; Camurlu, P. Sensitivity enhancement for microbial biosensors through cell Self-Coating with polypyrrole. *Int. J. Polym. Mater. Polym. Biomater.* **2019**, *68*, 1058–1067.
137. Ramanavicius, A.; Kausaite, A.; Ramanaviciene, A. Polypyrrole-coated glucose oxidase nanoparticles for biosensor design. *Sens. Actuators B Chem.* **2005**, *111*, 532–539.
138. Olea, D.; Viratelle, O.; Faure, C. Polypyrrole-glucose oxidase biosensor: Effect of enzyme encapsulation in multilamellar vesicles on analytical properties. *Biosens. Bioelectron.* **2008**, *23*, 788–794.
139. Mazur, M.; Krywko-Cendrowska, A.; Krysiński, P.; Rogalski, J. Encapsulation of lacase in a conducting polymer matrix: A simple route towards polypyrrole microcontainers. *Synth. Met.* **2009**, *159*, 1731–1738.
140. Ramanavicius, A.; Kausaite, A.; Ramanaviciene, A.; Acaite, J.; Malinauskas, A. Redox enzyme-glucose oxidase-initiated synthesis of polypyrrole. *Synth. Met.* **2006**, *156*, 409–413.
141. Apetrei, R.-M.; Cărac, G.; Bahrim, G.; Camurlu, P. Utilization of enzyme extract self-encapsulated within polypyrrole in sensitive detection of catechol. *Enzym. Microb. Technol.* **2019**, *128*, 34–39.
142. Sherman, H.G.; Hicks, J.M.; Jain, A.; Titman, J.J.; Alexander, C.; Stolnik, S.; Rawson, F.J. Mammalian-Cell-Driven Polymerisation of Pyrrole. *ChemBioChem* **2019**, *20*, 1008–1013.
143. Bennett, M.R.; Gurnani, P.; Hill, P.J.; Alexander, C.; Rawson, F.J. Iron-Catalysed Radical Polymerisation by Living Bacteria. *Angew. Chem. Int. Ed.* **2020**, *59*, 4750–4755.
144. Liu, S.-R.; Cai, L.-F.; Wang, L.-Y.; Yi, X.-F.; Peng, Y.-J.; He, N.; Wu, X.; Wang, Y.-P. Polycodamine coating on individual cells for enhanced extracellular electron transfer. *Chem. Commun.* **2019**, *55*, 10535–10538.
145. Yu, Y.-Y.; Wang, Y.-Z.; Fang, Z.; Shi, Y.-T.; Cheng, Q.-W.; Chen, Y.-X.; Shi, W.; Yong, Y.-C. Single cell electron collectors for highly efficient wiring-up electronic abiotic/biotic interfaces. *Nat. Commun.* **2020**, *11*, 4087.
146. Yang, C.; Aslan, H.; Zhang, P.; Zhu, S.; Xiao, Y.; Chen, L.; Khan, N.; Boesen, T.; Wang, Y.; Liu, Y.; et al. Carbon dots-fed *Shewanella oneidensis* MR-1 for bioelectricity enhancement. *Nat. Commun.* **2020**, *11*, 1379.
147. Liu, S.; Yi, X.; Wu, X.; Li, Q.; Wang, Y. Internalized Carbon Dots for Enhanced Extracellular Electron Transfer in the Dark and Light. *Smold* **2020**, *16*, 2004194.
148. Aslan, S.; Conghaile, P.Ó.; Leech, D.; Gorton, L.; Timur, S.; Anik, U. Development of an Osmium Redox Polymer Mediated Bioanode and Examination of its Performance in Gluconobacter oxydans Based Microbial Fuel Cell. *Electroanalysis* **2017**, *29*, 1651–1657.
149. Yuan, Y.; Shin, H.; Kang, C.; Kim, S. Wiring microbial biofilms to the electrode by osmium redox polymer for the performance enhancement of microbial fuel cells. *Bioelectrochemistry* **2016**, *108*, 8–12.
150. Timur, S.; Haghighi, B.; Tkac, J.; Pazarlıoğlu, N.; Telefoncu, A.; Gorton, L. Electrical wiring of *Pseudomonas putida* and *Pseudomonas fluorescens* with osmium redox polymers. *Bioelectrochemistry* **2007**, *71*, 38–45.
151. Hasan, K.; Çevik, E.; Sperling, E.; Packer, M.A.; Leech, D.; Gorton, L. Photoelectrochemical Wiring of *Paulschulzia pseudovolvax* (Algae) to Osmium Polymer Modified Electrodes for Harnessing Solar Energy. *Adv. Energy Mater.* **2015**, *5*, 1501100.

NOTES

NOTES

Vilniaus universiteto leidykla
Saulėtekio al. 9, III rūmai, LT-10222 Vilnius
El. p. info@leidykla.vu.lt, www.leidykla.vu.lt
bookshop.vu.lt, journals.vu.lt
Tiražas 15 egz.